

UNIVERSITI MALAYA

ORIGINAL LITERARY WORK DECLARATION

Name of Candidate: Nurul Husna Binti Zainol (I.C/Passport No: 871214-35-5522)

Registration/Matric No: SGR 100 100

Name of Degree: Master of Science (MSc)

Title of Project Paper/Research Report/Dissertation/Thesis (“this Work”):

Studies of PMMA-(MgCF₃SO₃)₂ Gel Polymer Electrolytes for Magnesium Battery Applications

Field of Study: Advance Materials

I do solemnly and sincerely declare that:

- (1) I am the sole author/writer of this Work;
- (2) This Work is original;
- (3) Any use of any work in which copyright exists was done by way of fair dealing and for permitted purposes and any excerpt or extract from, or reference to or reproduction of any copyright work has been disclosed expressly and sufficiently and the title of the Work and its authorship have been acknowledged in this Work;
- (4) I do not have any actual knowledge nor do I ought reasonably to know that the making of this work constitutes an infringement of any copyright work;
- (5) I hereby assign all and every rights in the copyright to this Work to the University of Malaya (“UM”), who henceforth shall be owner of the copyright in this Work and that any reproduction or use in any form or by any means whatsoever is prohibited without the written consent of UM having been first had and obtained;
- (6) I am fully aware that if in the course of making this Work I have infringed any copyright whether intentionally or otherwise, I may be subject to legal action or any other action as may be determined by UM.

Candidate’s Signature

Date 18 July 2013

Subscribed and solemnly declared before,

Witness’s Signature

Date 18 July 2013

Name:

Designation:

ABSTRACT

In the present work, the gel polymer electrolytes (GPEs) comprising of poly(methyl methacrylate) (PMMA) as a host polymer in a mixture of ethylene carbonate (EC) and propylene carbonate (PC) as a plasticizing solvent with various concentrations of magnesium triflate as a dopant salt have been prepared by the solution casting technique. The ionic conductivity of the GPE films was determined using AC impedance spectroscopy. The film containing 20 wt.% of magnesium triflate salt exhibited the highest room temperature ionic conductivity of $1.27 \times 10^{-3} \text{ S cm}^{-1}$. The conductivity-temperature studies of the GPE films follow the Arrhenius behavior with activation energy determined to be in the range of 0.18 - 0.26 eV. The transport number of magnesium ions in the GPEs was evaluated using the combination of AC impedance spectroscopy and DC polarization techniques. Fourier Transform Infrared Spectroscopy (FTIR) studies confirmed the increased in conductivity is due to increase of free ions and decrease in ion aggregates. The increase and decrease in the number of free ions can also be implied from the dielectric constant, ϵ_r -frequency plots. Thermal studies indicate that the GPE films are stable over a wide temperature range, 30 °C – 130 °C. XRD and FESEM studies revealed that the increased in amorphous region of GPE films lead to higher conductivity of the films. The electrochemical stability of the GPE film has been tested using linear sweep voltammetry (LSV). Studies based on AC impedance and cyclic voltammetry (CV) confirm Mg^{2+} ion conduction in the GPE film. The highest conducting GPE film was used as an electrolyte in Mg|GPE|MnO₂ cell. The GPE film appears to be excellent substitute for the liquid electrolyte in rechargeable magnesium batteries.

ABSTRAK

Dalam kajian ini, elektrolit-elektrolit polimer gel (GPEs) yang terdiri daripada polimetil metakrilat (PMMA) sebagai polimer dalam campuran etilena karbonat (EC) dan propilena karbonat (PC) sebagai pelarut pemplastik dengan pelbagai kuantiti magnesium triflate sebagai garam pendopan telah disediakan dengan menggunakan teknik tuangan larutan. Kekonduksian ionik filem GPE ini telah ditentukan menggunakan spektroskopi impedans AC. Filem yang mengandungi 20 wt% garam magnesium triflate menunjukkan kekonduksian yang tertinggi pada suhu bilik ialah $1.27 \times 10^{-3} \text{ S cm}^{-1}$. Kajian kekonduksian-suhu filem-filem GPE mengikut tingkah laku Arrhenius dengan tenaga pengaktifan dalam julat 0.18-0.26 eV. Bilangan pengangkutan ion magnesium dalam filem GPE telah dinilai menggunakan gabungan spektroskopi impedans AC dan polarisasi teknik DC. Kajian Spektroskopi inframerah transformasi Fourier (FTIR) pula mengesahkan peningkatan dalam kekonduksian adalah disebabkan oleh peningkatan ion-ion bebas dan pengurangan ion agregat. Peningkatan dan penurunan dalam bilangan ion bebas juga boleh dilihat daripada plot pemalar dielektrik, ϵ_r - frekuensi. Kajian Terma menunjukkan bahawa filem GPE adalah stabil pada julat suhu yang luas iaitu $30^\circ\text{C} - 130^\circ\text{C}$. Kajian XRD dan FESEM menunjukkan bahawa peningkatan rantau amorfus pada filem-filem GPE membawa kepada kekonduksian yang lebih tinggi pada filem-filem tersebut. Kestabilan elektrokimia filem GPE telah diuji dengan menggunakan kaedah voltammetri sapu linear (LSV). Kajian yang berdasarkan AC impedans dan voltammetri berkitar (CV) mengesahkan pengkonduksian ion Mg^{2+} dalam filem GPE. Filem GPE dengan kekonduksian tertinggi telah digunakan sebagai elektrolit dalam sel Mg|GPE|MnO_2 . Filem GPE merupakan pengganti yang sangat baik bagi elektrolit cecair dalam bateri magnesium boleh dicas semula.

ACKNOWLEDGEMENTS

In the name of Allah, the Almighty Lord, the Most Gracious and the Most Merciful. Praise be to Allah who has given me the strength and inspirations for establishing me to complete my dissertation successfully. Peace be upon His messenger Muhammad and his honourable family.

I wish to express the deepest appreciation to my supervisor, Associate Professor Dr. Zurina Osman for her constant encouragement. I am extremely grateful and indebted to her for her expert, patience, support, understanding and valuable guidance extended to me throughout the project. I would also like to acknowledge Physics department and University of Malaya for providing me financial support and laboratory facilities.

I am particularly grateful for the assistance given by my lab mates, especially my seniors, Lisani Othman and Khairul Bahiyah Md. Isa. My special thanks are extended to Siti Mariam Samin and Chong Woon Gie for their willing to help and sharing the ideas during the experimental works. Thanks also to the technicians and laboratory assistance that helped me in handling the instruments and for the technical support rendered.

Most of all, I take this opportunity to record sincerely thanks to my beloved family and friends for their prayers and unceasing encouragement. They were always supporting me both on and off water by not letting me give up with their best wishes. Last but not certainly least, my sense of gratitude to all the individuals who directly or indirectly have lent their helping hand during the preparation of this dissertation.

CONTENTS

CONTENTS	PAGE
Declaration	ii
Abstract	iii
Abstrak	iv
Acknowledgements	v
Contents	vi
List of Figures	x
List of Tables	xv
List of Published and Presented Papers	xvi
CHAPTER 1 : INTRODUCTION	
1.1 Introduction to the Present Work	1
1.2 Objectives of the Present Work	3
1.3 Organization of the Dissertation	4
CHAPTER 2 : LITERATURE REVIEW	
2.1 Polymer	
2.1.1 <i>Polymerization</i>	9
2.1.2 <i>Polymer properties</i>	10
2.1.3 <i>Polymer Characterization</i>	12
2.2 Polymer electrolytes	
2.2.1 <i>Liquid Polymer Electrolytes</i>	14
2.2.2 <i>Solid Polymer Electrolytes</i>	14
2.2.3 <i>Gel Polymer Electrolytes</i>	15

2.3	Poly(methylmethacrylate) – PMMA	16
2.4	Salts	17
2.5	Plasticizers / Plasticizing Solvent	19
2.6	Complexation of Polymer Salt – based Gel Polymer Electrolytes	21
2.7	Applications	
2.7.1	<i>Batteries</i>	22
2.7.2	<i>Fuel cells</i>	23
2.7.3	<i>Electrochromic Devices</i>	24
CHAPTER 3 : EXPERIMENTAL TECHNIQUES		
3.1	Sample preparation	26
3.2	Electrochemical Impedance Spectroscopy (EIS)	
3.2.1	<i>A.C Impedance Theory</i>	30
3.2.2	<i>Conductivity measurements</i>	32
3.2.3	<i>Dielectric properties</i>	33
3.3	Transference number measurements	34
3.4	Fourier Transform Infra-Red Spectroscopy (FTIR)	36
3.5	X-Ray Diffraction (XRD)	41
3.6	Field Emission Scanning Electron Microscopy (FESEM)	44
3.7	Differential Scanning Calorimetry (DSC)	48
3.8	Linear Sweep Voltammetry (LSV)	50
3.9	Cyclic Voltammetry (CV)	52
3.10	Battery Performance and Characteristics	53

CHAPTER 4 : RESULTS AND DISCUSSION

4.1 Electrical Studies

Impedance Spectroscopy (IS) Analysis

4.1.1 Room temperature conductivity studies

4.1.1.1 *PMMA – EC - PC system* 55

4.1.1.2 *PMMA – EC – PC – Mg(CF₃SO₃)₂ system* 56

4.1.2 Conductivity-temperature dependence studies

4.1.2.1 *PMMA – EC – PC – Mg(CF₃SO₃)₂ system* 59

4.2 Dielectric Studies 62

4.3 Transport Number Studies

4.3.1 *Ionic Transport Number* 68

4.3.2 *Transport Number of Mg²⁺ ions* 69

Structural Studies

4.4 Fourier Transform Infra-Red (FTIR) Analysis

4.4.1 *Pure PMMA film* 72

4.4.2 *Pure Mg(CF₃SO₃)₂ film* 74

4.4.3 *PMMA – EC – PC system* 77

4.4.4 *PMMA – EC – PC – Mg(CF₃SO₃)₂ system* 80

4.5 X-Ray Diffraction (XRD) Analysis

4.5.1 *Pure PMMA film* 87

4.5.2 *PMMA – EC – PC system* 88

4.5.3 *Pure Mg(CF₃SO₃)₂ film* 89

4.5.4 *PMMA – EC – PC – Mg(CF₃SO₃)₂ system* 91

Morphological Studies

4.6 Field Emission Scanning Electron Microscopy (FESEM)

Analysis

4.6.1	<i>Pure PMMA film</i>	92
4.6.2	<i>Pure Mg(CF₃SO₃)₂ film</i>	93
4.6.3	<i>PMMA – EC – PC system</i>	94
4.6.4	<i>PMMA – EC – PC – Mg(CF₃SO₃)₂ system</i>	95

Thermal Studies

4.7 Differential Scanning Calorimetry (DSC) Studies

4.7.1	<i>Pure PMMA film</i>	99
4.7.2	<i>PMMA – EC – PC system</i>	100
4.7.3	<i>PMMA – EC – PC – Mg(CF₃SO₃)₂ system</i>	102

Electrochemical Studies

4.8 Electroanalytical Techniques Analysis

4.8.1	<i>Linear Sweep Voltammetry (LSV)</i>	107
4.8.2	<i>Cyclic Voltammetry (CV)</i>	108

4.9 Battery Performance / Characteristics 111

CHAPTER 5 : DISCUSSION, CONCLUSION AND SUGGESTIONS FOR FUTURE WORK 115

REFERENCES 120

LIST OF FIGURES	PAGE	
Figure 2.1	Schematic representations of (a) a linear polymer (b) a branched polymer, and (c) a network or crosslinked polymer	7
Figure 2.2	Structures of the repeating units of some common polymers	7
Figure 2.3	Glass transition temperature diagram	10
Figure 2.4	The chemical structure of PMMA	16
Figure 2.5	The chemical structure of a) magnesium triflate and b) lithium triflate	17
Figure 2.6	The chemical and molecular structure of ethylene carbonate (EC)	20
Figure 2.7	The chemical and molecular structure of propylene carbonate (PC)	20
Figure 2.8	Schematic diagram of rechargeable polymer ion battery	23
Figure 2.9	Schematic diagram of fuel cell	24
Figure 2.10	Schematic diagram of Electrochromic Devices	25
Figure 3.1	Gel Polymer Electrolyte containing $\text{Mg}(\text{CF}_3\text{SO}_3)_2$ salt	27
Figure 3.2	The complex impedance plot	30
Figure 3.3	Cole-Cole or Nyquist plot	31
Figure 3.4	Basic diagram of FTIR Spectrometer	36
Figure 3.5	Schematic diagram of FTIR spectrometry	38
Figure 3.6	The sample analysis process	39
Figure 3.7	Vibrational modes	40
Figure 3.8	Instrumentation of FTIR measurement	41

Figure 3.9	Schematic diagram of X-Ray diffraction (XRD)	42
Figure 3.10	Bragg's Law reflection. The diffracted x-rays exhibit constructive interference when the distance between paths ABC and A'B'C' differs by an integer number of wavelengths (λ)	43
Figure 3.11	Instrumentation of XRD measurement	44
Figure 3.12	Principal features of an optical microscope, a transmission electron microscope and a scanning electron microscope, drawn to emphasize the similarities of overall design	45
Figure 3.13	The schematic diagram of SEM experiment	46
Figure 3.14	Instrumentation of FESEM	47
Figure 3.15	Typical DSC thermogram	48
Figure 3.16	Instrumentation of DSC measurement	50
Figure 3.17	linear sweep voltammograms as the change of the rate constant	51
Figure 3.18	Cyclic voltammogram (CV)	52
Figure 4.1	Cole-Cole plot for the PMMA-EC-PC film	56
Figure 4.2	Conductivity (σ) of GPE films as a function of $\text{Mg}(\text{CF}_3\text{SO}_3)_2$ salt concentration	58
Figure 4.3	Temperature dependence of ionic conductivity of PMMA-EC-PC- $\text{Mg}(\text{CF}_3\text{SO}_3)_2$ gel polymer electrolyte films for the films containing (a) 5wt.%, (b) 30wt.% and (c) 20wt.% of $\text{Mg}(\text{CF}_3\text{SO}_3)_2$ salt	60
Figure 4.4	Dielectric constant versus frequency for all the films in PMMA-EC-PC- $\text{Mg}(\text{CF}_3\text{SO}_3)_2$ system	63
Figure 4.5	Dielectric loss versus frequency for all the films in PMMA-EC-PC- $\text{Mg}(\text{CF}_3\text{SO}_3)_2$ system	63
Figure 4.6	Real part of electrical modulus versus frequency for various concentrations of $\text{Mg}(\text{CF}_3\text{SO}_3)_2$ salt in PMMA-EC-PC- $\text{Mg}(\text{CF}_3\text{SO}_3)_2$ system	64

Figure 4.7	Loss tangent versus frequency for various concentrations of $\text{Mg}(\text{CF}_3\text{SO}_3)_2$ salt in PMMA-EC-PC- $\text{Mg}(\text{CF}_3\text{SO}_3)_2$ system	64
Figure 4.8	Loss tangent versus frequency for various concentrations of salt for film in the PMMA-EC-PC- $\text{Mg}(\text{CF}_3\text{SO}_3)_2$ system	66
Figure 4.9	The variation of conductivity and relaxation time with amounts of $\text{Mg}(\text{CF}_3\text{SO}_3)_2$ salt in PMMA-EC-PC- $\text{Mg}(\text{CF}_3\text{SO}_3)_2$ system	66
Figure 4.10	Variation of dielectric constant of optimized GPE film as a function of frequencies at various temperatures	67
Figure 4.11	Variation of dielectric loss of optimized GPE film as a function of frequencies at various temperatures	67
Figure 4.12	Normalized current versus time plots for GPE films containing (a) 5wt%, (b) 20wt%, and (c) 30wt% of $\text{Mg}(\text{CF}_3\text{SO}_3)_2$ salt	68
Figure 4.13	A.C complex impedance plot before and after DC polarization of a typical symmetric Mg GPE Mg cell	70
Figure 4.14	Polarization current plot as a function of time for the highest conducting film in PMMA-EC-PC- $\text{Mg}(\text{CF}_3\text{SO}_3)_2$ system with Mg GPE Mg cell	71
Figure 4.15	FTIR spectra of pure PMMA film in the region 650 cm^{-1} and 3000 cm^{-1}	73
Figure 4.16	FTIR spectrum of pure $\text{Mg}(\text{CF}_3\text{SO}_3)_2$ salt in the range of 700 cm^{-1} and 1600 cm^{-1}	76
Figure 4.17	FTIR spectra of (a) pure PC and (b) pure EC in the range of 1000 cm^{-1} and 2000 cm^{-1}	77
Figure 4.18	The FTIR spectrum of PMMA-EC-PC film in the range of 1000 cm^{-1} and 2000 cm^{-1}	79
Figure 4.19	FTIR spectra of pure PMMA, pure $\text{Mg}(\text{CF}_3\text{SO}_3)_2$ and PMMA based GPE films with 5 wt% to 30 wt% of $\text{Mg}(\text{CF}_3\text{SO}_3)_2$	82
Figure 4.20	FTIR spectra of pure PMMA, pure $\text{Mg}(\text{CF}_3\text{SO}_3)_2$ and PMMA based GPE films with 5 wt% to 30 wt% of	83

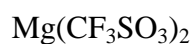


Figure 4.21	FTIR spectra of pure PMMA, pure $\text{Mg}(\text{CF}_3\text{SO}_3)_2$ and PMMA based GPE films with 5 wt% to 30 wt% of $\text{Mg}(\text{CF}_3\text{SO}_3)_2$	84
Figure 4.22	FTIR spectra of pure PMMA, pure $\text{Mg}(\text{CF}_3\text{SO}_3)_2$ and PMMA based GPE films with 5 wt% to 30 wt% of $\text{Mg}(\text{CF}_3\text{SO}_3)_2$	85
Figure 4.23	Deconvolution part for all the GPE films containing (i) free ions, (ii) ions pair and (iii) ions aggregates in the range of 1000 cm^{-1} to 1100 cm^{-1}	86
Figure 4.24	X-ray diffractogram of pure PMMA film	87
Figure 4.25	X-ray diffractogram of pure EC	88
Figure 4.26	X-ray diffractogram of PMMA-EC-PC film	89
Figure 4.27	X-ray diffractogram of pure PMMA and PMMA-EC-PC films	89
Figure 4.28	X-ray diffractogram of $\text{Mg}(\text{CF}_3\text{SO}_3)_2$ salt	90
Figure 4.29	X-ray diffractogram of PMMA-EC-PC film and GPE film containing 5 wt%, 20 wt% and 30 wt% of $\text{Mg}(\text{CF}_3\text{SO}_3)_2$	91
Figure 4.30	FESEM micrograph of pure PMMA film	93
Figure 4.31	FESEM micrograph of pure $\text{Mg}(\text{CF}_3\text{SO}_3)_2$	94
Figure 4.32	FESEM micrograph of PMMA-EC-PC film	95
Figure 4.33	FESEM micrograph for GPE film containing 5 wt.% of $\text{Mg}(\text{CF}_3\text{SO}_3)_2$ salt	96
Figure 4.34	FESEM micrograph for GPE film containing 20 wt.% of $\text{Mg}(\text{CF}_3\text{SO}_3)_2$ salt	97
Figure 4.35	FESEM micrograph for GPE film containing 30 wt.% of $\text{Mg}(\text{CF}_3\text{SO}_3)_2$ salt	97
Figure 4.36	DSC thermogram of pure PMMA film	99
Figure 4.37	DSC thermogram of PMMA-EC-PC film	100

Figure 4.38	DSC thermogram of GPE film containing 5 wt% of Mg(CF ₃ SO ₃) ₂ salt	102
Figure 4.39	DSC thermogram of GPE film containing 10 wt% of Mg(CF ₃ SO ₃) ₂ salt	102
Figure 4.40	DSC thermogram of GPE film containing 15 wt% of Mg(CF ₃ SO ₃) ₂ salt	103
Figure 4.41	DSC thermogram of GPE film containing 20 wt% of Mg(CF ₃ SO ₃) ₂ salt	103
Figure 4.42	DSC thermogram of GPE film containing 25 wt% of Mg(CF ₃ SO ₃) ₂ salt	104
Figure 4.43	DSC thermogram of GPE film containing 30 wt% of Mg(CF ₃ SO ₃) ₂ salt	104
Figure 4.44	Linear sweep voltammogram of SS GPE Mg cell for GPE containing 20 wt.% of Mg(CF ₃ SO ₃) ₂ salt at scan rate of 5 mV s ⁻¹	107
Figure 4.45	Complex impedance plots for Cell-I: SS GPE SS and Cell-II: Mg GPE Mg at room temperature	110
Figure 4.46	Cyclic voltammogram of cell-I: SS GPE SS with 20 wt.% of Mg(CF ₃ SO ₃) ₂ salt at scan rate of 5 mV s ⁻¹	110
Figure 4.47	Cyclic voltammogram of cell-II: Mg GPE Mg with 20 wt.% of Mg(CF ₃ SO ₃) ₂ salt at scan rate of 5 mV s ⁻¹	111
Figure 4.48	Charge-discharge cycles as a function of time of Mg GPE MnO ₂ cell.	113
Figure 4.49	Discharge curves against specific capacity of Mg GPE MnO ₂ cell with constant current of 0.2 mA.	114

LIST OF TABLES**PAGE**

Table 4.1	Constituents of the prepared GPE films in PMMA-EC-PC-Mg(CF ₃ SO ₃) ₂ system	57
Table 4.2	Conductivity and activation energy values of GPE films using various types of polymer host and magnesium salt	61
Table 4.3	The vibrational modes and wavenumbers of pure PMMA film	74
Table 4.4	The vibrational modes and wavenumbers of pure Mg(CF ₃ SO ₃) ₂ salt	75
Table 4.5	T _g and T _m values for pure PMMA, PMMA-EC-PC and PMMA-EC-PC- Mg(CF ₃ SO ₃) ₂ GPE films	105
Table 5.1	The ionic conductivity for the GPE films from PMMA-EC-PC-Mg(CF ₃ SO ₃) ₂ system.	116

LIST OF PUBLISHED AND PRESENTED PAPERS

1. **N.H. Zainol**, Z. Osman, L. Othman and K.B. Md. Isa, “Transport, Structural and Morphological Properties of Gel Polymer Electrolytes containing $\text{Mg}(\text{CF}_3\text{SO}_3)_2$ ” – Advanced Material Research 686.137 (2013).
2. **N. H. Zainol**, S.M. Samin, L. Othman, W.G. Chong, K.B. Md Isa and Z. Osman, “Magnesium-based Gel Polymer Electrolytes: Ionic Transport and Infrared Spectroscopy Studies” International Journal of Electrochemical Science, 8 (2013) 3602-3614.
3. **N.H.Zainol**, Z. Osman and L.Othman, “Studies of Magnesium Ion Conduction in PMMA- based Gel Polymer Electrolytes”. Progress in Polymer Research, Vol. 2 (2013).
4. **N. H. Zainol** and Z. Osman, “Studies of Ionic Transport and Morphological Properties of PMMA-Gel Polymer Electrolytes Containing Magnesium Ions”, presented at International Conference of Young Researchers on Advanced Materials (ICYRAM), 1- 6 July 2012, Biopolis, Singapore.

CHAPTER 1

1.1 Introduction to the Present Work

Nowadays, major research on gel polymer electrolytes (GPEs) has attracted much attention compared to both solid polymer electrolytes (SPEs) and liquid electrolytes in view of its potential application in solid state rechargeable polymer batteries. It is because of the use of a gel polymer electrolyte that makes the fabrication of safe batteries possible and permits the development of thin batteries with design flexibility (Park, Kim, Prakash, & Sun, 2003). GPEs are prepared by incorporating a large quantity of low molecular weight organic solvents or plasticizing solvents to a host polymer matrix that is capable of forming a stable gel (Girish Kumar & Sampath, 2005). The plasticizing solvents such as ethylene carbonate (EC) and propylene carbonate (PC) can be used to improve the polymer electrolyte conductivity due to their high dielectric constant and low viscosity (Pitawala, Dissanayake, & Seneviratne, 2007). Hence, it is expected that the GPEs have high ionic conductivity as well as good dimensional stability. GPEs usually exhibit ionic conductivity ranging from 10^{-4} to 10^{-3} S cm^{-1} at room temperature which is close to the value of commercial liquid electrolyte. SPEs possess good mechanical strength but its conductivity at ambient temperature is lower than GPEs which is in the range of 10^{-5} to 10^{-4} S cm^{-1} (Girish Kumar & Munichandraiah, 2002).

At present, much research effort has been directed towards advanced battery technology based on lithium. Rechargeable lithium-ion batteries have been one of the best choices in view of its specific capacity and cycle stability. However, lithium-ion batteries are relatively expensive and suffered from some safety problems and it requires a high purity argon or helium atmosphere to be handled.

Therefore, magnesium-based systems have attracted interest in electrochemical research and development of solid-state rechargeable batteries due to their electrochemical properties which are close to lithium-based systems (Chusid et al., 2003). Thus, magnesium is a promising candidate since it possesses a number of important characteristics such as free from hazards, high stability with highly negative standard potential (-2.375V versus SHE), relatively low equivalent weight (12g per Faraday), high melting point (649°C), low cost, high safety, ease of handling, and low toxicity which allows for urban waste disposal (Novák, Imhof, & Haas, 1999).

In addition, it is cost effective due to natural abundance and it is safer than lithium. The use of magnesium as a negative electrode in aqueous primary and rechargeable batteries has been reported (Yoshimoto, Yakushiji, Ishikawa, & Morita, 2003). Work on solid-state rechargeable magnesium batteries using gel polymer electrolytes have been investigated by Kumar and Muchandriah (Kumar & Munichandriah, 2000). They claimed that the poly(methyl) methacrylate (PMMA) was chosen as a polymer host in the development of a gel polymer electrolyte since it can give high ionic conductivity at room temperature and a good solvent retention ability.

In this work, we report the preparation of GPE films comprising of PMMA, EC, PC and magnesium triflate, $\text{Mg}(\text{CF}_3\text{SO}_3)_2$, with the fixed ratio of polymer and plasticizing solvent. For the purpose of arriving at an appropriate composition, several GPE films were prepared by varying the quantities of $\text{Mg}(\text{CF}_3\text{SO}_3)_2$ ranging from 5wt.% to 30wt.%. Ionic conductivity and transport number of the GPE films will be evaluated using impedance spectroscopy and DC polarization or Wagner's method, respectively.

Structural, morphological, and thermal properties will be investigated using Fourier Transform Infrared Spectroscopy (FTIR), X-Ray Diffraction (XRD), Field Emission Scanning Electron Microscopy (FESEM) and Differential Scanning Calorimetry (DSC) techniques. The electrochemical properties of the GPE films will be studied using linear sweep voltammetry (LSV) and cyclic voltammetry (CV). The highest conducting GPE film will be used as an electrolyte in magnesium battery and its charge-discharge characteristics will be studied.

1.2 Objectives of the Present Work

The main objective of this work is to study the electrical, morphological, thermal and electrochemical properties of poly(methyl)methacrylate (PMMA) – based gel polymer electrolyte films containing magnesium triflate, $\text{Mg}(\text{CF}_3\text{SO}_3)_2$ as an inorganic salt while ethylene carbonate (EC) and propylene carbonate (PC) will act as a plasticizing solvent. In this study, gel polymer electrolyte (GPE) films are prepared by using the solution casting technique. Thus, the specific objectives of this study are:

- 1) To determine the ionic conductivity of GPE films using AC impedance spectroscopy.
- 2) To investigate the effect of salt and plasticizing solvent to the enhancement of conductivity in GPE films. The conductivity-temperature dependence and dielectric properties of the GPE films will also be studied.
- 3) To evaluate the value of ionic transport number that will be carried out using DC polarization method or known as Wagner's method. The transport number of Mg^{2+} ions will also be determined by using the combination of AC and DC methods.

- 4) To study the physical properties of gel polymer electrolyte films including thermal, structural, morphological and electrochemical characteristics.
- 5) To fabricate magnesium batteries using the highest conducting GPE film as an electrolyte and study the performance of the battery.

1.3 Organization of the Dissertation

This report illustrates the study of ionic conductivity, transport number, structural, morphological, thermal and electrochemical properties of PMMA-based gel polymer electrolyte films containing magnesium triflate. The report is organized into five chapters. The first chapter states the background of the research interest and the objectives of the research work including the organization of the report.

Chapter two of this report provides the reviews of polymer electrolytes including the brief explanations on polymer properties and characterization. It also describes the differences between solid, liquid and gel polymer electrolytes. The basic information of polymer, salt and plasticizing solvent used in this work will be presented. The applications of the gel polymer electrolyte will also be discussed in this chapter.

Chapter three reveals the experimental techniques carried out in preparation and characterization of GPE films. The techniques used in this work include impedance spectroscopy, transport number measurements, Fourier Transform Infrared Spectroscopy (FTIR), X-Ray Diffraction (XRD), Field Emission Scanning Electron Microscopy (FESEM), Differential Scanning Calorimetry (DSC), linear sweep voltammetry (LSV) and cyclic voltammetry (CV) will be provided.

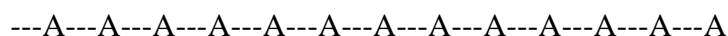
The results and discussion are presented in chapter four. The ionic conductivity, transport number and dielectric properties of gel polymer electrolyte films will be studied. The structural, morphological and thermal studies using FTIR, XRD, FESEM and DSC techniques will be discussed. The electrochemical properties of the highest conducting GPE film will be characterized using electroanalytical techniques, LSV and CV while battery performance will be analyzed through charge-discharge cycles. Finally, chapter five concludes the research work with some suggestions for future work.

CHAPTER 2

2.1 Polymer

Polymer is a large molecules or known as macromolecules that composed by joining repeating structural units. Most of the polymers are linear polymers which is made up of small molecule or called monomer after another and hooked together in a long chain called backbone. The atoms that make up the backbone of the polymer chain come in a regular order and this order repeat itself along the polymer chain. If there is only one type of chemical unit, the corresponding polymer is a homopolymer but if there is more than one type, it is called a copolymer. Copolymers are the most common form of heteropolymers. They are often formed from a sequence of two types of monomer unit. It should be noted that the term monomer or monomer unit is often used to mean either the chemical repeat unit or the small molecule which polymerises to form the polymer.

The simplest polymers are chain-like molecules of the type



where A is a small group of covalent bonded atoms and the groups are covalently linked. The simplest useful polymer is polyethylene



wherein a typical length of chain, n correspond to the order of repeating monomer. The phrase ‘typical length of chain’ was used because the molecules of polymers are not all identical, unlike those of other chemical compounds. Commercial polymers often have average values of molar masses, M between 100 000 and 1 000 000 g mol^{-1} , although lower values are not infrequent.

The real shapes of polymer molecules do not consist of simple linear chains. There are several types of polymer chain and structure as shown in Figure 2.1.

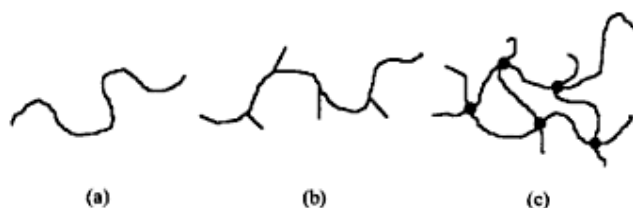


Figure 2.1: Schematic representations of (a) a linear polymer (b) a branched polymer, and (c) a network or crosslinked polymer.

Figure 2.2 shows the structures of repeating units of some common polymers that has been used in preparation of polymer electrolytes. Poly(methylmethacrylate) or PMMA is widely used as a host polymer because of its good transparency that makes it suitable to be used as an electrolyte in rechargeable batteries or electronic devices.

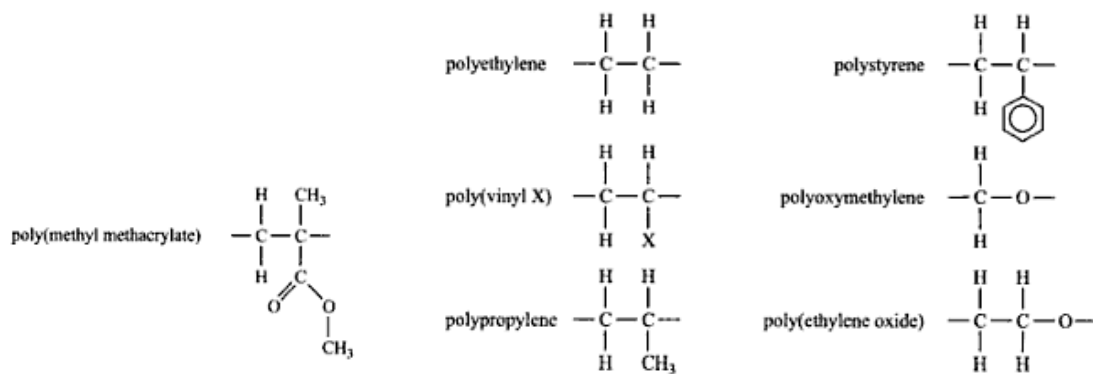


Figure 2.2: Structures of the repeating units of some common polymers.

Types of polymer:

a) Thermoplastics

Thermoplastics form the bulk of polymers in use. They consist of linear or branched molecules and they soften or melt when heated, so that they can be moulded and remoulded by heating. In the molten state, they consist of a tangled mass of molecules and may form a glass or crystallise on cooling below a temperature called the glass transition temperature, T_g . If they crystallize they do so only partially, the rest remaining in a liquid-like state which is usually called amorphous or non-crystalline.

b) Rubbers or elastomers

Rubbers or elastomers, are network polymers that are lightly cross-linked and they are reversibly stretchable to high extensions. When unstretched they have fairly tightly randomly coiled molecules that are stretched out when the polymer is stretched. This causes the chains to be less random, so that the material has lower entropy, and the retractive force observed is due to this lowering of the entropy. Rubbers become glassy or crystallize (partially) on cooling and cannot melt when the temperature increases because the cross-links prevent the molecules from flowing past each other.

c) Thermosets

Thermosets are network polymers that are heavily cross-linked to give a dense three-dimensional network. They are normally rigid and cannot melt on heating and also may decompose if the temperature is high enough. Example of thermoset is the epoxy resins such as Araldites.

2.1.1 Polymerization

The process that converts a monomer to a polymer is called polymerization. Converting monomer to long polymer chain is the final step in the polymer manufacturing sequence. Some hundreds of monomer molecules are combined to form a polymer that has strong physical properties such as elasticity, highly tensile strength or the ability to form fibers. Polymerization is usually highly favourable in thermodynamic terms, mainly on energetic grounds because ordering molecules into linked chains is a process where the entropy is decreased. There are two types of polymerization process, which is step-growth and chain-growth polymerization.

Step-growth polymers are obtained by the repeated process of joining together smaller molecules, which are usually of two different kinds at the beginning of the polymerization process. It is formed by stepwise reaction between functional groups of monomers. Most of them are classified as condensation polymers but not all step-growth polymers release condensates. They increase in molecular weight at lower conversions and moderately higher molecular weight only at high conversion.

Chain-growth polymerization involves several consecutive stages which is initiation, propagation, and termination. Each chain is individually initiated and grows very rapidly to a high molar mass until its growth is terminated. Chain-growth polymerization leads to living polymerization. Other forms of chain growth polymerization include cationic addition and anionic addition which are not used to a large extent but are ideally suited for living polymerizations. All polymerizations are exothermic (heat is liberated due to bond formation) and the heat must be conducted away to maintain a uniform reaction temperature.

2.1.2 Polymer properties

Properties of polymer are basically divided into several classes which are structural properties, physical properties and mechanical properties. Structural properties play a major role in determining bulk physical properties of the polymer, which describe how the polymer behaves as a continuous macroscopic material. The physical properties of polymer are strongly dependent on the size or length of the polymer chain. Increasing chain length furthermore tends to decrease chain mobility, increase strength and toughness and increase the glass transition temperature, (T_g).

2.1.2.1 Glass transition temperature (T_g)

The temperature at which the polymer experiences the transition from rubbery to rigid state is called glass transition temperature, as shown in Figure 2.3. The glass transition is a property of only the amorphous portion of a semi-crystalline solid. The crystalline portion remains crystalline during glass transition. At low temperature, the amorphous regions of a polymer are in the glassy state where it generally will be hard, rigid, and brittle. As the temperature rises above T_g , the polymer becomes more rubber-like. Thus, knowledge of T_g is essential in the selection of materials for various applications.

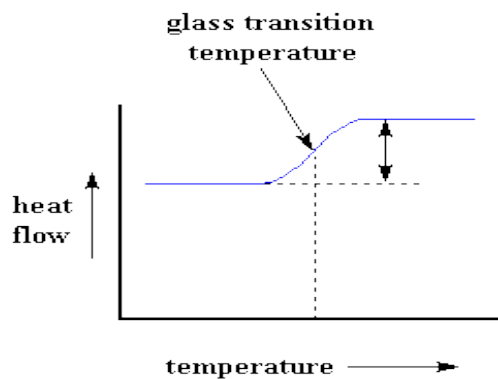


Figure 2.3: Glass transition temperature diagram

2.1.2.2 Crystallinity

The crystallinity of polymers is characterized by their degree of crystallinity, ranging from zero for a completely non-crystalline polymer to one for a theoretical completely crystalline polymer. The degree of crystallinity may be expressed in terms of a weight fraction or volume fraction of crystalline material. Polymers with a degree of crystallinity approaching zero or one will tend to be transparent, while polymers with intermediate degrees of crystallinity will tend to be opaque due to light scattering by crystalline or glassy regions. Thus, transparency of the polymers can be increased by reducing the degree of crystallinity.

2.1.2.3 Tensile strength

A major test of the mechanical behavior of polymers, especially those plastics below their glass transition temperature, involves the measurement of tensile strength. Tensile strength refers to how much stress a sample can withstand before failing while being stretched. It is measured by stretching a polymer under constant force and measuring how much it stretches before it fails. Tensile modulus, which is a measure of tensile stress, can then be calculated by the ratio of stress to strain. Where stress is the ratio of Force to cross sectional area of the polymer and strain is the ratio of change in the length before failing to the original length of the polymer. In general, tensile strength increases with polymer chain length and crosslinking of polymer chains. Tensile strength is important to many applications of polymers, it allows a material to flex and bend without breaking thus making the material reliable.

2.1.2.4 Transport properties

Transport properties are important in many applications of polymers for films and membranes. It will reveal how fast molecules move through the polymer matrix and electric current produced is generally caused by the transport of charge carriers. Electrons only can flow in metals, whereas solutions of electrolytes exhibit only ion conduction. In an electrolytic solution, cations and anions both contribute to charge transport in an electric field. The contribution of one ionic species to the total current is called the transport number and it holds only for examined total electrolytes, because they depend on the mobility of the counter-ion.

2.1.3 Characterization of Polymer Electrolytes

There are several techniques used to characterize the properties of polymer electrolytes. Impedance spectroscopy is a useful technique to determine the ionic conductivity and dielectric properties of the polymer electrolytes. Transport properties were characterized using transport number measurements in order to confirm the charge carrier of the polymer electrolytes is either ionic or electronic. Techniques such as X-Ray diffraction and FTIR are used to determine the crystalline structure and the composition of the polymers, respectively. Surface morphology of the polymer electrolytes can be studied by using SEM/FESEM technique. The thermal properties such as the glass transition temperature and melting point can be determined by Differential Scanning Calorimetry (DSC). Electrochemical properties and battery performance of highest conducting GPE film can be investigated using linear sweep voltammetry (LSV), Cyclic Voltammetry (CV) and charge-discharge cycles.

2.2 Polymer Electrolytes

Polymer electrolytes are ionic conductors which provides medium for charge transfer through ions inside the cell between anode and cathode. It intended for many applications in various electrochemical devices. Good electrolyte must have high ionic conductivity, not electronically conductive because it would cause internal short-circuiting, non reactivity with electrode materials, safety in handling and low cost materials. An ideal electrolyte for electrochemical devices should be able to completely dissolve and dissociate in the nonaqueous media, and the solvated ions should be able to travel in the media with high mobility (Ahmad, 2009). It also should meet the following criteria with respect to its anionic part:

- a) The anion should be stable against oxidative decomposition at the cathode.
- b) The anion should be inert to electrolyte solvents.
- c) The anion should be nontoxic and remains stable against thermally induced reactions with electrolyte solvents and other cell components.
- d) Both anion and cation should remain inert toward the other cell components such as separator, electrode substrate, and cell packaging materials.

There are three types of polymer electrolytes that have been studied until nowadays which is liquid polymer electrolytes, solid polymer electrolytes, and gel polymer electrolytes.

2.2.1 Liquid Polymer Electrolytes

Liquid polymer electrolyte is formed by the dissolution of the polymer electrolyte in the proper solvent. Liquid electrolytes are comprised entirely ions and are liquid at room temperature. Its offer the potential advantages such as low vapour pressure, high ionic conductivity, greater thermal and electrochemical stability. The use of liquid polymer electrolytes for enhancement of ionic conductivity has been reported. Despite its have high conductivity, solid polymer electrolytes (SPEs) are more preferred in battery industries because liquid electrolytes have leaking problem and have poorer fabrication properties.

2.2.2 Solid Polymer Electrolytes

During last three decades, little progress was made concerning the actual application of solid polymer electrolyte (SPEs) as practical materials for applied electrochemistry, has been proposed by Armand (Armand, 1994) The suggestion of Armand et al. was mainly brought by the following advantages of these polymer electrolytes i.e good mechanical strength and high dimensional stability, no leakage, easy processing, low self-discharge and high energy density. On the basis of a general survey of the most SPE systems so far, ionic conductivity seems to be $\sim 10^{-4} \text{ S cm}^{-1}$ at room temperature for any polymer host whose mechanical strength could afford the formation of a free standing film (Song, Wang, & Wan, 1999). Wright and coworkers (Payne & Wright, 1982) were the first to discover that the PEO-based solid polymer electrolyte was able to dissolve inorganic salts and exhibit ion conduction at room temperature. Although the ionic conductivity is poor, SPEs remain the materials of material scientist interest for their applications while gel polymer electrolytes (GPEs) have shown much higher feasibility.

2.2.3 Gel Polymer Electrolytes

Gel polymer electrolytes (GPEs) are alternatives to both solid polymer electrolytes (SPEs) and liquid electrolytes for battery applications. A liquid electrolyte has very high conductivity, but it also bears the high risk of leakage and can cause corrosion during packaging. SPE conversely, poses no problem with leakage or packaging, but possesses only low conductivity. In order to overcome the problems related to liquid and solid polymer electrolytes while also maintaining high ionic conductivity as well as good mechanical strength, GPEs have been proposed. GPE essentially contains a liquid electrolyte that retained in a polymer matrix. Its have important advantages over liquid electrolytes such as the risk of leakage is reduced and electrode-electrolyte interfacial contact can be maintained during charge and discharge cycles of the batteries. In particular, PMMA-based gel polymer electrolytes have been found to be most preferred potential candidates as electrolytes in electrochromic windows due to their high transparency as well as good gelatinizing and solvent retention ability (Deepa, Agnihotry, Gupta, & Chandra, 2004). Scrosati et al. (Appetecchi, Croce, & Scrosati, 1995) have been established that PMMA-based GPEs are able to induce a more favorable surface.

2.3 Poly(methylmethacrylate) – PMMA

PMMA is one of the potential polymers that are widely used for making membranes due to its good solvent retention stability. PMMA is a transparent polymeric material that possesses many desirable properties such as light weight, colorless, high light transmittance, chemical resistance, resistance to weathering corrosion and good insulating properties. PMMA is an uncrystallized polymer which has an amorphous morphology and glass transition temperature at 125°C. The general chemical structure of PMMA is shown in Figure 2.4 below.

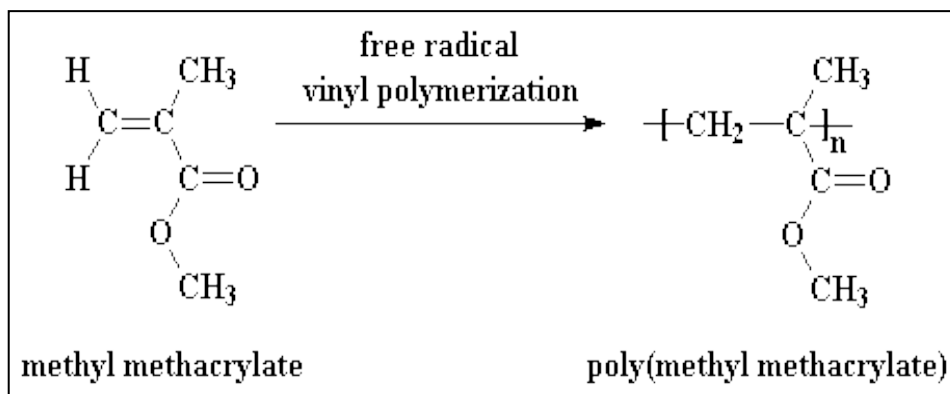


Figure 2.4: The chemical structure of PMMA

Almost all PMMA resins are copolymers made from the mixtures of monomer with acrylics as the main component. PMMA has a polar functional group so as to exhibit a high affinity for both lithium ions and plasticizing organic solvents. This feature allows the PMMA-based gel electrolytes to have high ionic conductivity even at ambient temperature.

2.4 Ionic Salts

Salts are ionic compounds consisting of cations (positively charge ions) and anions (negative ions) that result from the neutralization of an acid and a base. It can be either inorganic such as chloride, or organic such as acetate and monoatomic ions such as fluoride as well as polyatomic ions such as sulfate. Salts having low lattice energies are generally expected to promote greater dissociation of the salt, thus providing higher conducting of ions. Recently, inorganic salts such as lithium triflate and magnesium triflate are widely being studied in polymer-based gel electrolytes. Figure 2.5 shows the chemical structure of magnesium triflate and lithium triflate.

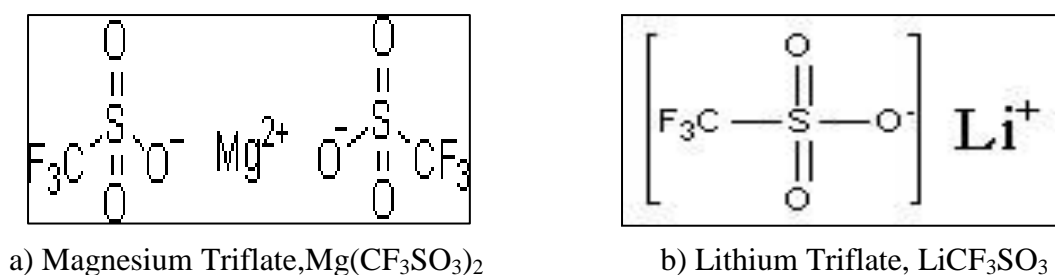


Figure 2.5: The chemical structure of a) magnesium triflate and b) lithium triflate

2.4.1 Magnesium salt versus Lithium salt

Most of the works on polymer electrolytes are focusing on lithium ion conducting gel polymer electrolytes which is due to their use as electrolytes in high energy density lithium batteries (Scrosati, 2000). Since the first report of high conductivity in lithium ion conducting gel polymer electrolytes (Feuillade & Perche, 1975), these materials are receiving much attention due to some of their unique properties like ease of preparation, wide range of composition and hence wider control of properties, good adhesive properties suitable for lamination and have good thermal/electrochemical stability (Sekhon, 2003).

Although exploratory research has been made on monovalent salt systems like Li^+ , little attention has been given to the polymer electrolytes in which multivalent cations are the mobile species. In view of negligible hazards and enhanced safety, studies on magnesium ion conducting gel polymer electrolyte are expected to have wide scope in future (Oh, Ko, & Kim, 2004). Magnesium is positioned next to lithium in the electrochemical series and its electrochemical performance characteristics are also attractive next to lithium. The ionic radii of Li^+ and Mg^{2+} are comparable in magnitude; hence it is possible to replace Li^+ ions with Mg^{2+} ions as the charge carrier in gel polymer electrolytes. Nevertheless, it is worthy to note that the magnesium is more stable and less reactive towards oxygen and water in comparison with lithium, which requires a high purity argon or helium atmosphere. Therefore safety problems associated with magnesium metal are minimal since it can be handled safely in open air. Besides that, natural resources of the magnesium are plentiful and thus, it is much cheaper than lithium. Owing to these merits, investigations on electrochemistry of magnesium-based rechargeable battery systems are significantly important.

2.4 Plasticizing solvent

Plasticizing solvent is a substance, usually a liquid that acts as dissolving agent or an additive to reduce the viscosity of the electrolyte. Low molecular weight organic nonaqueous solvent or known as plasticizing solvent such as ethylene carbonate (EC) and propylene carbonate (PC) is added in order to enhance the conductivity by facilitates the movement of the ionic charge carriers along the polymer backbone. An ideal plasticizing solvent should meet the following criteria:

- a) It must be able to dissolve salts to sufficient concentration, i.e., it should have a high dielectric constant, ϵ .
- b) It should have low viscosity, so that facile ion transport can occur.
- c) It should remain liquid in a wide temperature range, i.e., it must have low melting point (T_m) and high boiling point (T_b).
- d) It should be a good ionic conductor and electronic conductor so that self-discharge can be minimized.
- e) It should has a wide electrochemical window so that electrolyte degradation would not occur within the range of the working potentials of the electrodes.
- f) It should be inert to other cell components such as cell separators, electrode substrates and cell packaging materials.
- g) It should be robust against electrical, mechanical, or thermal abuses.
- h) It should also be safe (low vapour pressure), nontoxic, economical and environmental friendly.

The main function of plasticizing solvent in the polymer electrolyte is to decrease the glass transition, T_g of the polymer and dissolving the crystallite of the polymer. Ethylene carbonate (EC) has been considered as an electrolyte solvent due to its high dielectric constant ($\epsilon = 89.78$) and low viscosity which would help ion conductivity. Compared to EC, propylene carbonate (PC) has certainly attracted attention as a favored solvent since it also have high dielectric constant with low melting point, T_m and high boiling point, T_b . As a matter of fact, many commercially available electrolytes are thus based on the mixture of EC and PC (Ahmad, 2009). Figure 2.6 and Figure 2.7 show the chemical and molecular structure of the plasticizing solvent used in this research work.

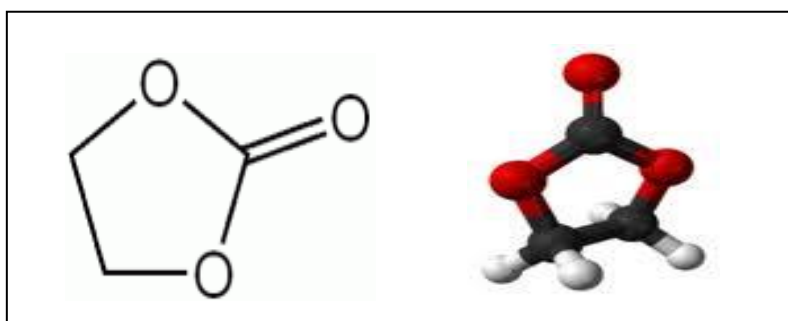


Figure 2.6: The chemical and molecular structure of ethylene carbonate (EC)

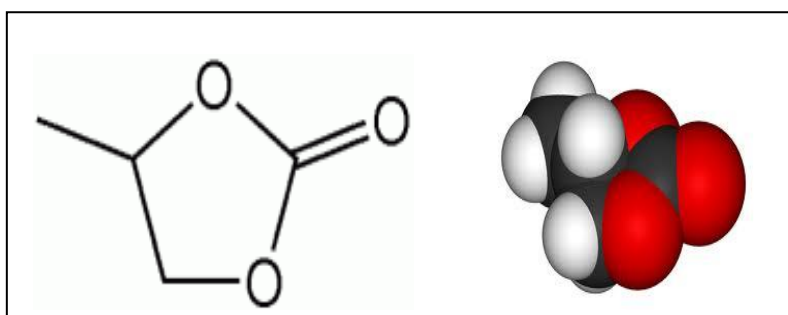


Figure 2.7: The chemical and molecular structure of propylene carbonate (PC)

2.6 Complexation of Polymer Salt- based Gel Polymer Electrolytes

In gel polymer electrolytes (GPEs), the salt generally provides free/mobile ions which take part in the conduction process and the solvent helps in solvating the salt and also acts as a conducting medium whereas the polymer is reported to provide mechanical stability by increasing the viscosity of electrolyte (Agnihotry, Pradeep, & Sekhon, 1999). The salt used should generally have large anions and low dissociation energy so that it easily dissociates. The plasticizing solvent used should have high dielectric constant, low viscosity, high boiling point and low melting point in order to prevent ion aggregation and increase the number of charge carriers thereby enhancing the ionic conductivity of GPEs.

In this research work, PMMA has been used as a polymer host with the mixtures of EC and PC as a plasticizing solvent while $\text{Mg}(\text{CF}_3\text{SO}_3)_2$ will act as the source of magnesium ions. The structural properties of the GPE films will be characterized using Fourier Transform Infrared Spectroscopy (FTIR) and X-Ray Diffraction (XRD) techniques. The complexation in the GPE films will be confirmed and discussed in Chapter 4.

2.7 Applications of GPE films

Polymer electrolytes are an important component of many electrochemical devices such as high performance batteries, fuel and electrolysis cells and electrochromic devices. These devices are of tremendous practical interest in view of our energy and environment needs.

2.7.1 Batteries

Battery is a device that converts the chemical energy contained in its active materials directly into electric energy by means of an electrochemical oxidation-reduction (redox) reaction. For rechargeable system, the battery is recharged by a reversal of the process. This type of reaction involves the transfer of electrons from anode to cathode through an electric circuit. A battery consisted of one or more cell, connected in series or parallel or both, depending on the desired output voltage and capacity (David Linden, 2001). Figure 2.8 shows the schematic diagram of rechargeable polymer ion battery. Three major components are:

- 1) Anode or negative electrode (the reducing electrode) - which gives up electrons to the external circuit and is oxidized during the electrochemical reaction.
- 2) Cathode or positive electrode (the oxidizing electrode) - which accepts electrons from the external circuit and is reduced during the electrochemical reaction.
- 3) Electrolyte (the ionic conductor) – which provides the medium for transfer of charge, as ions, inside the cell between anode and cathode. The electrolyte must has good ionic conductivity but not be electronically conductive, as this would cause internal short-circuiting.

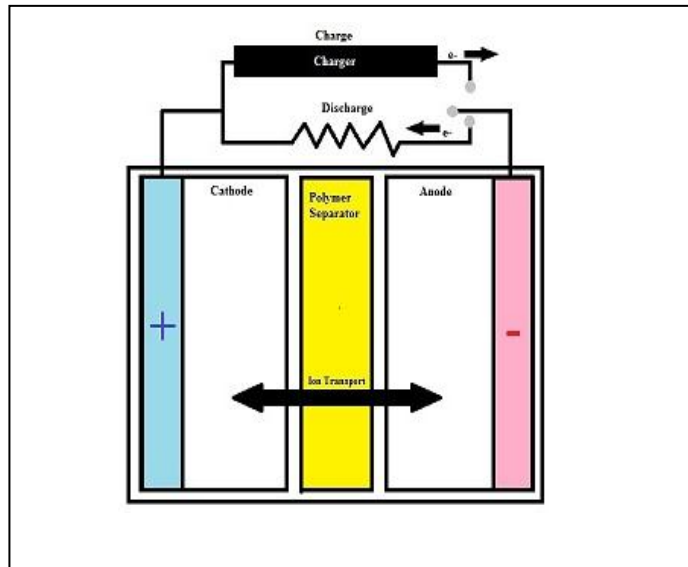


Figure 2.8: Schematic diagram of rechargeable polymer ion battery (battery_diagram, 2012)

2.7.1 Fuel cells

Similar to battery, fuel cells are electrochemical galvanic cells that convert chemical energy directly into electrical energy. The fuel cell differs from a battery in that the active materials are not an integral of the device (as in battery), but are fed into the fuel cell from an external source when power is desired. The electrode materials of the fuel cell are inert in that they are not consumed during the cell reaction, but have catalytic properties which enhance the electro-reduction or electro-oxidation of the reactants. The anode active materials used in fuel cells are generally gaseous or liquid and are fed into the anode side of the fuel cell. Oxygen or air is the predominant oxidant and is fed into cathode side of the fuel cell. Use of the fuel cell in a variety of applications has been developing slowly, including utility power, dispersed or on-site electric generators and electric vehicles. Fuel cell systems can take a number of configurations depending on the combination of the fuel and oxidant, the type of electrolyte, the temperature of operation and the application.

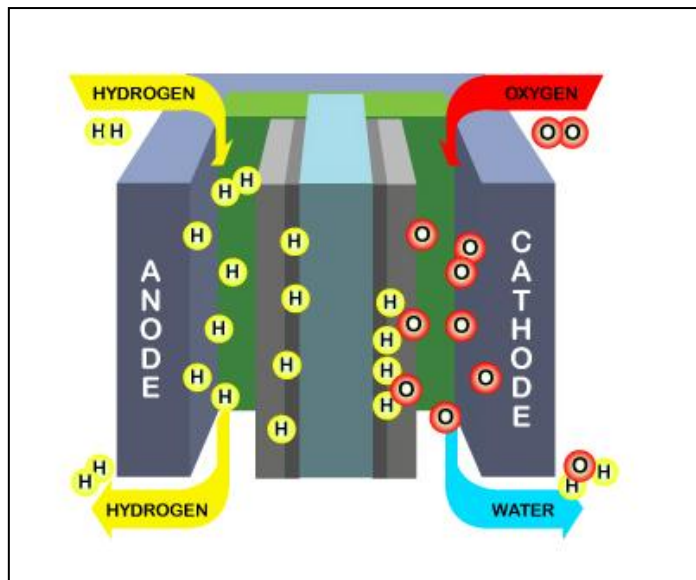


Figure 2.9: Schematic diagram of fuel cell (cell, 2012)

2.7.2 Electrochromic Devices

Electrochromism has a long history of fundamental and practical interest. It can be defined as the phenomenon of the reversible color change in optical properties when a material is electrochemically oxidized or reduced. They showed marked visible color changes when the materials were considered ‘electrochromic’. Electrochromic materials can change their optical properties upon charge insertion/extraction. When thin films of such materials are integrated in devices, it becomes possible to modulate the transmittance (T), reflectance (R), absorptance (A), and emittance (E) between widely separated extreme (Granqvist, 1995). Electrochromic devices are now being studied for modulation of radiation in the near infrared and microwave regions and ‘color’ can mean response of detectors of these wavelengths, not just the human eyes. There has been a growing interest in electrochromic (EC) materials these days for use in practical electrooptical devices such as EC displays, optical modulator, adjustable reflectance mirrors for vehicles, sunglasses, and smart windows for buildings and vehicles.

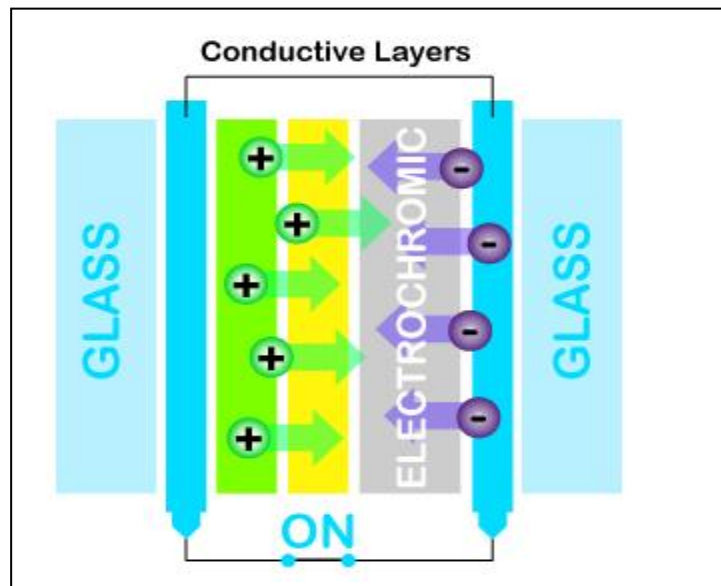


Figure 2.10: Schematic diagram of Electrochromic Devices (Device, 2012)

A schematic diagram of electrochromic devices is shown in Figure 2.10. An electrochromic film is positioned between the two substrates in laminate configuration which the substrate is normally made of glass or flexible polyester foil. The conductive layers at the central part consisted of pure ion conductor (electrolyte) that can be inorganic or organic materials. This ion conductor bounds on an electrochromic film that is capable of conducting electrons as well as ions. This central part of structure is positioned between electrically conducting transparent films. Ions can be shuttled between the ion storage film and the electrochromic film when voltage of the order of one volt is applied between the transparent electrical conductors. The electrons injected from the transparent conductors (electrochromic film) then alter the optical properties. A reversal of the voltage, or short-circuiting, brings back the original properties. The coloration can be stopped at any intermediate level, and the device exhibits open-circuit memory.

CHAPTER 3

Materials

Poly(methylmethacrylate) PMMA with molecular weight of 996,000 g/mol as host polymer, magnesium triflate ($\text{Mg}(\text{CF}_3\text{SO}_3)_2$) as an organic salt, propylene carbonate (PC) and ethylene carbonate (EC) as plasticizing solvent were purchased from Sigma-Aldrich. All these materials were used as received without further purification to prepare gel polymer electrolyte films.

3.1 Sample Preparation

In this research work, gel polymer electrolyte (GPE) system comprising poly(methyl methacrylate) (PMMA), ethylene carbonate (EC), propylene carbonate (PC) and magnesium trifluorosulfonate or magnesium triflate ($\text{Mg}(\text{CF}_3\text{SO}_3)_2$) which has been purchased from Sigma-Aldrich were prepared through solution casting technique. In this system, the amount of polymer and plasticizing solvent are fixed but amount of salt are varied ranging from 5 wt% to 30 wt%. The pure PMMA film will be served as a reference.

The pure PMMA film is prepared by dissolving 2 g of poly(methyl methacrylate) with molecular weight of 9.96×10^5 g/mol in tetrahydrofuran (THF). The mixture was slowly stirred for several hours until complete dissolution is achieved. Then the solution is cast into petri dish and left to dry at room temperature until the standing film is formed. The PMMA-EC-PC film is then prepared by dissolving 2 g of PMMA in the mixture of EC and PC with weight ratio of EC:PC was 2:1. The mixture was stirred at 60°C until homogenous solution obtained and was cast into petri dish. This film was left to dry in a dessicator until clear and stable film is formed. The conductivity of the film was evaluated by using impedance spectroscopy.

For the purpose in obtaining the optimum conductivity value, several GPE films were prepared by varying the amounts of magnesium triflate salt from 5 wt% to 30 wt% in a fixed amount of PMMA and plasticizing solvent, EC and PC. Magnesium triflate was continuously stirred with the plasticizing solvent and heated at 60°C for several hours. Then PMMA is added into the mixture and this solution was continuing stirred until the homogenous solution is formed. This solution was subsequently cast on a petri dish and allowed to dry at room temperature. The films formed are mechanically stable and free standing with thickness range of 0.07 to 0.15 cm. Figure 3.1 shows the prepared GPE film.



Figure 3.1: Gel Polymer Electrolyte containing $\text{Mg}(\text{CF}_3\text{SO}_3)_2$ salt

3.2 Electrochemical Impedance Spectroscopy (EIS)

Electrochemical Impedance Spectroscopy (EIS) is a powerful diagnostic tool that we can use to characterize limitations and improve the performance of electrochemical devices. EIS is useful for research and development of new materials and electrode structures, as well as for product verification and quality assurance in manufacturing operations.

The analysis involves the linear excitation of the electrochemical process by application of small sinusoidal stimulus voltage or current. Normally impedance is measured using a small excitation signal and the cell's response is pseudo-linear. The excitation signal, expressed as a function of time, has the form

$$E_t = E_0 \sin(\omega t) \quad (3.1)$$

E_t is the potential at time t , E_0 is the amplitude of the signal, and ω is the radial frequency. The relationship between radial frequency ω (expressed in radians/second) and frequency f (expressed in Hertz) is:

$$\omega = 2\pi f \quad (3.2)$$

In a linear system, the response signal, it's shifted in phase (φ) and has different amplitude, I_0 .

$$I_t = I_0 \sin(\omega t + \varphi) \quad (3.3)$$

An expression analogous to Ohm's Law allows us to calculate the impedance of the system as:

$$Z = \frac{E_t}{I_t} = \frac{E_0 \sin(\omega t)}{I \sin(\omega t + \phi)} = Z_0 \frac{\sin \omega t}{\sin(\omega t + \phi)} \quad (3.4)$$

The impedance is therefore expressed in terms of magnitude, Z_0 and phase shift, ϕ with Eulers relationship,

$$\exp(j\phi) = \cos \phi + j \sin \phi \quad (3.5)$$

It is possible to express the impedance as a complex function. The potential is described as:

$$E_t = E_0 \exp(\omega j t) \quad (3.6)$$

And the current response as:

$$I_t = I_0 \exp(j\omega t - \phi) \quad (3.7)$$

The impedance is then represented as a complex number,

$$Z(\omega) = \frac{E}{I} = Z_0 \exp(j\phi) = Z_0 (\cos \phi + j \sin \phi) = Z' + Z'' \quad (3.8)$$

And the phase angle given by:

$$\phi(\omega) = \tan^{-1} (Z''(\omega) | Z'(\omega)) \quad (3.9)$$

The expression for $Z(\omega)$ is composed of a real and imaginary part. If the real part is plotted on the X axis and the imaginary part on the Y axis, a ‘Cole-Cole plot’ or Nyquist plot will obtain. There are two method of measuring the electrochemical properties of electrolytes which is A.C and D.C techniques. In this work, we used A.C impedance technique in order to find the value of conductivity of the GPE films.

3.2.1 A.C Impedance Theory

The primary advantage of A.C method over D.C method is that it eliminates the concentration polarization problem associated with D.C measurements. This is because the passage of current in D.C method is only one direction therefore leads to the build up of a concentration gradient which eventually opposes the effect of the applied field. In an A.C measurement, a sinusoidal voltage is applied to a cell and the sinusoidal current passing through the cell a result of this perturbation is determined. Two parameters are required to relate the current flowing to the applied potential. One represents the opposition to the flow of charge and is equal to the ratio of the voltage and current maxima, and is analogous to the resistance in D.C method. The other parameter is the phase shift, of the voltage and current. The combination of these parameters represents the impedance, Z .

An A.C method consists of determining the complex impedance of a cell as a function of the signal frequency and presenting the results in the form of a complex impedance plot. Figure 3.2 shows a diagram of complex plane plot.

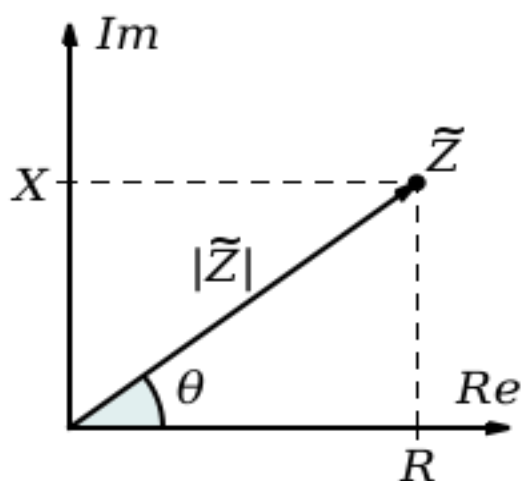


Figure 3.2: The complex impedance plot

EIS data for electrochemical cells are most often represented in Nyquist plot or Cole-Cole plot. A complex plane or Nyquist plot depicts the imaginary impedance, which is indicative of the capacitive and inductive character of the cell, versus the real impedance of the cell as shown in Figure 3.3. Nyquist plot have the advantage that activation-controlled processes with distinct time-constants show up as unique impedance arcs and the shape of the curve provides insight into possible mechanism or governing phenomena.

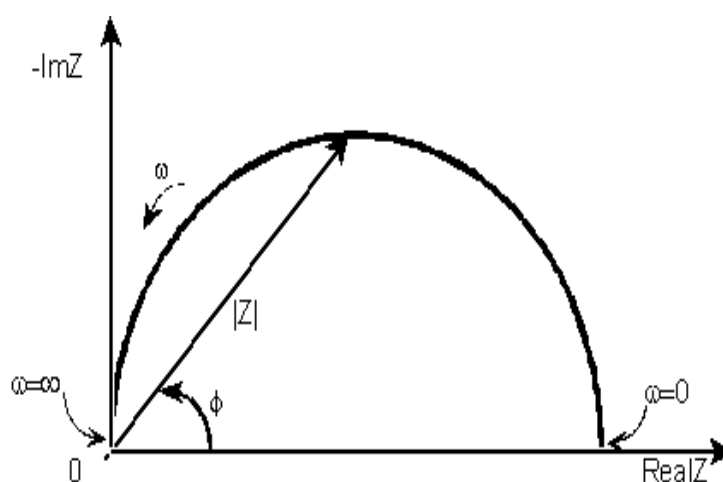


Figure 3.3: Cole-Cole or Nyquist plot

From the Cole-Cole plot with the horizontal and vertical axes having the same scale, the bulk resistance, R_b can be obtained. Whenever R_b was difficult to obtain from the complex impedance data, the impedance data was converted into admittance data and plotted according to the admittance formalism from which $1/R_b$ maybe easier to obtain.

3.2.2 Conductivity measurements

The ionic conductivity of the polymer electrolytes can be expressed in the equation by the sum of the product of the concentration of ionic charge carriers and their mobility:

$$\sigma = \sum n_i z_i \mu_i \quad (3.10)$$

where n_i is the number of charge carriers, z_i is the ionic charge and μ_i is the mobility. In this work, the ionic conductivity of the films was measured using A.C method over the frequency range from 50 Hz to 1MHz using HIOKI 3532 LCR. The films were sandwiched between stainless steel (SS) blocking electrodes and the R_b was determined from the Cole-Cole plot. The conductivity for each film is measured for six times with different parts of the film. The ionic conductivity of the film can be calculated using the following equation:

$$\sigma = \frac{t}{R_b A} \quad (3.11)$$

where t is thickness of the GPE films, R_b is a bulk resistance and A is area of SS electrodes.

The conductivity-temperature dependence of the gel polymer electrolytes are carried out in the temperature range between 303 K and 373 K to indicate an activated process occurred in the mechanism of ionic conduction. It obeys Arrhenius behavior if it shows the linear variation of $\log \sigma$ versus $1000/T$. The conductivity can be expressed by:

$$\sigma = \sigma_o \exp\left(\frac{-E_a}{kT}\right) \quad (3.12)$$

where σ_o is a pre-exponential factor, E_a is the activation energy, k is Boltzmann constant and T is the absolute temperature in K. The activation energy value can be evaluated from the slope of the Arrhenius plot (C. Julien, 1994).

3.2.3 Dielectric properties

In order to understand the conductivity enhancement mechanism in the sample, the impedance data were converted into the complex permittivity. In the complex permittivity plot, the value of the dielectric constant, ϵ_r and dielectric loss, ϵ_i increases at low frequency which is due to the electrode polarization effect. At high frequencies, the periodic reversal of the electric field occurs very fast, hence there is no ion diffusion in the direction of the field. The polarization due to the charge accumulation decrease and the decrease in the value of ϵ' and ϵ'' can be observed.

The relationships between complex impedance, admittance, permittivity and electrical modulus can be obtained from MacDonald, (MacDonald, 1987). From these relationships and writing $Z = Z_r + jZ_i$ where Z_r and Z_i are the magnitudes of the real and imaginary impedance, the equations for the dielectric constant, ϵ_r , and the dielectric loss, ϵ_i can be shown as:

$$\epsilon_r = \frac{Z_i}{\omega C_o (Z_r^2 + Z_i^2)} \quad (3.13)$$

$$\epsilon_i = \frac{Z_r}{\omega C_o (Z_r^2 + Z_i^2)} \quad (3.14)$$

where Z_r and Z_i are related to the magnitude of the complex impedance via the equation, $Z_r(\omega) = Z(\omega)\cos \theta(\omega)$, $Z_i(\omega) = Z(\omega)\sin \theta(\omega)$ and $C_o = \epsilon_o A/t$. ϵ_o is permittivity of free space and $\omega = 2\pi f$, where f is frequency. The electrical modulus, Mr and Mi was then obtained using the following equation:

$$M_r = \frac{\varepsilon_r}{(\varepsilon_r^2 + \varepsilon_i^2)} \quad (3.15)$$

and

$$M_i = \frac{\varepsilon_i}{(\varepsilon_r^2 + \varepsilon_i^2)} \quad (3.16)$$

The loss tangent equation can be written as:

$$\tan \delta = \frac{M_i}{M_r} \quad (3.17)$$

or

$$\tan \delta = \frac{\varepsilon_i}{\varepsilon_r} \quad (3.18)$$

In the present work, dielectric properties of GPE films was further studied in order to better understand the ionic transport phenomenon of polymer electrolyte system.

3.3 Transference number measurements

The transference number of a charge carrier is defined as the ratio of the conductivity due to itself and the total conductivity, σ_T . The total conductivity of a sample given by:

$$\sigma_T = \sigma_i + \sigma_e \quad (3.19)$$

where σ_i and σ_e are the conductivities contributed by ions (cations/anions) and electron/holes, respectively. The fraction of the conductivity due to different charge carriers gives respective transference numbers given by:

$$\text{Ionic transference number, } t_i = \sigma_i / \sigma_T \quad (3.20)$$

$$\text{Electronic transference number, } t_e = \sigma_e / \sigma_T \quad (3.21)$$

The transference number of the polymer electrolytes can be measured by the direct current (DC) polarization method or also known as Wagner's method (Pandey, Agrawal, & Hashmi, 2009). In this work, D.C polarization method was used to measure the ionic transport number from the sample containing 5wt.%, 20wt.% and 30wt.% of magnesium triflate, $\text{Mg}(\text{CF}_3\text{SO}_3)_2$ salt. In this method, the D.C current is monitored as a function of time on the application of fixed dc voltage (0.5 V) across the GPE films using stainless steel blocking electrodes. If the electrical conductivity of the polymer electrolytes is primarily ionic, the current will decrease with time. The polarization current versus time will be plotted and the ionic transference number will be evaluated using the following equations:

$$t_e = \sigma_e / \sigma_T = i_e / i_T \quad (3.22)$$

and

$$t_i = 1 - i_e / i_T = 1 - t_e \quad (3.23)$$

where i_e and i_T are the electronic and total current, respectively.

The transport number, t_+ of Mg^{2+} ions in the GPE films was evaluated by the method that proposed by Evans et al. (Bruce, Evans, & Vincent, 1988) using the combination of A.C impedance spectroscopy and D.C. polarization of $\text{Mg}|\text{GPE}|\text{Mg}$ cell. According to this method, the cells were polarized by applying a constant voltage, $\Delta V = 0.3$ V for 20 hours and subsequently initial and final currents were recorded. The cells were subjected to A.C. impedance measurements prior to and after the polarization. The values of electrode-electrolyte contact resistances were obtained from the impedance plots. The transport number, t_+ values were determined using the equation;

$$t_i = \frac{I_s(\Delta V - R_o I_o)}{I_o(\Delta V - R_s I_s)} \quad (3.24)$$

where I_o and I_s are initial current and final current, respectively. R_o and R_s are cell resistances before and after the polarization, respectively.

3.4 Fourier Transform Infra-Red Spectroscopy

Fourier Transform Infra-Red Spectroscopy (FTIR) has been a workhorse technique for materials analysis in the laboratory for over seventy years. In infrared spectroscopy, IR radiation is passed through a sample. Some of the infrared radiation is absorbed by the sample and some of it is passed through (transmitted). Figure 3.4 shows the basic diagram of spectrometer used in FTIR spectroscopy.

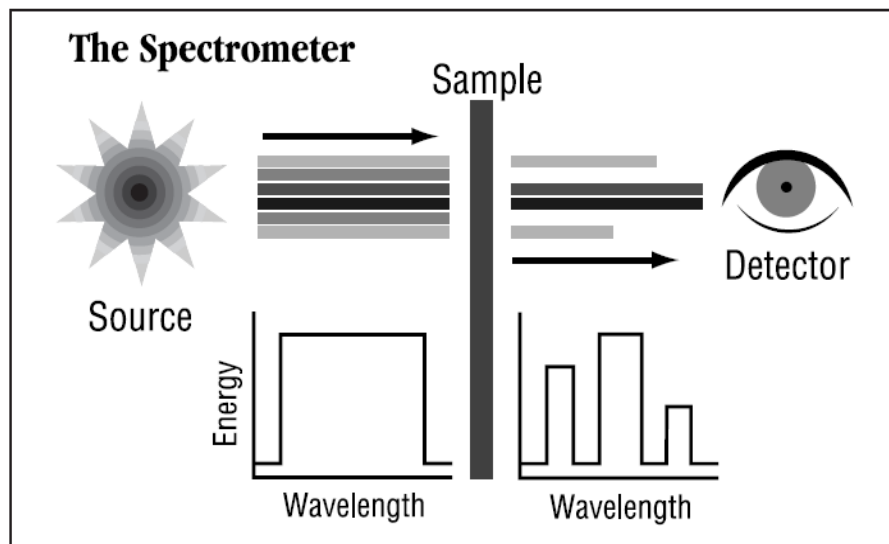


Figure 3.4: Basic diagram of FTIR Spectrometer (basic_FTIR, 2012)

The infrared region of the electromagnetic radiation lies in the range from 14000 cm^{-1} to 10 cm^{-1} . Typically, mid-infrared region (4000 cm^{-1} to 400 cm^{-1}) is used to study organic compounds by analysis of their constituent bonds. An infrared spectrum represents a fingerprint of a sample with absorption peaks which correspond to the frequencies of vibrations between the bonds of the atoms making up the material. Because each different material is a unique combination of atoms, no two compounds produce the same infrared spectrum. Therefore, infrared spectroscopy can result in a positive identification (qualitative analysis) of every different kind of material. In addition, the size of the peaks in the spectrum is a direct indication of the amount of material present. This makes infrared spectroscopy useful for several types of analysis and with modern software algorithms, infrared is an excellent tool for quantitative analysis.

FTIR spectrometry was developed by employed a very simple optical device called an interferometer. Figure 3.5 shows the schematic diagram of FTIR spectrometry. The interferometer produces a unique type of signal which has all of the infrared frequencies “encoded” into it. Most interferometers employ a beam splitter which takes the incoming infrared beam and divides it into two optical beams. One beam reflects off of a flat mirror which is fixed in place. The other beam reflects off of a flat mirror which is on a mechanism which allows this mirror to move a very short distance (typically a few millimeters) away from the beam splitter. The two beams reflect off of their respective mirrors and are recombined when they meet back at the beam splitter. Because the path that one beam travels is a fixed length and the other is constantly changing as its mirror moves, the signal which exits the interferometer is the result of these two beams “interfering” with each other.

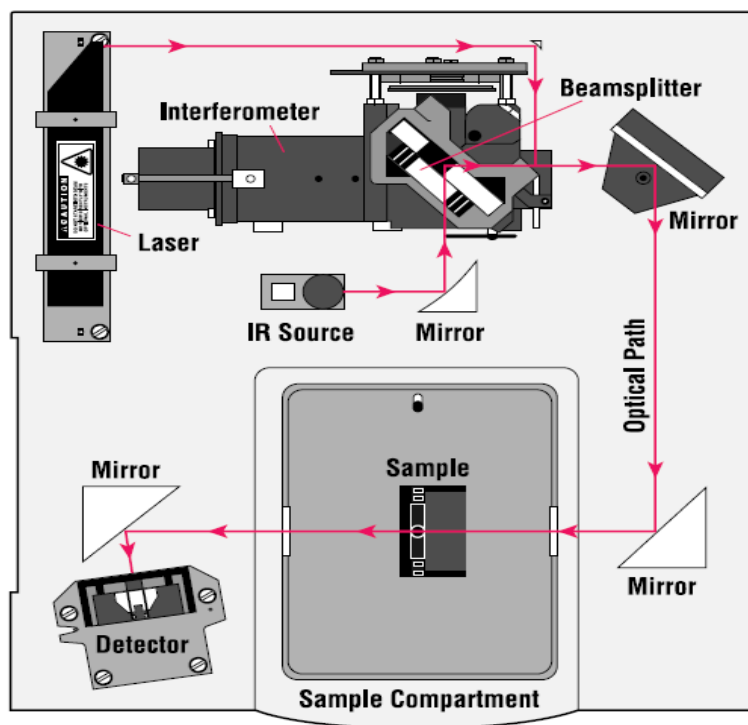


Figure 3.5: Schematic diagram of FTIR spectrometry (schematic_FTIR, 2012)

The resulting signal is called an interferogram which has the unique property that every data point (a function of the moving mirror position) which makes up the signal has information about every infrared frequency which comes from the source. This means that as the interferogram is measured, all frequencies are being measured simultaneously. Thus, the use of the interferometer results in extremely fast measurements. Because the analyst requires a frequency spectrum (a plot of the intensity at each individual frequency) in order to make an identification, the measured interferogram signal can not be interpreted directly. A means of “decoding” the individual frequencies is required. This can be accomplished via a well-known mathematical technique called the Fourier transformation. This transformation is performed by the computer which then presents the user with the desired spectral information for analysis.

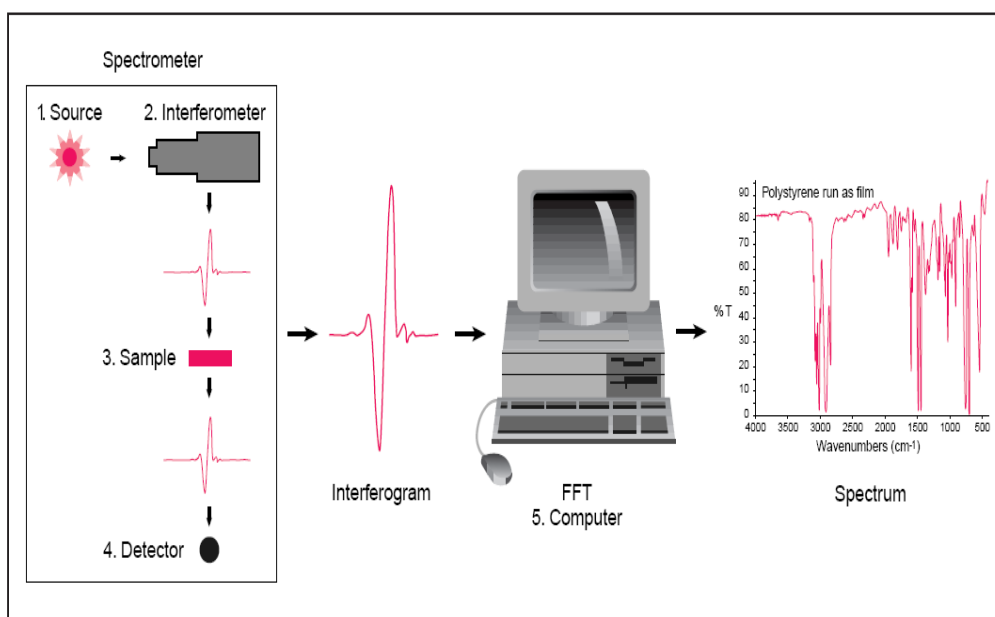


Figure 3.6: The sample analysis process (sample_analysis, 2012)

Figure 3.6 represents the sample analysis process of IR spectrum obtained from analysis process can be used to gain information about the sample composition in terms of chemical group presents and also to verify the various vibrational modes of a molecule. Vibrations can be in the form of a bend or a stretch for each bond. Not all possible vibrations within a molecule will result in an absorption band in the infrared region. Deconvolution method can be used to decompose the overlapping spectrum that can not be resolved by collecting data at a higher resolution setting in the IR spectra. By knowing the basic vibration modes and deformation types of the molecules, the much complex polymer chain vibrations could be understood. Figure 3.7 illustrates the possible vibrational motions for the simple molecule.

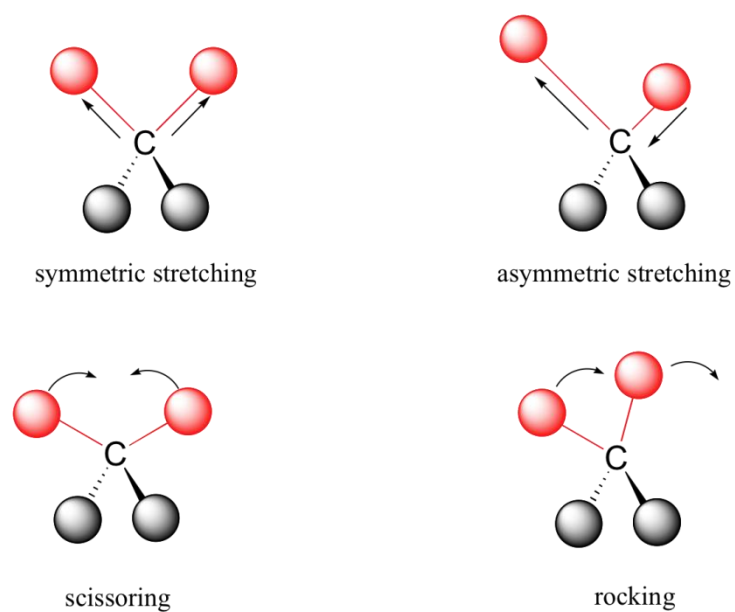


Figure 3.7: Vibrational modes (vibrational_modes, 2012)

In this present work, infrared spectra exhibited from all the GPE films were taken by using Nicolet is10 (Thermo Scientific) as shown in Figure 3.8 in the wavenumber region between 650 cm^{-1} and 4000 cm^{-1} . The resolution of this spectrometer was 1 cm^{-1} .



Figure 3.8: Instrumentation of FTIR measurement

3.5 X-ray Diffraction (XRD)

X-ray diffraction is a non-destructive analytical technique for identification and quantitative determination of the various crystalline forms, known as ‘phases’. Identification is achieved by comparing the x-ray diffraction (XRD) pattern because every crystalline substance produces its own XRD pattern. Bragg's law was used to explain the interference pattern of x-rays scattered by crystals. Crystals consist of planes of atoms that are spaced a distance d apart, but can be resolved into many atomic planes, each with a different d spacing. The atomic planes of a crystal cause an incident beam of x-rays to interfere with one another as they leave the crystal. The phenomenon is called x-ray diffraction. Figure 3.9 shows the schematic of x-ray diffraction.

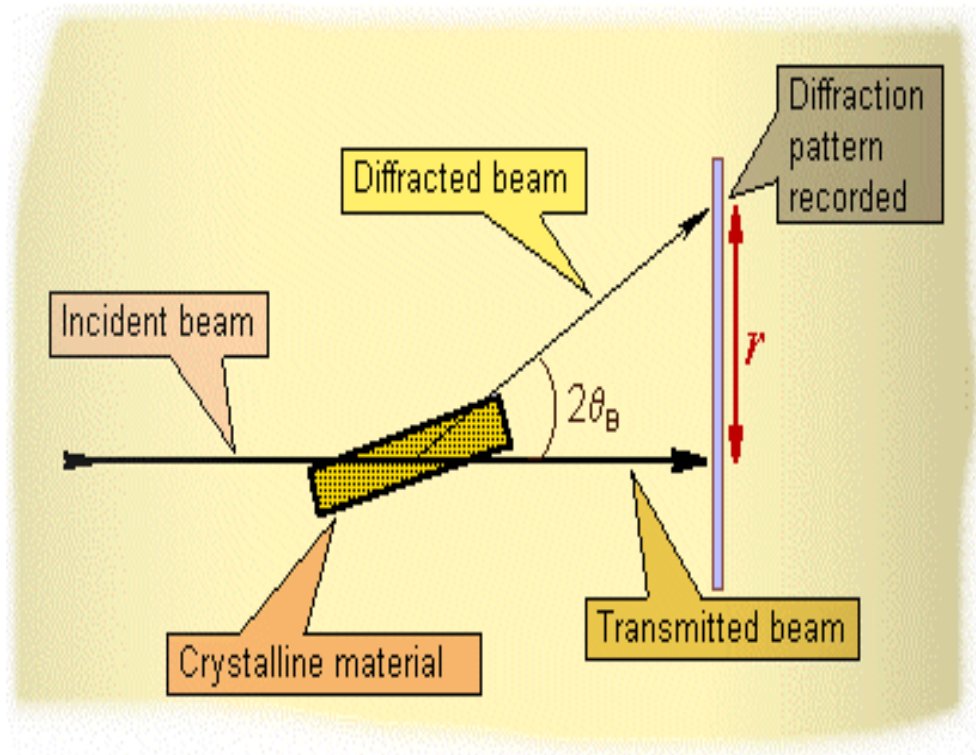


Figure 3.9: Schematic diagram of X-Ray diffraction (XRD) (schematic_XRD, 2012)

When a monochromatic x-ray beam with wavelength λ is incident on the lattice planes in a crystal at an angle θ , diffraction occurs only when the distance traveled by the rays reflected from successive planes differs by a complete number n of wavelengths. Diffraction occurs only when Bragg's law is satisfied condition for constructive interference from planes with spacing d . Figure 3.10 shows the Bragg's Law reflection.

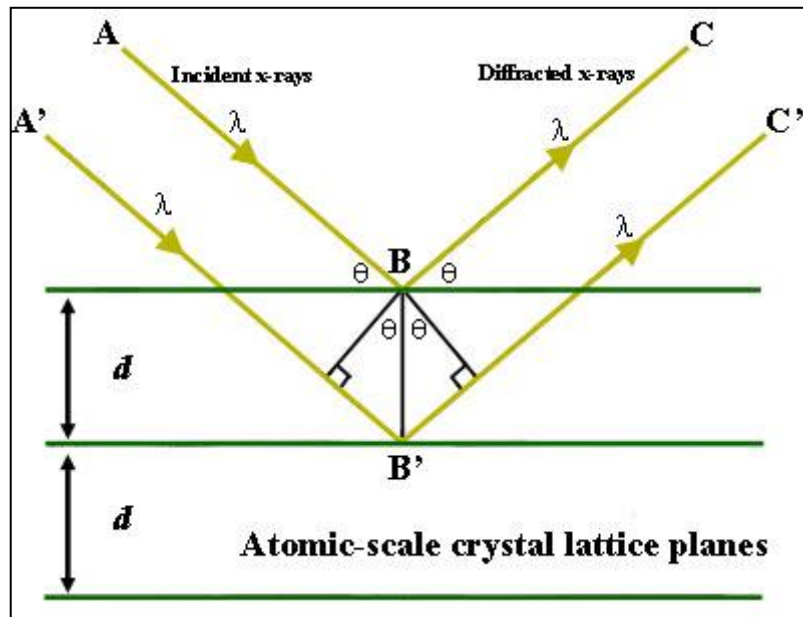


Figure 3.10: Bragg's Law reflection. The diffracted x-rays exhibit constructive interference when the distance between paths ABC and A'B'C' differs by an integer number of wavelengths (λ). (braggs_law, 2012)

The general relationship between the wavelength of the incident x-ray, angle of incident and spacing between the crystal lattice planes of atoms can be expressed as:

$$n\lambda = 2d \sin \theta \quad (3.21)$$

where n (an integer) is the "order" of reflection, λ is the wavelength of the incident x-rays, d is the interplanar spacing of the crystal and θ is the angle of incident.

In this work, XRD studies were carried out using X'Pert PRO PANalytical diffractometer as shown in Figure 3.11 on the pure PMMA film, PMMA-EC-PC film, pure $\text{Mg}(\text{CF}_3\text{SO}_3)_2$ salt, and also for the GPE films containing 5 wt.% to 30 wt.% of $\text{Mg}(\text{CF}_3\text{SO}_3)_2$ salt in order to examine the nature of crystallinity and the amorphousness of the GPE films.



Figure 3.11: Instrumentation of XRD measurement

3.6 Field Emission Scanning Electron Microscopy (FESEM)

Electron microscopes are scientific instruments that use a beam of energetic electrons to examine objects on a very fine scale. Electron microscopes were developed due to the limitations of light microscopes which are limited by the physics of light. In the early 1930's, this theoretical limit had been reached and there was a scientific desire to see the fine details of the interior structures of organic cells. This requires 10,000x plus magnification which was not possible using current optical microscopes.

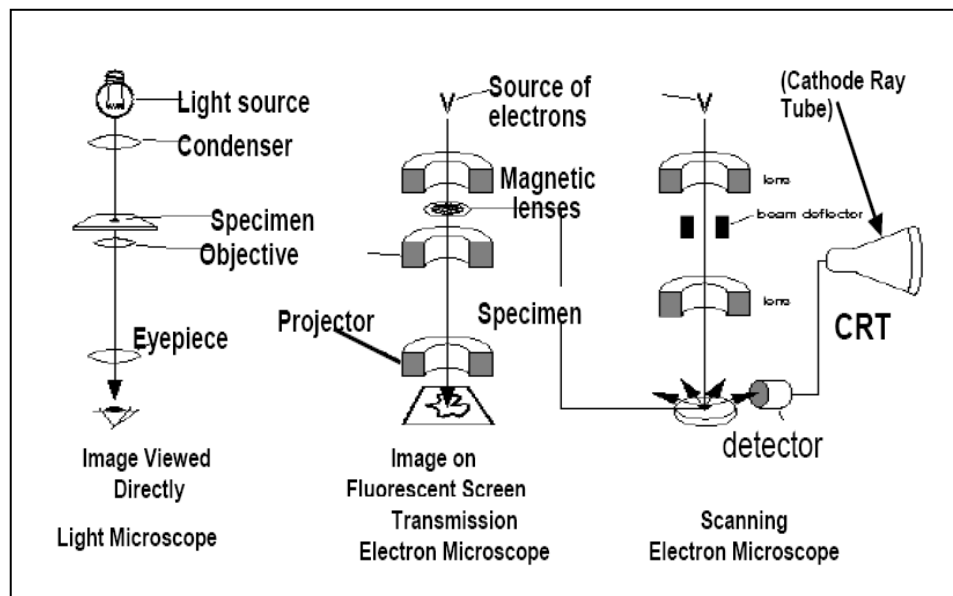


Figure 3.12: Principal features of an optical microscope, a transmission electron microscope and a scanning electron microscope, drawn to emphasize the similarities of overall design. (SEM_principal, 2012)

Transmission electron microscope (TEM) is patterned exactly on the light transmission microscope except that a focused beam of electrons is used instead of light to form an image. Scanning electron microscope (SEM) was developed due to the electronics involved in “scanning” the beam of electrons across the sample.

It has a large depth of field, which allows a large amount of the sample to be in focus at one time and higher resolution so that closely spaced specimens can be magnified at much higher levels. These advantages make the SEM one of the most useful instruments in many research areas. Figure 3.12 and 3.13 show the principal features of an optical microscope, a transmission electron microscope and a scanning electron microscope and the schematic diagram of SEM experiment, respectively.

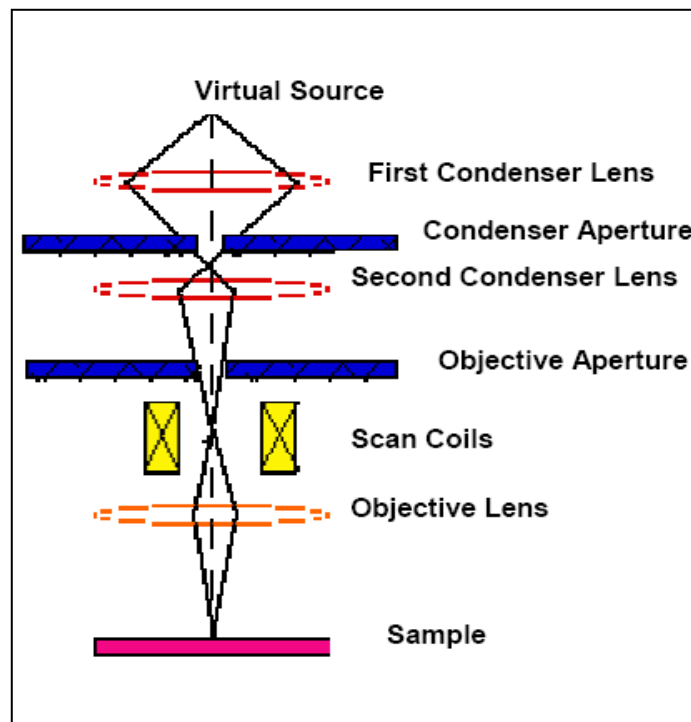


Figure 3.13: The schematic diagram of SEM experiment (schematic_SEM, 2012)

The “virtual source” at the top represents the electron gun, producing a stream of monochromatic electrons. The stream is condensed by the first condenser lens. This lens is used to both form the beam and limit the amount of current in the beam. It works in conjunction with the condenser aperture to eliminate the high-angle electrons from the beam. The beam is then constricted by the condenser aperture, eliminating some high-angle electrons. The second condenser lens forms the electrons into a thin, tight, coherent beam and is usually controlled by the ‘fine probe current knob’. A user selectable objective aperture further eliminates high angle electrons from the beam. A set of coils then “scan” or “sweep” the beam in a grid fashion, dwelling on points for a period of time determined by the scan speed. The final lens, the objective, focuses the scanning beam onto the part of the specimen desired.

When the beam strikes the sample, interactions occur inside the sample and are detected with various instruments. Detectors collect these x-rays, backscattered electrons, and secondary electrons and convert them into a signal which then produced an image. In Field Emission Scanning Electron Microscopy (FESEM), we are using field emission gun where electric field at the tip is very strong due to the sharp point effect and the electrons are pulled out from the tip by the strong field. Figure 3.14 shows the instrumentation of FESEM used in this study.

In this work, gel polymer electrolytes were analyzed using FESEM technique through FEI Quanta 200 system in order to investigate the surface morphology of the samples. From the images, we will evaluate the direct relation between the morphological properties and the conductivity studies as well as the structural properties of the GPE samples.



Figure 3.14: Instrumentation of FESEM

3.7 Differential Scanning Calorimetry (DSC)

Differential Scanning Calorimetry (DSC) is the most widely used technique of all the thermal analysis methods. It is a thermoanalytical technique in which the difference in the amount of heat required to increase the temperature of a sample and reference is measured as a function of temperature. The basic principle underlying in this technique is the heat flux where the sample undergoes a physical transformation such as phase transitions. In this process, the sample which shall be measured is placed in an aluminium pan whereas an empty aluminium pan serves as the reference. These two pans are put on a electrically heated plate in order to make sure that the temperature in the sample is the same as in the reference. Heat is transferred to the sample and the reference via those plates and the pans by using a defined computer controlled heating program. The differential heat flux to the sample and the reference as well as the sample temperature are measured.

The result of a DSC measurement called thermogram shows a plot of heat difference delivered to the sample and reference as a function of the sample temperature as shown in Figure 3.15.

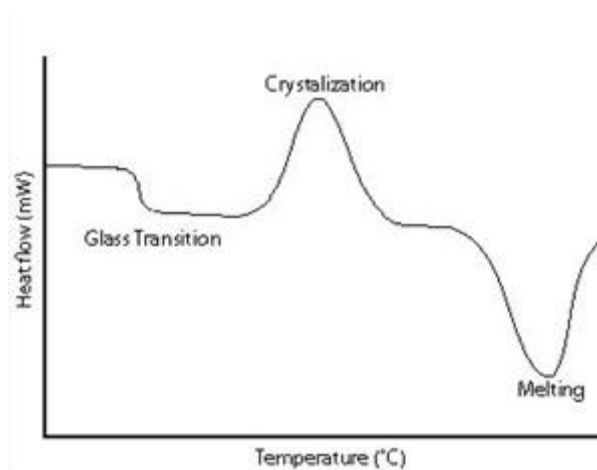


Figure 3.15: Typical DSC thermogram (DSC_thermogram, 2012)

From DSC process, the changes in the sample that is associated with absorption or evolution of heat cause a change in the differential heat flow which is then recorded as a peak. The area under the peak is directly proportional to the enthalpic change and its direction indicates whether the thermal process is endothermic or exothermic. Endothermic process occurs due the absorption of heat by the sample as it is require more heat flowing to the sample to increase its temperature at the same rate as the reference. Likewise, less heat is required to increase the sample temperature as the sample undergoes exothermic process where the heat will be released during the phase transitions.

Differential scanning calorimetry can be used to measure a number of characteristic properties of a sample. It can be used to observe the chemical reactions that may occur such as heat fusion, oxidation, crystallization process as well as glass transition temperature, T_g . Glass transition temperature, T_g is the phase when the sample turn from the rubbery state to the glassy state and this is due to the sample undergoing an exothermic process. As the temperature of the sample is increased, the sample eventually reaches its melting temperature, T_m and this process results in an endothermic peak in the DSC curve.

In this work, DSC results of the GPE samples are obtained using Perkin Elmer DSC Instrument at Physics Department, as shown in Figure 3.16. The temperature range used ranging from room temperature until 300°C with heating/cooling rate at 10°/min. The DSC plot will be analyzed using TA Instrument Explorer software in order to find the glass transition temperature T_g (midpoint), melting point (T_m) and decomposition temperature (T_d) of the GPE films.



Figure 3.16: Instrumentation of DSC measurement

3.8 Linear Sweep Voltammetry (LSV)

In linear sweep voltammetry (LSV) measurements, the voltage is scanned from a lower limit to an upper limit and the current response is plotted as a function of voltage as shown in Figure 3.17. The scan begins from the left hand side, V_1 of the current/voltage plot where no current flows. However, a current begins to flow as the voltage is swept to the right, V_2 and eventually reaches a peak before dropping. The peak occurs since the surface of the electrode is completely covered in the reactant. This means the diffusion layer has grown sufficiently above the electrode so that the flux of reactant to the electrode is not fast enough.

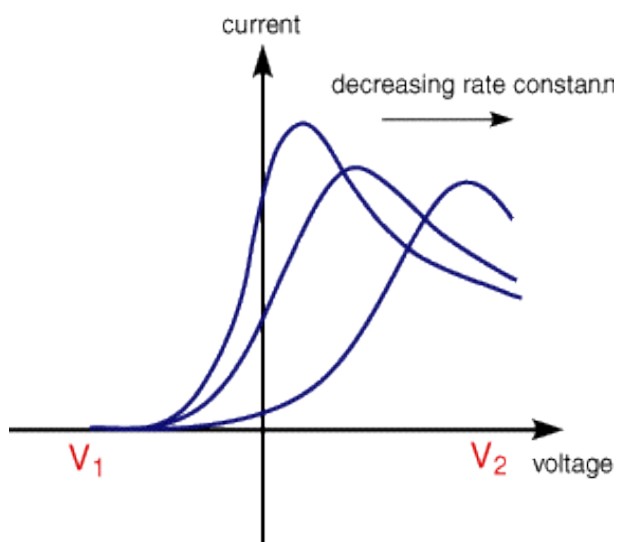


Figure 3.17: linear sweep voltammograms as the change of the rate constant (LSV_voltammogram, 2012)

The above voltammogram was recorded at a single scan rate. If the scan rate is altered, the current response will also change. Even though each curve from the plot has the same form but it is apparent that total current will decrease with decreasing scan rate. This again can be rationalized by considering the size of the diffusion layer and the time taken to record the scan. In a slow voltage scan, the diffusion layer will grow much further from the electrode in comparison to fast scan. Consequently, the flux to the electrode surface is considerably smaller at a slow scan rate than it is at faster rates. As the current is proportional to the flux towards the electrode, the magnitude of the current will be higher at high rates and lower at slow scan rates.

In this research work, highest conducting film containing 20 wt.% of $\text{Mg}(\text{CF}_3\text{SO}_3)_2$ salt was characterized through LSV technique by using WonATech system recorded on a SS|GPE|Mg cell in order to estimate the electrochemical stability window (ESW) or working voltage limit of the gel polymer electrolyte film and the results obtained will be analyzed. In this technique, the stainless steel (SS) will act as a working electrode while Mg foil as the combined of counter and reference electrodes. The cell was charged up to 2.3 V with a scan rate of 5 mV s^{-1} .

3.9 Cyclic Voltammetry (CV)

Cyclic voltammetry is a simple and direct method for measuring the formal potential of a half reaction when both oxidized and reduced forms are stable during the time required to obtain the voltammogram (current-potential curve). In cyclic voltammetry, the potential of a working electrode is changed linearly with time starting from a potential where no electrode reaction occurs and moving to potentials where reduction and oxidation of a solute occurs. The forward sweep produces an identical response to that seen in LSV experiment. When the direction of the linear sweep is reversed, the electrode reactions of intermediates and products that formed during the forward scan can be detected.

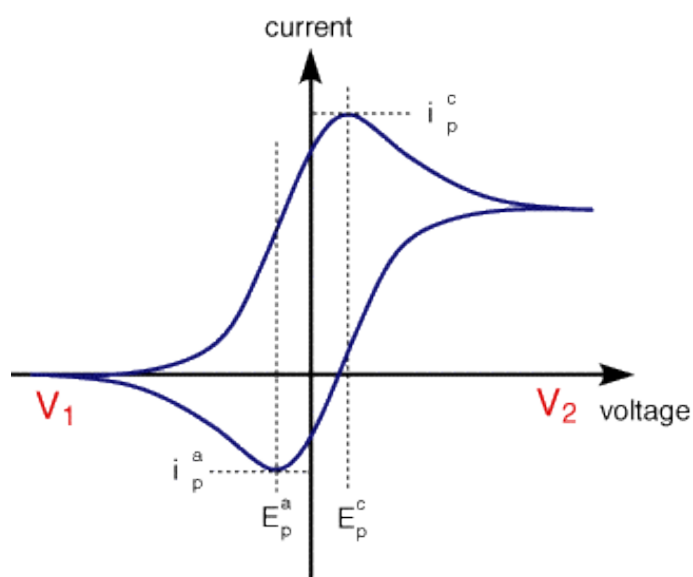


Figure 3.18: Cyclic voltammogram (CV) (CV_voltammogram, 2012)

The CV is characterized by several important parameters which is the cathodic (E_{pc}) and anodic (E_{pa}) peak potentials, and also the cathodic (i_{pc}) and anodic (i_{pa}) peak currents, as illustrates in Figure 3.18. The cathodic peak in the CV results from the competition of two factors, the increase in the (net) rate of reduction as the potential is made more negative and the development of a thickening depletion layer across which reactant must diffuse. Meanwhile, an anodic peak in the CV is obtained for reasons analogous to those underlying the cathodic peak where the surface concentration of reactant becomes small and the current is limited by the rate of diffusion through the depletion layer (diffusion-controlled current).

Cyclic voltammetry is a powerful technique for detection and characterization of such coupled chemical reactions. In this work, cyclic voltammetry and complex impedance studies have been carried out in order to confirm the Mg^{2+} ion conduction in the gel polymer electrolyte. It has been performed on symmetrical cells SS|GPE|SS (Cell-I) and Mg|GPE|Mg (Cell-II) for the GPE film containing 20 wt.% of $Mg(CF_3SO_3)_2$ salt at room temperature where the stainless steel (SS) and Mg foil will act as a working electrode and the combined of counter and reference electrodes respectively.

3.10 Battery Performance and Characteristics

In order to obtain high energy density battery system, highly reactive component should be used, i.e. anode materials of the lowest redox potential possible, and cathode materials whose redox potential is sufficiently high compared with that of the anode, thus enabling the composition of battery systems of high working potentials. Natural candidates for anode materials for high energy density batteries are active metals such as lithium, magnesium, zinc, calcium, etc.

Among of these active materials, lithium ion conduction has been much focused due to their use as electrolytes in high energy density lithium battery systems. Li^+ ion battery, with significantly high energy density is found to be the most promising battery materials for portable electronic devices. However, this battery system cannot fulfill the increasing needs of the global battery market since the Li-ion batteries are relatively expensive and suffer from some safety problems. Thus, new rechargeable battery systems which are much cheaper and environment friendly material has been developed. A natural candidate for anode material with high energy density is obviously magnesium which are highly abundant in the earth, low toxicity, ease of handling and environmental friendly (Aurbach et al., 2001).

In this present work, the MnO_2 electrodes were prepared using a mixture of manganese dioxide powder (80 wt.%), super-P carbon (10 wt.%) and PVdF (10 wt.%) as the binder. The mixtures was thoroughly ground in a mortar and applied on to an aluminium grid which was subjected to prior degreasing in acetone. The grid along with the electrode material was weighted and heated at 100°C for 1 hour. The weight of cathode material used in this work is about 0.0504 g. A Mg/GPE/ MnO_2 cell was assembled by sandwiching the respective electrodes and the GPE film in a sealed container. Charge/discharge cycling was carried out by using an electrochemical analyzer, WPG100e potentiostat/galvanostat system with a constant current of 0.2 mA and the cell was charged up to 2.3 V.

CHAPTER 4

4.1 Impedance Spectroscopy (IS) Studies

The study of electrical conductivity concerning on polymer electrolytes is very important in order to understand the ionic behavior and transport mechanism in the polymer electrolytes. An understanding of this mechanism is of considerable interest in view of possible applications such as solid-state rechargeable batteries, sensors, fuel cells and electrochromic windows. Therefore, impedance spectroscopy analysis was performed on PMMA based gel polymer electrolytes system to obtain the conductivity at room temperature. The impedance was measured from 50 Hz to 1 MHz. The conductivity-temperature studies were also performed on the GPE films from the PMMA-EC-PC-Mg(CF₃SO₃)₂ system in the temperature range between 303 K and 373 K.

4.1.1 Room temperature Impedance Spectroscopy Studies

4.1.1.1 PMMA-EC-PC film

Figure 4.1 shows the Cole-Cole plot of plasticized PMMA film containing a fixed amount of EC and PC with the mass ratio of EC: PC = 2:1. The amount of PMMA used in this film is 2g. The room temperature conductivity value of this film is $1.81 \times 10^{-6} \text{ S cm}^{-1}$. It can be seen that the conductivity of the PMMA film increases as the plasticizers, EC and PC were added. This shows that the plasticizer has reduced the rigidity of the polymer backbone and hence increases the mobility of segmental chain of the polymer.

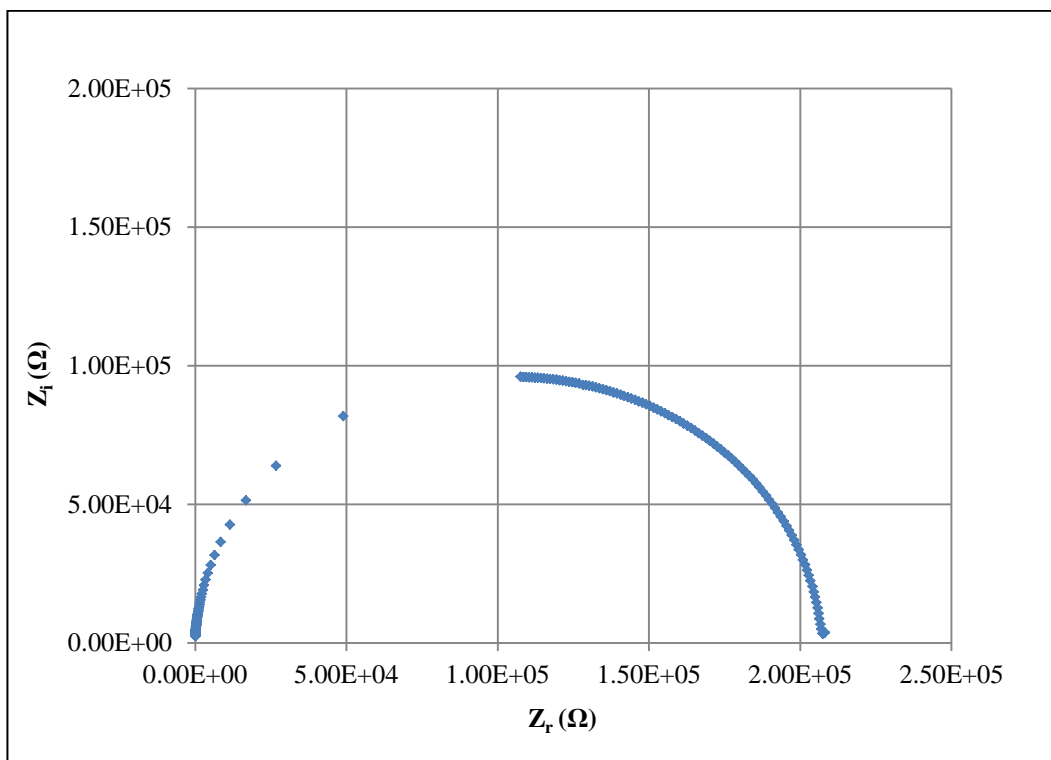


Figure 4.1: Cole-Cole plot for the PMMA-EC-PC film.

4.1.1.2 PMMA-EC-PC-Mg(CF₃SO₃)₂ system

Table 4.1 lists the compositions of the prepared GPE films at room temperature, the values of bulk resistance, R_b and the conductivities films in the PMMA-EC-PC-Mg(CF₃SO₃)₂ system. In this work, the GPE films were prepared by varying the amounts of Mg(CF₃SO₃)₂ salt from 5wt% to 30wt% in a fixed amount (by weight) of PMMA and the plasticizing solvent, (EC + PC). The mass ratio of (EC+PC) to PMMA was 3:2. The highest conductivity achieved is $1.27 \times 10^{-3} \text{ S cm}^{-1}$ from the film containing 20 wt. % of Mg(CF₃SO₃)₂. Figure 4.2 shows the variation of conductivity of the plasticized PMMA films containing different amounts of Mg(CF₃SO₃)₂ salt by weight percentage. The bulk resistance, R_b values can be calculated from the intercept on the real impedance axis of Cole-Cole plot.

Table 4.1: Constituents of the prepared GPE films in PMMA-EC-PC-Mg(CF₃SO₃)₂ system

Amount of Mg(CF ₃ SO ₃) ₂ (wt.%)	Average Conductivity (S cm ⁻¹)	Standard deviation (S cm ⁻¹)
5	4.65 x 10 ⁻⁵	5.34 x 10 ⁻⁶
10	8.34 x 10 ⁻⁵	1.68 x 10 ⁻⁵
15	5.58 x 10 ⁻⁴	1.57 x 10 ⁻⁴
20	1.27 x 10 ⁻³	3.48 x 10 ⁻⁴
25	1.49 x 10 ⁻⁴	2.60 x 10 ⁻⁵
30	1.56 x 10 ⁻⁴	4.43 x 10 ⁻⁵

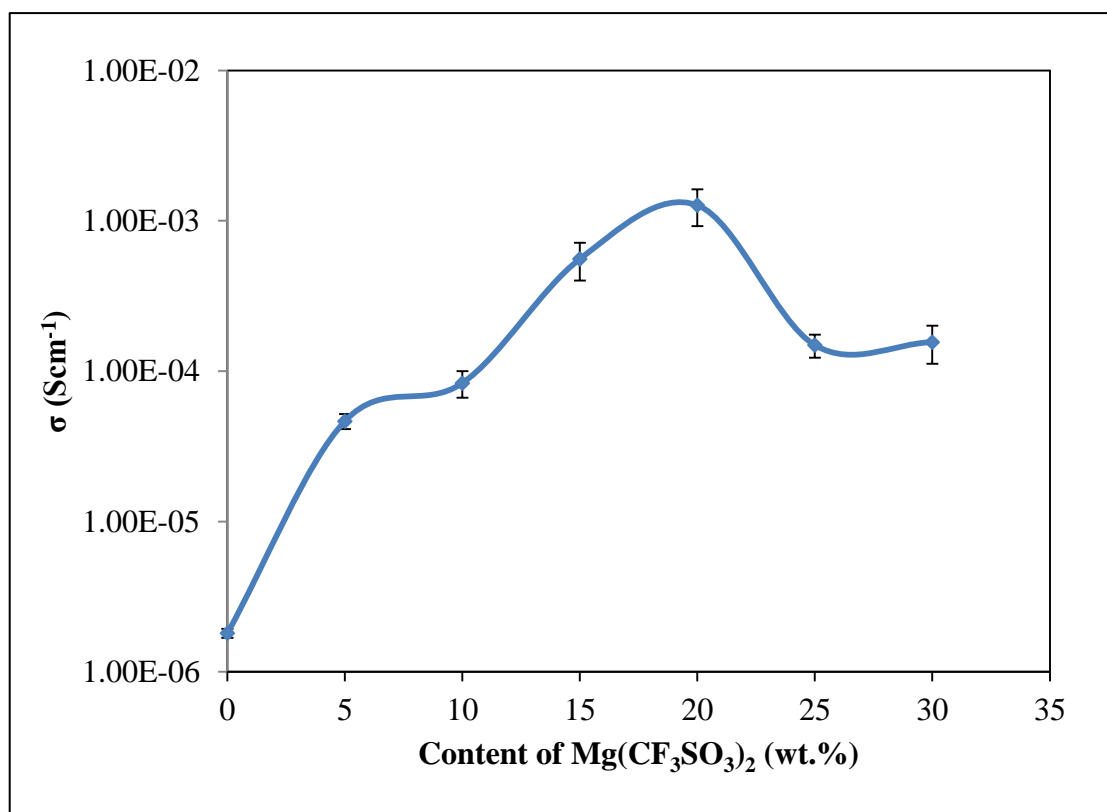


Figure 4.2: Conductivity (σ) of GPE films as a function of $\text{Mg}(\text{CF}_3\text{SO}_3)_2$ salt concentration

From the Figure 4.2, it can be observed that the conductivity of the plasticized PMMA film has increased to $10^{-5} \text{ S cm}^{-1}$ on addition of 5 wt.% of $\text{Mg}(\text{CF}_3\text{SO}_3)_2$ salt. Then, the value of conductivity keep increases until it reaches a maximum value of $1.27 \times 10^{-3} \text{ S cm}^{-1}$ when 20 wt.% of $\text{Mg}(\text{CF}_3\text{SO}_3)_2$ salt has been added. The GPE films exhibits high ionic conductivity due to the presence of $\text{Mg}(\text{CF}_3\text{SO}_3)_2$ salt dissolved in EC and PC, which is encapsulated in the matrix of PMMA (Girish Kumar & Munichandraiah, 2000). The increase in the ionic conductivity with the increase of salt concentration can be related to the increase in the number of mobile charge carriers or free ions in the polymer electrolytes (Ramya, Selvasekarapandian, Savitha, Hirankumar, & Angelo, 2007).

Further increase in concentration of $\text{Mg}(\text{CF}_3\text{SO}_3)_2$ salt (25 wt.% and 30 wt.%), the conductivity decreased to order of $10^{-4} \text{ S cm}^{-1}$. This result may be attributed to the ions aggregation, leading to the formation of ion pairs and ion aggregates, thus reduces the number of mobile charge carriers (MacCallum, Tomlin, & Vincent, 1986).

4.1.2 Conductivity-temperature dependence studies

4.1.2.1 PMMA – EC – PC – $\text{Mg}(\text{CF}_3\text{SO}_3)_2$ system

The conductivity-temperature dependence measurements are carried out to analyze the mechanism of ionic conduction in polymer electrolytes. In this work, the conductivity-temperature dependence studies have been done on the GPE films containing 5 wt.%, 20 wt.% and 30 wt.% of $\text{Mg}(\text{CF}_3\text{SO}_3)_2$ salt. The films were sandwiched between two blocking electrodes (stainless steel) and were subjected to A.C impedance measurements in the temperature range from 303 K to 373 K. Figure 4.3 shows the plots are fairly linear with regression values, R^2 almost unity. The activation energies, E_a has been calculated from the films containing 5wt.%, 20wt.%, and 30wt.% of $\text{Mg}(\text{CF}_3\text{SO}_3)_2$ and the values obtained are 0.18 eV, 0.22 eV and 0.26 eV, respectively.

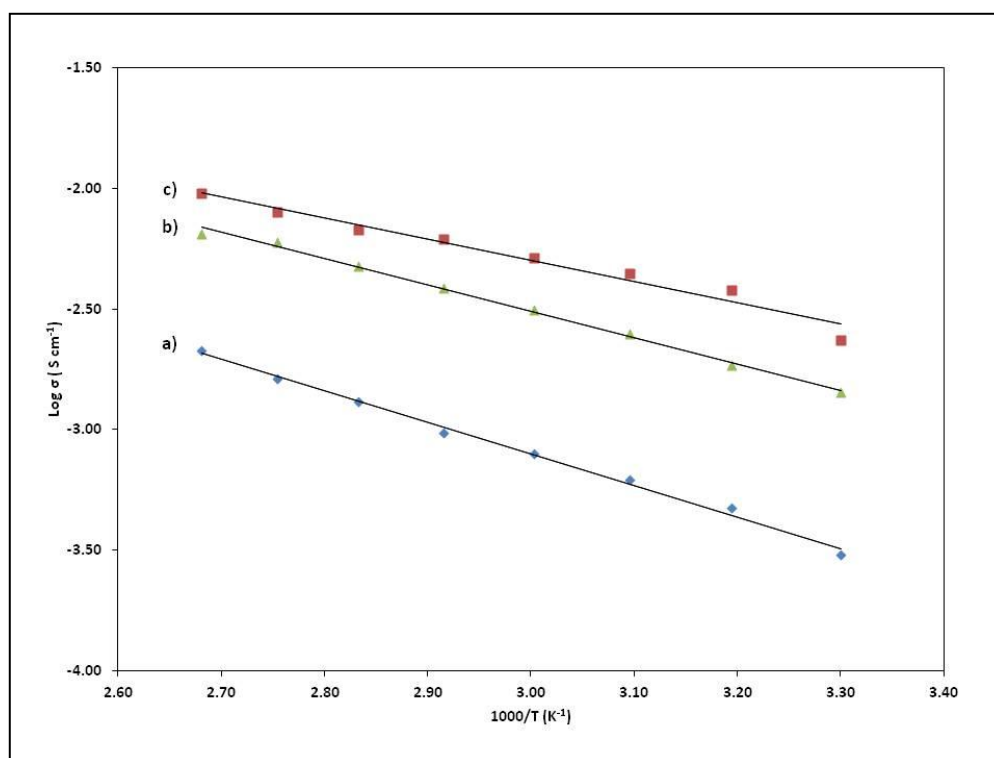


Figure 4.3: Temperature dependence of ionic conductivity of PMMA-EC-PC-Mg(CF₃SO₃)₂ GPE films for the films containing (a) 5wt.%, (b) 30wt.% and (c) 20wt.% of Mg(CF₃SO₃)₂ salt

From the plot, it can be proved that the ionic conductivity increases as the temperature increased for the electrolytes system. The increase in conductivity with temperature may be due to the decrease in viscosity and hence increased the chain flexibility (Uma, Mahalingam, & Stimming, 2003). The regression value, R^2 for the plot of $\log \sigma$ versus $1000/T$ is almost unity suggesting that the plot obeying the Arrhenius behavior and thermally activated processes. The low value of E_a shows that ionic conduction is facile in GPE films due to the completely amorphous nature of the system. Thus, it will provide greater free volume around the polymer chain and facilitates the fast Mg²⁺ ion motion in the polymer network. This inter-chain or intra-chain ion movements are responsible for the high ionic conductivity in the electrolyte system (Rajendran & Uma, 2000).

It is a well-established fact that for the application in devices operating over a wide range of temperature, it is desirable to have electrolytes with uniform conductivity and low activation energies (Uma, Mahalingam, & Stimming, 2005). In this study, the value of E_a is a minimum of 0.18 eV for the highest conducting GPE film. The values of conductivity, σ and activation energy, E_a obtained in this present work are within the range that reported by other researchers as presented in Table 4.2.

Table 4.2: Conductivity and activation energy values of GPE films using various types of polymer host and magnesium salt

GPE composition	Conductivity (Scm ⁻¹)	E _a (eV)	Reference
PMMA+PC+Mg(ClO ₄) ₂	1.59 x 10 ⁻² (Resistivity, $\rho = 62.8 \Omega \text{ cm}$)	0.21 (19.8 kJ/mol)	(Jiří Vondrák et al., 2003)
PMMA+PC+Mg(ClO ₄) ₂	2.38 x 10 ⁻⁴ (Resistivity, $\rho = 4200 \Omega \text{ cm}$)	0.21 (19.8 kJ/mol)	(Jiří Vondrák, Reiter, Velická, & Sedlářiková, 2004)
PMMA+PC+EC+Mg(CF ₃ SO ₃) ₂	4.20 x 10 ⁻⁴	0.038	(Girish Kumar & Munichandraiah, 2002)
PAN+PC+EC+Mg(CF ₃ SO ₃) ₂	1.80 x 10 ⁻³	0.13 – 0.16	(Girish Kumar & Munichandraiah, 2000)
PVdF-HFP+EC+PC+Mg(ClO ₄) ₂ +MgO	8.0 x 10 ⁻³	0.235	(Pandey, Agrawal, & Hashmi, 2009)

4.2 Dielectric Studies

Dielectric studies are an important tool in understanding the relaxation of dipoles in the polymer complex and the nature of ionic transport mechanism in the given system. Dielectric constant is known as a measure of charge carrier density that is being stored. Figure 4.4 and 4.5 show the plots of dielectric constant, ϵ_r and dielectric loss, ϵ_i against log frequency for the prepared GPE films. It can be seen that the variation in both ϵ_r and ϵ_i rise sharply towards low frequencies. The low frequencies dispersion region is basically attributed to the high contribution of charge accumulation at the electrode-electrolyte interface (D. Kumar & Hashmi, 2010). The highest conducting film with 20 wt.% of $\text{Mg}(\text{CF}_3\text{SO}_3)_2$ salt shows the highest value of dielectric constant, ϵ_r and dielectric loss, ϵ_i .

The increase in dielectric constant is in accordance to the conductivity value which is due to an increase in the number of free ions. This also can be perceived to be either due to electrode polarization effects or due to trace quantities of water that may be retained by the films (Jiří Vondrák et al., 2001). At high frequencies, the periodic reversal of the electric field at the interface occurs so fast that there is no excess ion diffusion in the direction of the field. Thus, the polarization due to the charge accumulation decreases and the drops in the values of ϵ_r and ϵ_i are observed with increasing frequency (Ramesh, Yahaya, & Arof, 2002).

From Figure 4.6 and 4.7, it can be observed that M_r and M_i decrease towards low frequencies. This was attributed to the electrode polarization phenomenon which makes a negligible contribution, and its effect seems to be clearly vanishing towards low-frequency domain. The existence of a long tail at lower frequencies is attributed to the large capacitance associated with the electrodes (S. K. Tripathi, Jain, Gupta, & Mishra, 2012).

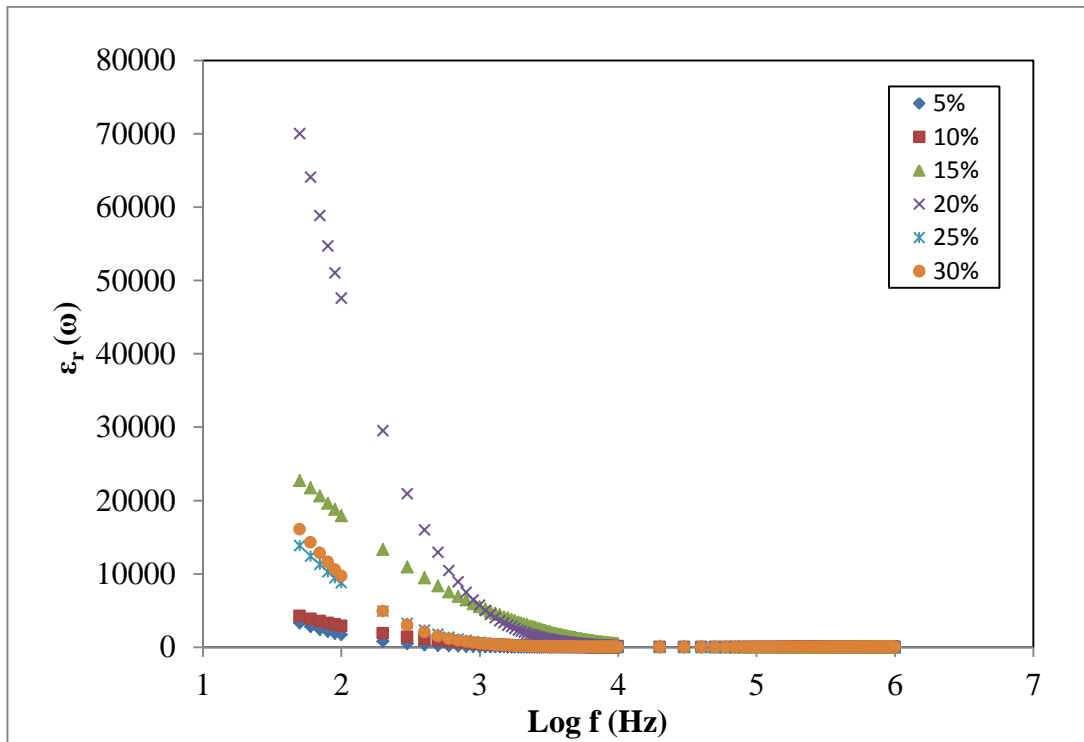


Figure 4.4: Dielectric constant versus frequency for all the films in PMMA-EC-PC-Mg(CF₃SO₃)₂ system.

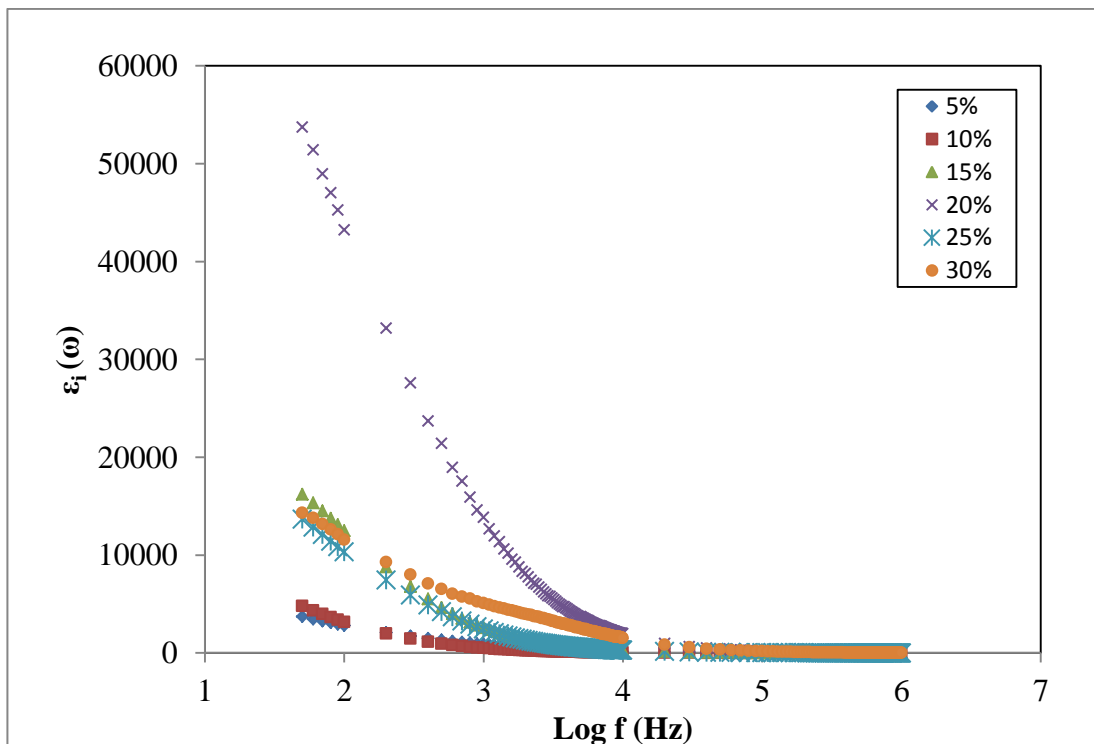


Figure 4.5: Dielectric loss versus frequency for all the films in PMMA-EC-PC-Mg(CF₃SO₃)₂ system.

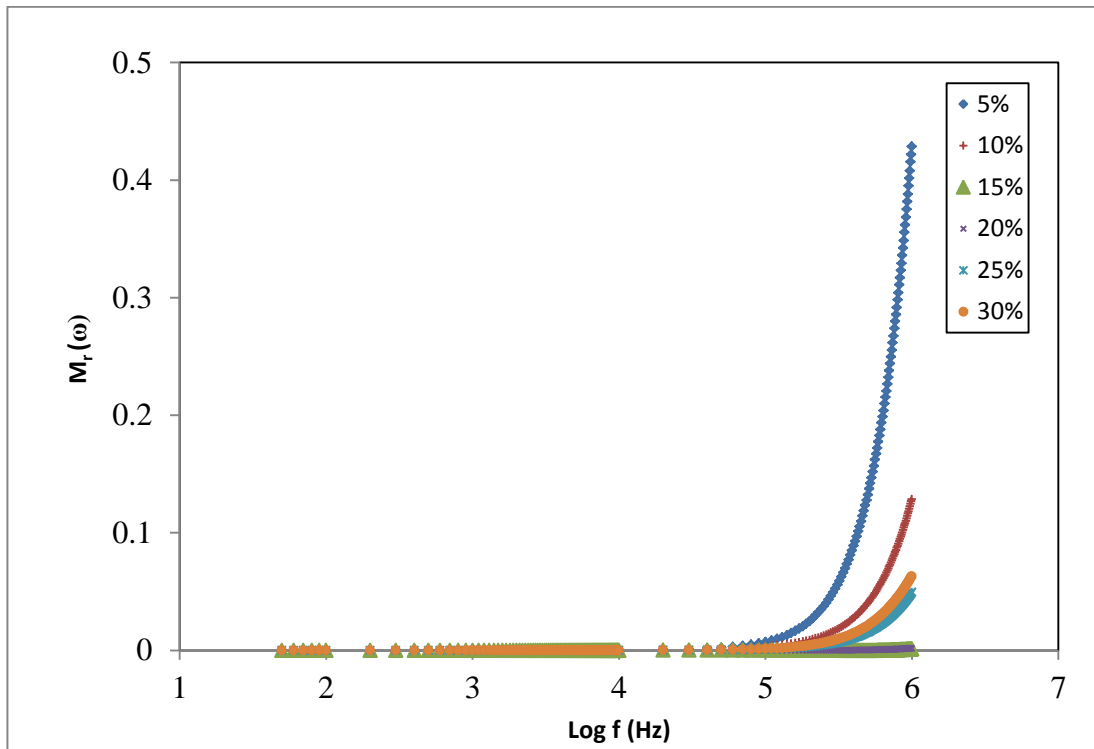


Figure 4.6: Real part of electrical modulus versus frequency for various concentrations of $\text{Mg}(\text{CF}_3\text{SO}_3)_2$ salt in PMMA-EC-PC- $\text{Mg}(\text{CF}_3\text{SO}_3)_2$ system.

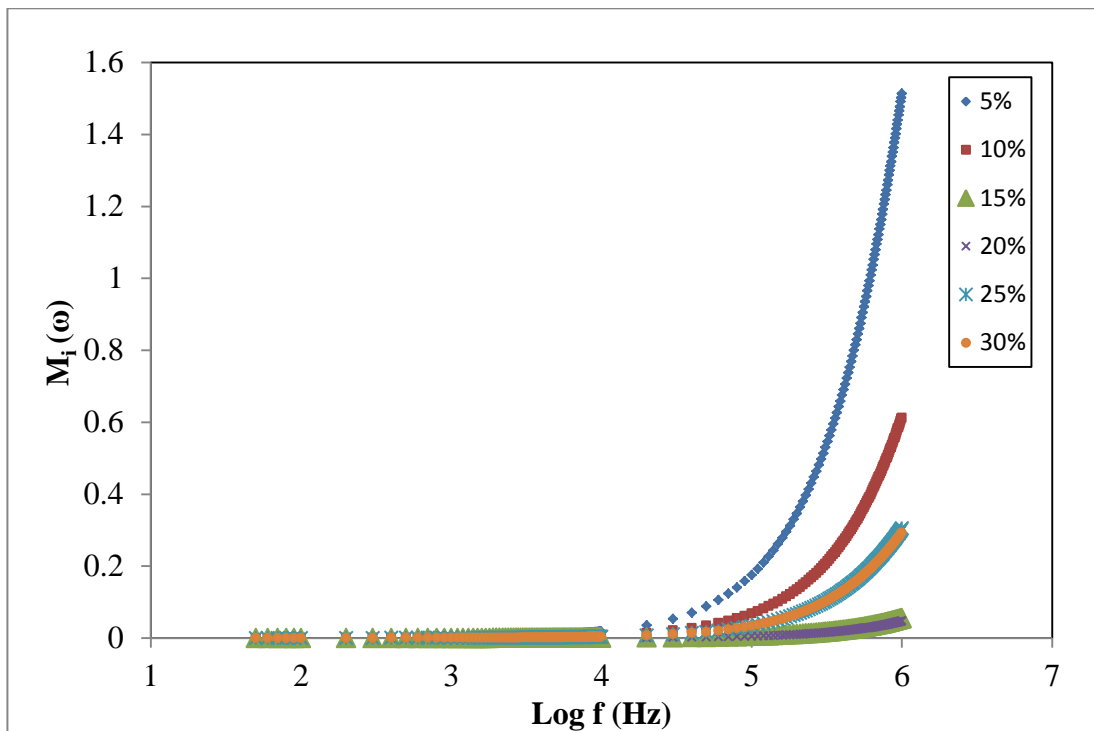


Figure 4.7: Loss tangent versus frequency for various concentrations of $\text{Mg}(\text{CF}_3\text{SO}_3)_2$ salt in PMMA-EC-PC- $\text{Mg}(\text{CF}_3\text{SO}_3)_2$ system.

The plot of loss tangent versus frequency for the GPE films containing various concentrations of salt is depicted in Figure 4.8. It is observed that the position of the peaks corresponds to the order of increased conductivity. The peak of the highest conducting film containing 20 wt.% of $\text{Mg}(\text{CF}_3\text{SO}_3)_2$ salt can be found at the highest frequency value. The plot of this film can be seen clearly in the inset figure. Figure 4.9 illustrates the variation of the conductivity and relaxation time, τ for all GPE films in this system. As the conductivity increases, the relaxation time decreases and this is due to the motion of free charge carriers within the material. When the values of conductivity are increasing, charge carriers will get sufficient time to build up at the electrode-electrolyte interfaces between the materials of electrolyte and electrode. This phenomenon is called “conductivity-relaxation” (Dyre, 1991).

The dielectric constant, ϵ_r and dielectric loss, ϵ_i of the highest conducting film were studied in temperature range between 303 K and 373 K. The trends of dielectric constant, ϵ_r and dielectric loss, ϵ_i show an increasing value with increasing temperature as indicated in the Figure 4.10 and 4.11. The higher values of dielectric constant, ϵ_r and dielectric loss, ϵ_i at higher temperatures can be attributed to the increase in charge carrier density. This also implies that temperature has increased the degree of salt dissociation causing an increase in the number of free ions and dissociation of ion aggregates. Therefore, the dielectric constant, ϵ_r and dielectric loss, ϵ_i are increased.

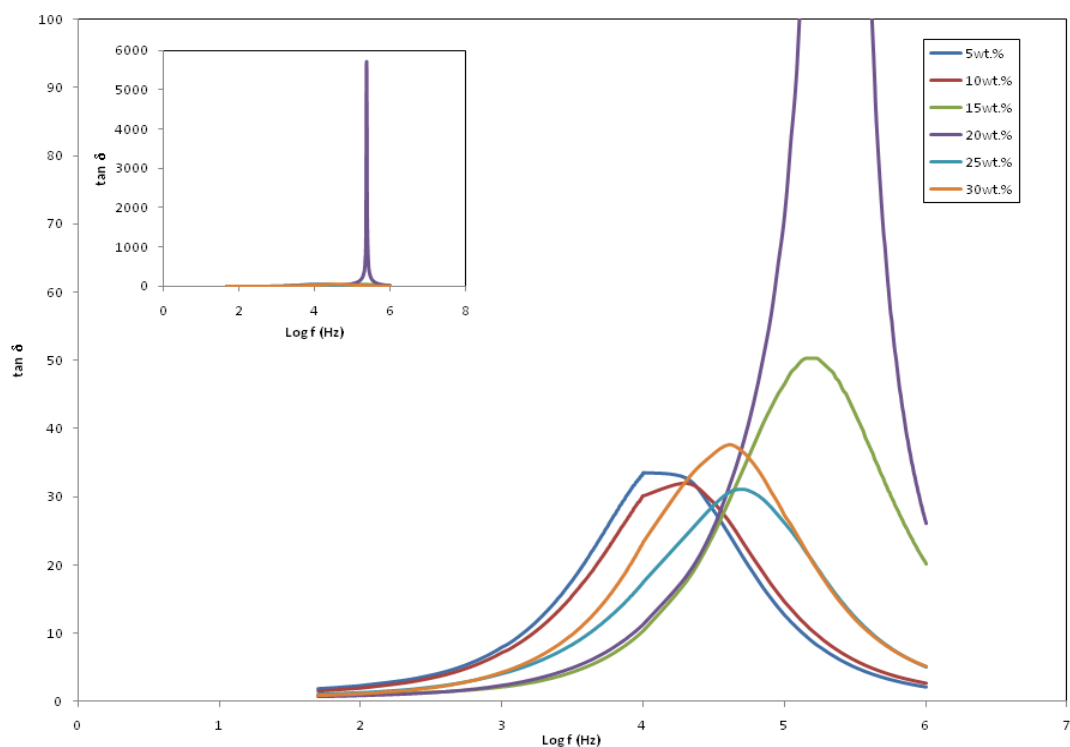


Figure 4.8: Loss tangent versus frequency for various concentrations of salt for film in the PMMA-EC-PC- $\text{Mg}(\text{CF}_3\text{SO}_3)_2$ system.

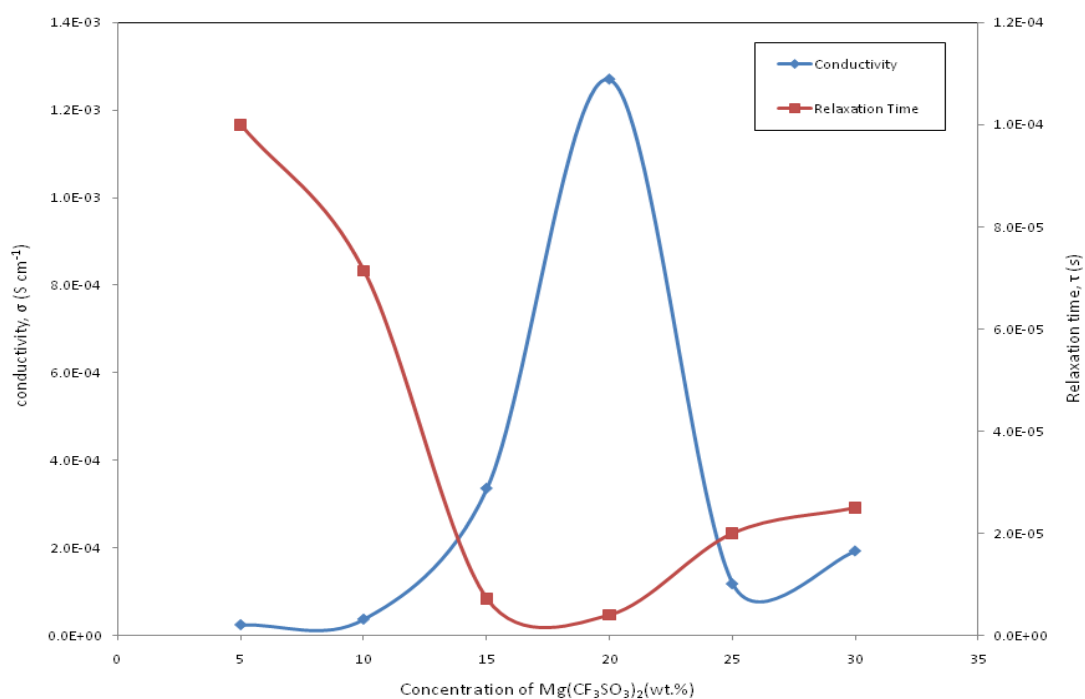


Figure 4.9: The variation of conductivity and relaxation time with amounts of $\text{Mg}(\text{CF}_3\text{SO}_3)_2$ salt in PMMA-EC-PC- $\text{Mg}(\text{CF}_3\text{SO}_3)_2$ system.

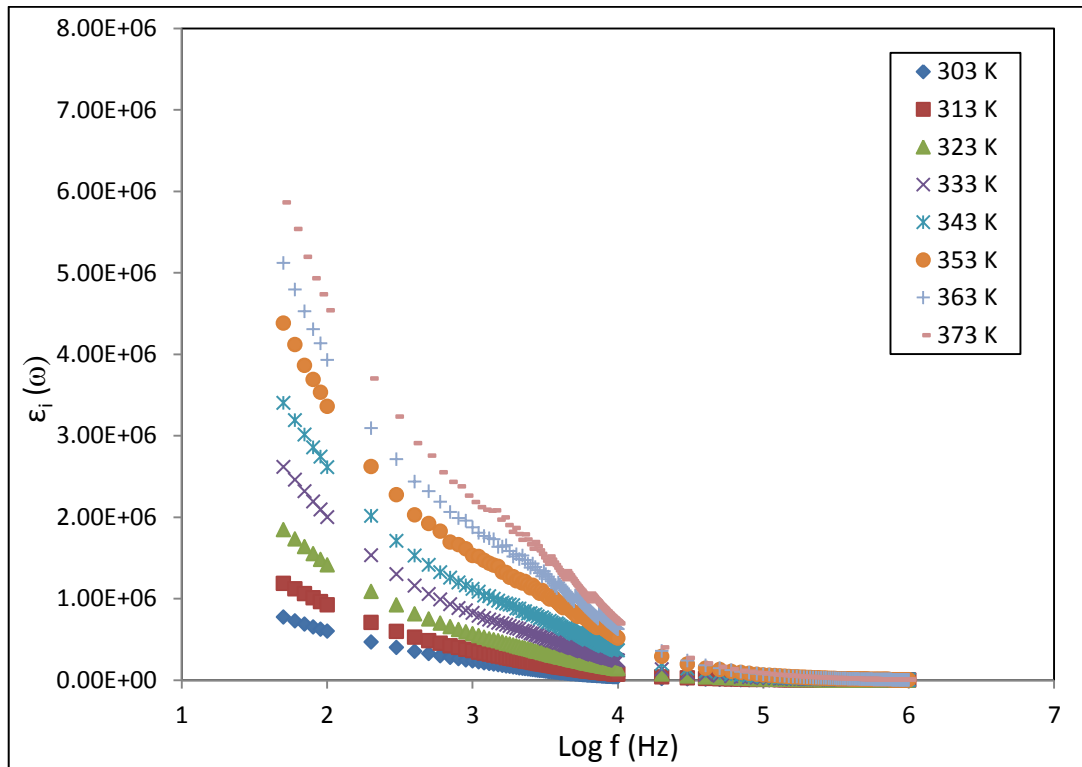


Figure 4.10: Variation of dielectric constant of optimized GPE film as a function of frequencies at various temperatures.

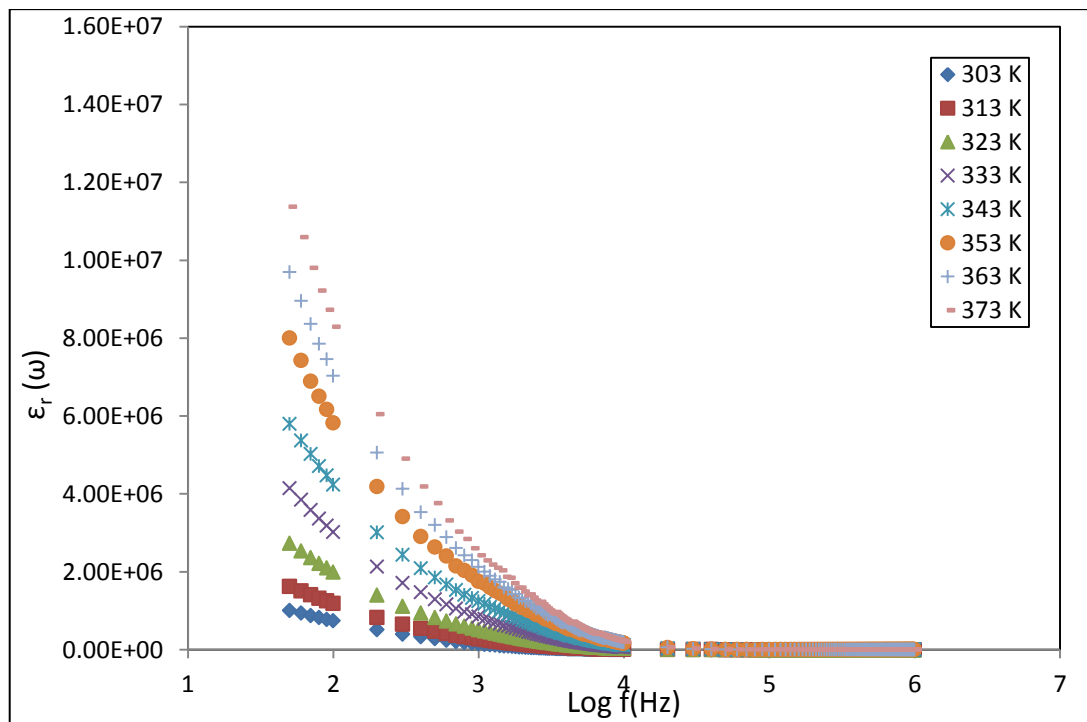


Figure 4.11: Variation of dielectric loss of optimized GPE film as a function of frequencies at various temperatures.

4.3 Transport Number Studies

4.3.1 Ionic Transport Number

Transport number measurements are very important parameters for ionic conductors in terms of their practical application. The total ionic transport number, t_{ion} was measured using the D.C polarization method. In this method, the D.C. current is monitored as a function of time on the application of fixed D.C. voltage (0.5 V) across the SS|GPE|SS (SS: stainless steel) for the films containing 5wt.%, 20wt.%, and 30wt.% of $Mg(CF_3SO_3)_2$ salt. The stainless steel electrodes act as blocking electrodes.

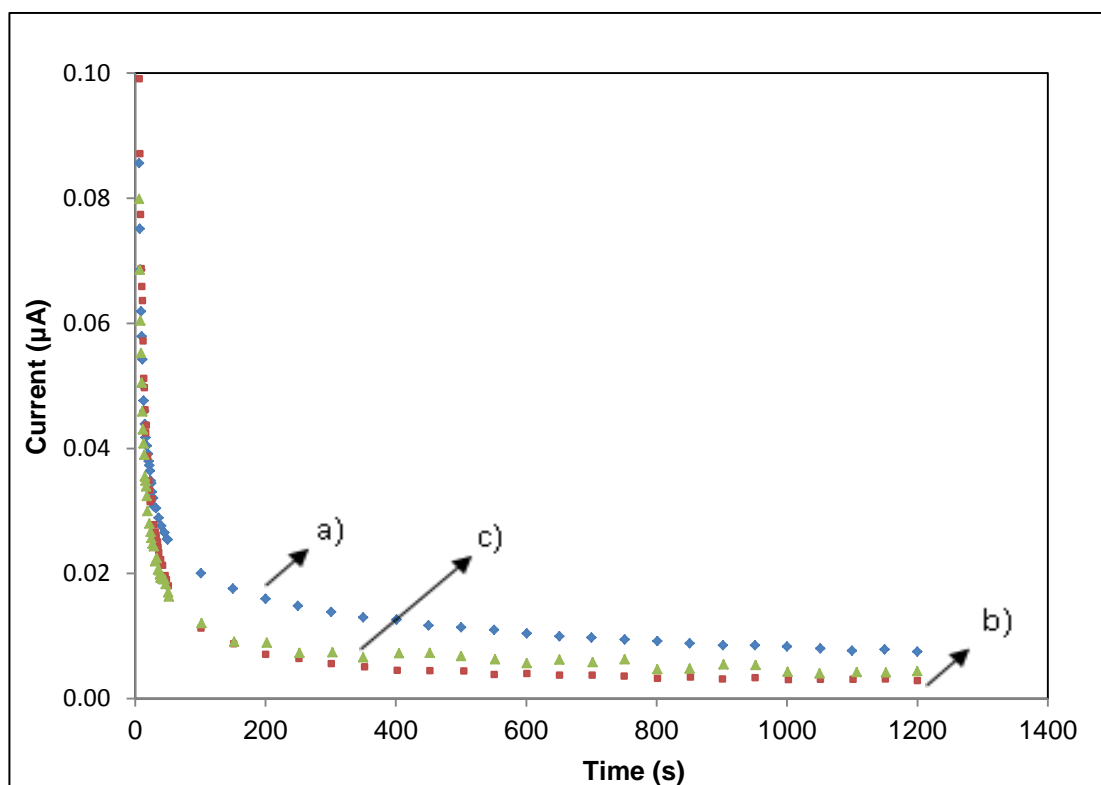


Figure 4.12: Normalized current versus time plots for GPE films containing (a) 5wt%, (b) 20wt%, and (c) 30wt% of $Mg(CF_3SO_3)_2$ salt.

Figure 4.12 shows the polarization current plot as a function of time at room temperature for GPE films containing 5wt.%, 20wt.%, and 30wt.% of $\text{Mg}(\text{CF}_3\text{SO}_3)_2$ salt. It is observed that the values of ionic transference number i.e. calculated using equation (3.19) for the films containing 5wt.%, 20wt.%, and 30wt.% of $\text{Mg}(\text{CF}_3\text{SO}_3)_2$ salt are found to be more than 0.99. The current decrease with time shows that the total conductivity of the polymer electrolytes is predominantly ionic. No electronic charge carriers that can contribute to conductivity are expected in the gel-like electrolytes where liquid electrolytes are entrapped in the polymer network. (Pandey & Hashmi, 2009).

4.3.2 Transport Number of Mg^{2+} ions

The cationic transport number measurement is an important study to determine the performance of the GPE film from its application point of view, i.e. magnesium rechargeable batteries. The transport number, t_+ of Mg^{2+} ions in the GPEs was evaluated by the method that was proposed by Evans et al. (Bruce, Evans, & Vincent, 1988) using the combination of A.C. impedance spectroscopy and D.C. polarizations of $\text{Mg}|\text{GPE}|\text{Mg}$ cell for the highest conducting film. According to this method, the cells were polarized by applying a constant voltage, $\Delta V = 0.3$ V for 20 hours and subsequently initial and final currents were recorded. The cells were subjected to A.C. impedance measurements prior to and after the polarization. The values of electrode-electrolyte contact resistances were obtained from the impedance plots.

The transport number, t_+ values were determined using the equation (3.20).

Figure 4.13 shows the impedance plot before and after D.C. polarization of a typical symmetric Mg|GPE|Mg cell. Figure 4.14 exhibits the polarization current plot as a function of time for the highest conducting GPE film containing 20 wt.% of $\text{Mg}(\text{CF}_3\text{SO}_3)_2$ salt in PMMA-EC-PC- $\text{Mg}(\text{CF}_3\text{SO}_3)_2$ system with Mg|GPE|Mg cell. The value of Mg^{2+} ions transport number was found to be 0.38 for the highest conducting GPE film. Kumar et al. (Girish Kumar & Munichandraiah, 2002) obtained the value of Mg^{2+} ions transport number of 0.33 at room temperature for PMMA-based GPE using 0.5 g of $\text{Mg}(\text{CF}_3\text{SO}_3)_2$ salt.

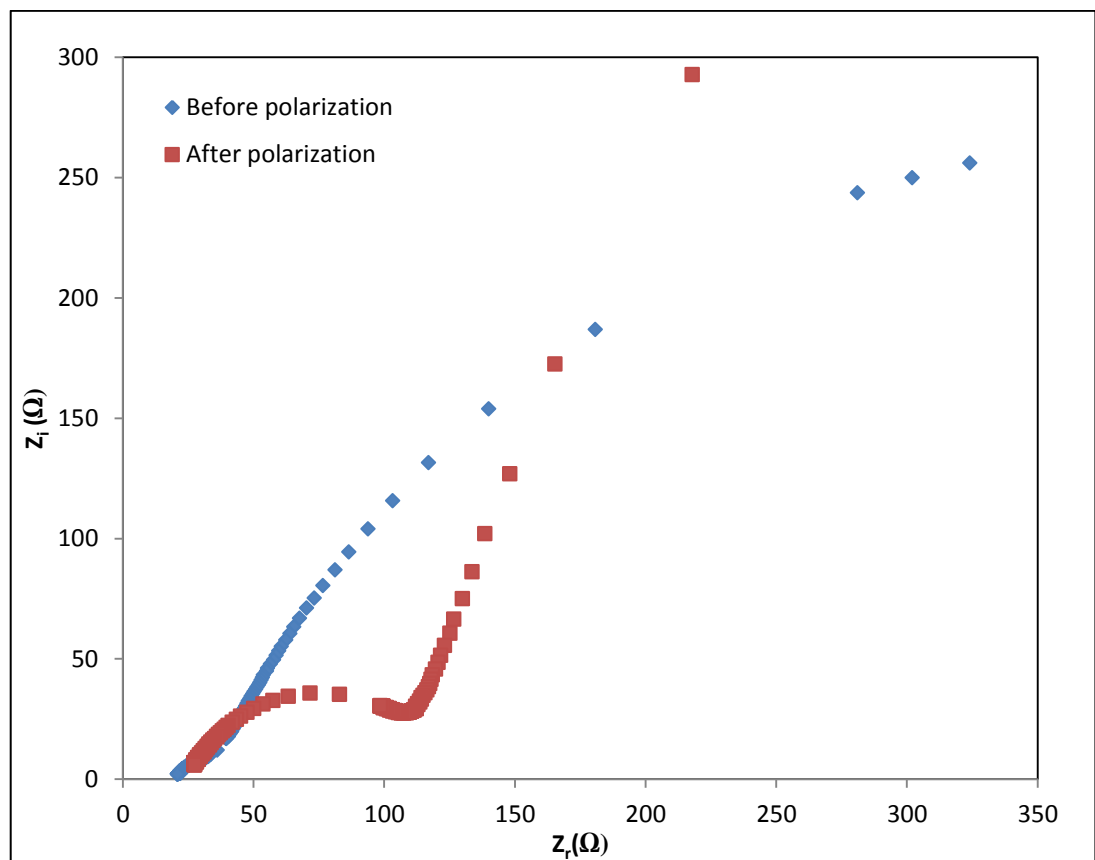


Figure 4.13: A.C. complex impedance plot before and after D.C. polarization of a typical symmetric Mg|GPE|Mg cell.

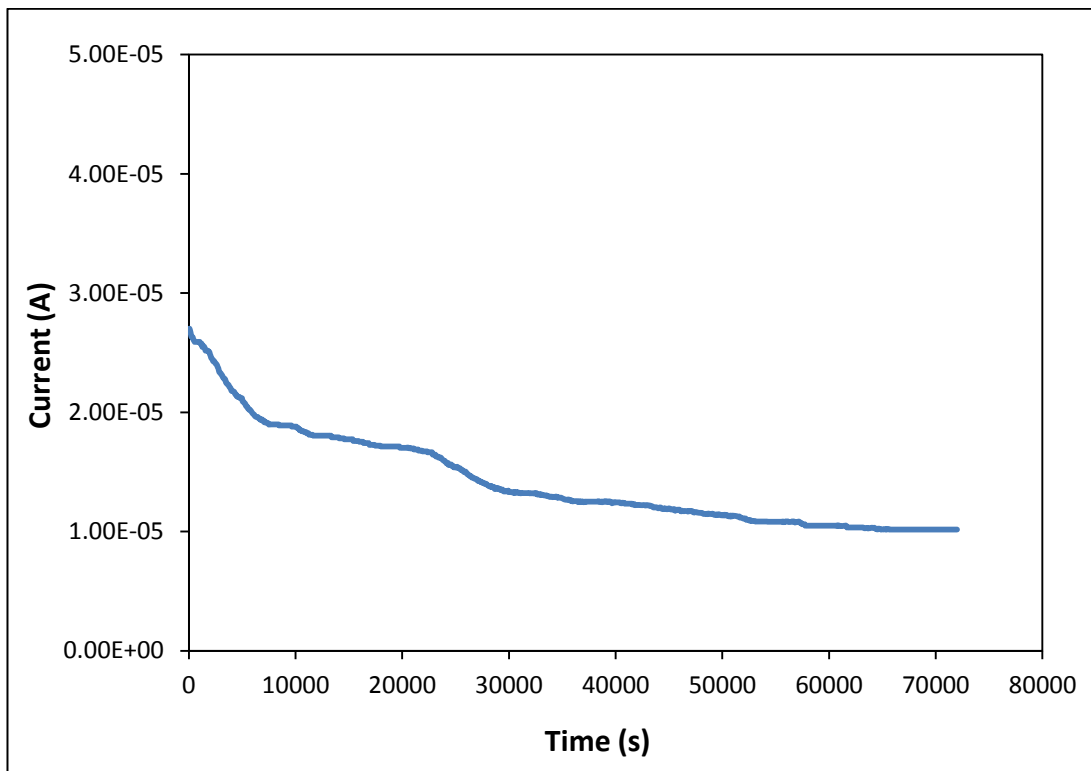


Figure 4.14: Polarization current plot as a function of time for the highest conducting film in PMMA-EC-PC-Mg(CF₃SO₃)₂ system with Mg|GPE|Mg cell.

Structural Studies

4.4 Fourier Transform Infra-Red Spectroscopy (FTIR) Analysis

An infrared spectrum represents a fingerprint of a sample with absorption peaks which correspond to the frequencies of vibrations between the bonds of atoms making up the material. Therefore, Infrared Spectroscopy has been a workhorse technique for analyzing the materials. This technique can be used to identify the unknown materials and to determine the interaction between components in the sample. In this study, the Fourier Transform Infrared (FTIR) analysis is performed by using Thermo Scientific Nicolet is10 Smart ATR spectrophotometer in the wave number range from 650 to 4000 cm^{-1} with resolution of 1 cm^{-1} . The purpose of this analysis is to investigate ion-polymer interaction of the prepared gel polymer electrolytes films in PMMA-EC-PC-Mg(CF₃SO₃)₂ system and the possible changes occurred in the films due to the effect of magnesium salt concentrations and the plasticizing solvent.

4.4.1 Pure PMMA film

The vibrational modes and wavenumbers of pure PMMA film are listed in Table 4.3. Figure 4.15 shows FTIR spectrum of pure PMMA film in the region of 650 cm^{-1} and 2000 cm^{-1} . As can be observed, the band that peaks at 837 cm^{-1} and 966 cm^{-1} are assigned to C – O – C symmetrical stretching. O – CH₃ stretching mode has been observed at band that peaks at 1149 cm^{-1} and 1160 cm^{-1} while the peak at 1230 cm^{-1} is due to C – O stretching. The absorption peaks appearing at 1388 cm^{-1} , 1460 cm^{-1} and 1725 cm^{-1} are correspond to O – CH₃ deformation, CH₃ bending and C = O stretching of PMMA, respectively. The vibrational mode that peak at 2960 cm^{-1} may be assigned to asymmetric stretching of CH₃.

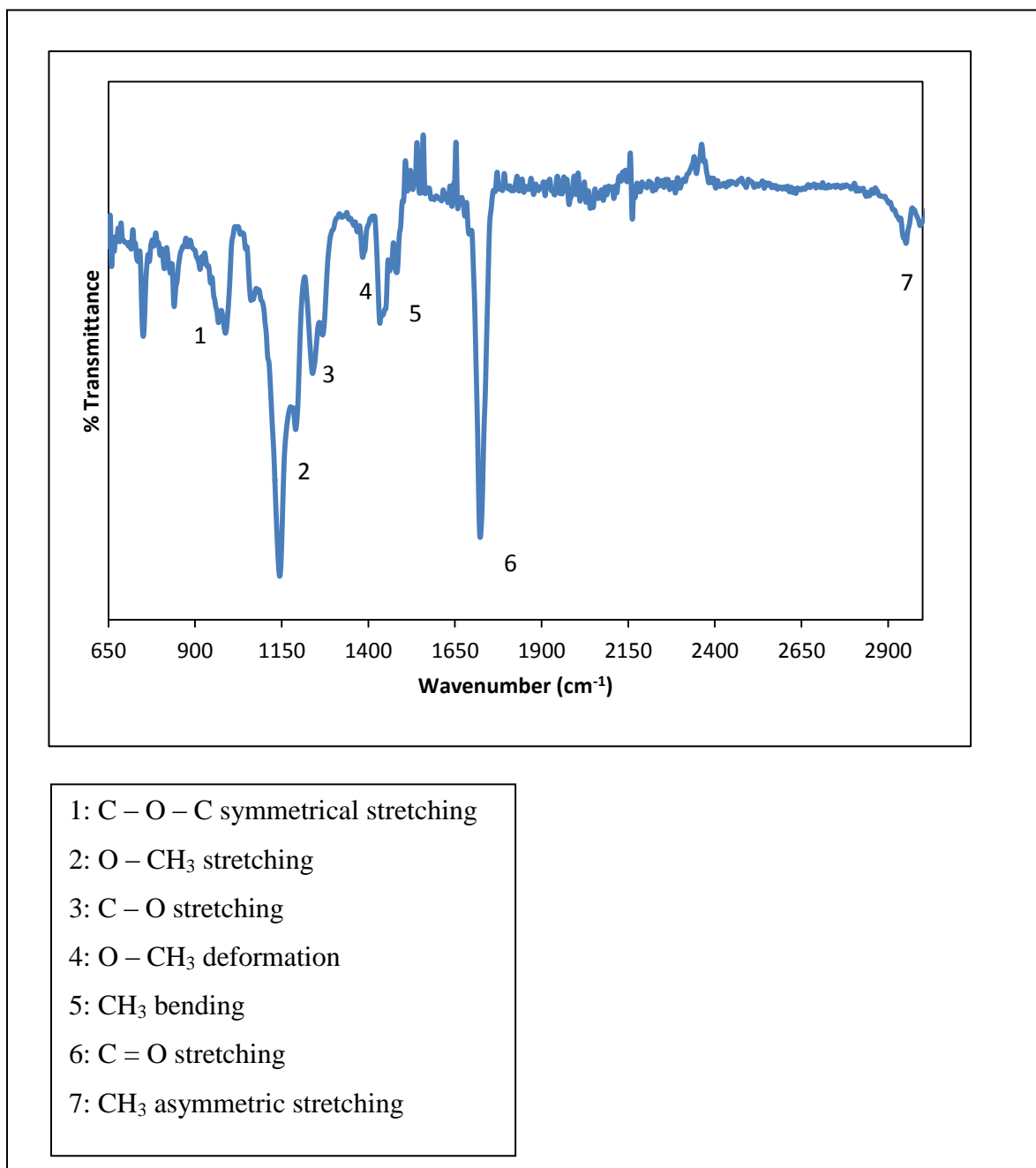


Figure 4.15: FTIR spectra of pure PMMA film in the region 650 cm⁻¹ and 3000 cm⁻¹.

Table 4.3: The vibrational modes and wavenumbers of pure PMMA film.

Vibrational modes	Wavenumbers (cm ⁻¹)	References	Results observed
C – O – C symmetrical stretching	874, 840, 964	(Uma et al., 2003)	837, 966
O - CH ₃ stretching	1159, 1152	(Rajendran, Kannan, & Mahendran, 2001)	1149, 1160
C – O stretching	1280, 1235	(Rajendran, Mahendran, & Kannan, 2002)	1230
O - CH ₃ deformation	1389	(Uma et al., 2005)	1384
CH ₃ bending	1452, 1440, 1458, 1448, 1443	(Rajendran et al., 2001)	1430, 1460
C = O stretching	1724, 1734, 1745	(Rajendran & Uma, 2000)	1722
CH ₃ stretching	3004	(Saikia & Kumar, 2005)	2960

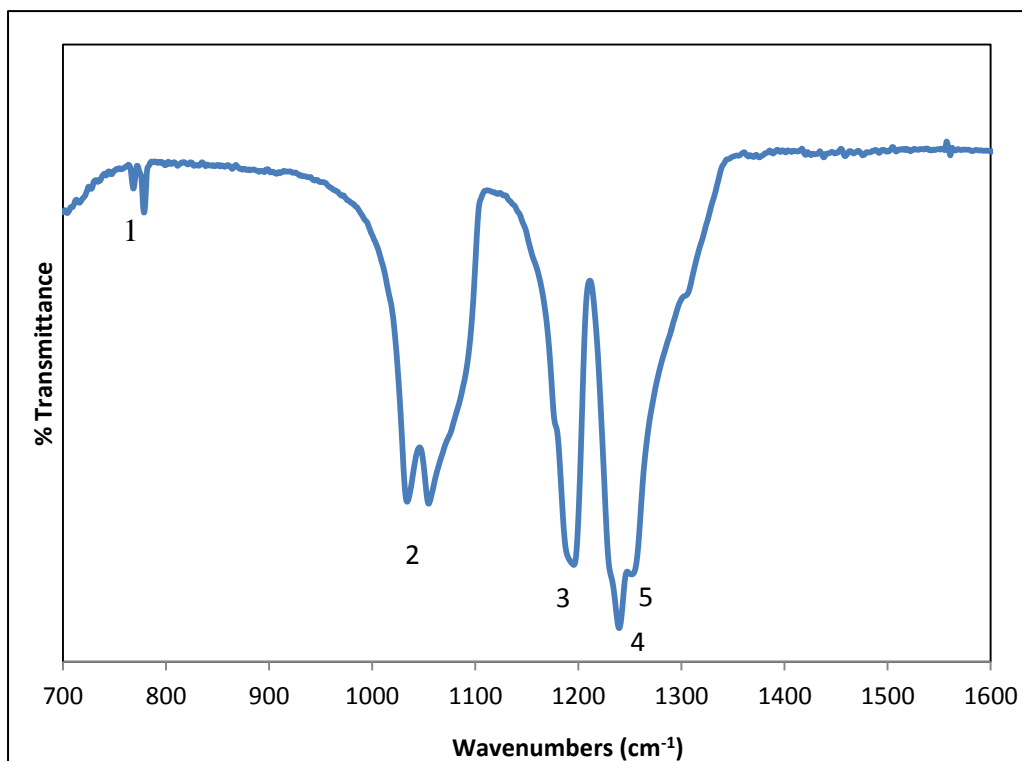
4.4.2 Mg(CF₃SO₃)₂ salt

The salt generally provides free ions which take part in the conduction process. Magnesium triflate or Mg(CF₃SO₃)₂ is an inorganic salt that have large anion and low lattice energy which may assisted in ion dissociation thus increase the conductivity. In these anions, the delocalization of the formal negative charge is practically realized by a combination of the inductive effect of the electron-withdrawing groups and the conjugated structures (Ahmad, 2009). The cation of the salt is expected to coordinate with the polar groups in the host polymer matrix and this interaction will affect the structure of the polymer backbone and also certain vibrational modes.

The vibrational modes and wavenumbers of $\text{Mg}(\text{CF}_3\text{SO}_3)_2$ salt are listed in Table 4.4. FTIR spectrum of pure $\text{Mg}(\text{CF}_3\text{SO}_3)_2$ salt was recorded in the region between 700 cm^{-1} and 1600 cm^{-1} as shown in Figure 4.16. In the present study, the FTIR bands due to free ions of $\text{Mg}(\text{CF}_3\text{SO}_3)_2$ salt are obtained at 777 cm^{-1} and 1030 cm^{-1} which is assigned to symmetric CF_3 deformation, ($\delta_s(\text{CF}_3)$) and symmetric SO_3 stretching, ($\nu_s(\text{SO}_3)$), respectively. The band due to ion pairs of triflate anions is observed at 1050 cm^{-1} while the absorption peaks at 1190 cm^{-1} and 1230 cm^{-1} are assigned to CF_3 asymmetric and symmetric stretching, respectively. The peak appearing at 1250 cm^{-1} is assigned to SO_3 asymmetric stretching modes of triflate.

Table 4.4: The vibrational modes and wavenumbers of pure $\text{Mg}(\text{CF}_3\text{SO}_3)_2$ salt.

Vibrational modes	Wavenumbers (cm^{-1})	References	Result observed
CF_3 symmetric deformation, δ_s	760; 752, 757, 762, 764, 756	(Chintapalli & Frech, 1996)	767, 777
SO_3 symmetric stretching, ν_s	1032, 1031	(Ramesh, Leen, Kumutha, & Arof, 2007)	1030
CF_3 asymmetric stretching, ν_{as}	1182	(Huang et al., 1996)	1190
SO_3 asymmetric stretching, ν_{as}	1272, 1257	(Uma et al., 2005)	1250
CF_3 symmetric stretching, ν_s	1222, 1157	(Uma et al., 2003)	1230



1: symmetric CF₃ deformation

2: symmetric SO₃ stretching

3: asymmetric CF₃ stretching

4: symmetric CF₃ stretching

5: asymmetric SO₃ stretching

Figure 4.16: FTIR spectrum of pure Mg(CF₃SO₃)₂ salt in the range of 700 cm⁻¹ and 1600 cm⁻¹.

4.4.3 PMMA-EC-PC film

Figure 4.17 show the infrared spectra of pure PC and pure EC in the range of 1000 cm^{-1} and 2000 cm^{-1} . In pure EC film, the skeletal stretching bands are observed at 1062 cm^{-1} and 1139 cm^{-1} while the band that peak at 1392 cm^{-1} is due to CH_2 wagging. The peak at 1472 cm^{-1} may be assigned to CH_2 bending. According to Wang and co-workers [11], EC has a pair of intense doublets that peak at 1774 cm^{-1} and 1803 cm^{-1} . These doublets are due to $\text{C} = \text{O}$ stretching mode. In this study, the doublets are observed at 1773 cm^{-1} and 1792 cm^{-1} .

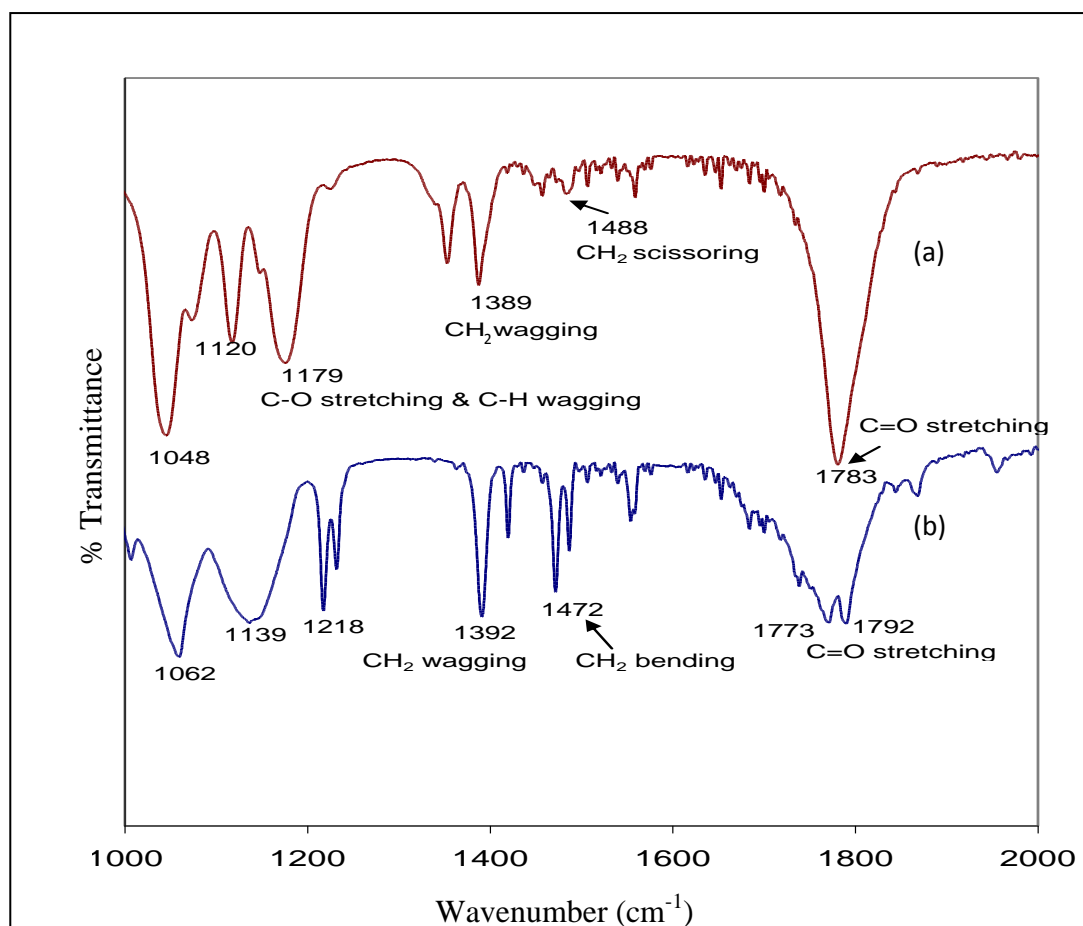


Figure 4.17: FTIR spectra of (a) pure PC and (b) pure EC in the range of 1000 cm^{-1} and 2000 cm^{-1} .

In pure PC, the absorption peaks at 1179 cm^{-1} is due to C – O stretching and C – H wagging. As can be seen from the Figure 4.17 (a), the bands of CH₂ wagging and scissoring were peak at 1389 cm^{-1} and 1488 cm^{-1} , respectively. The peak of C = O stretching band can be found at 1783 cm^{-1} .

Figure 4.18 depicts the FTIR spectrum of PMMA-EC-PC film in the range of 1000 cm^{-1} and 2000 cm^{-1} . From pure PMMA film, the band that peaks at 1056 cm^{-1} and 1074 cm^{-1} are shifted to 1053 cm^{-1} and 1072 cm^{-1} , respectively while the peak at 1159 cm^{-1} is shifted to 1161 cm^{-1} when plasticizing solvent, EC and PC were added. The C – O – C stretching bands at 1250 cm^{-1} and 1280 cm^{-1} of pure PMMA are decrease in intensity and shifted to 1248 cm^{-1} and 1278 cm^{-1} . It is also found that the peak at 1388 cm^{-1} of pure PC and 1392 cm^{-1} of pure EC are combined and formed a new peak at 1390 cm^{-1} . Due to the interaction between the EC and PC, the bands that peak at 1472 cm^{-1} and 1488 cm^{-1} which is assigned to CH₂ bending and scissoring, respectively appeared at 1480 cm^{-1} . The absorption peak at 1725 cm^{-1} which is due to C = O stretching is shifted to 1730 cm^{-1} in the complexes. It can be observed from the figure, the intensity peaks of C = O stretching at 1773 cm^{-1} and 1792 cm^{-1} of EC is increase in plasticized PMMA system. Intensity of these peaks increases due to the interaction with strong band at 1783 cm^{-1} of PC.

Thus, it can be suggested that the changes in the position and intensity of vibrational modes of the pure EC and PC in the polymer complexes indicated that the interaction between the polymer and the plasticizing solvent has occurred.

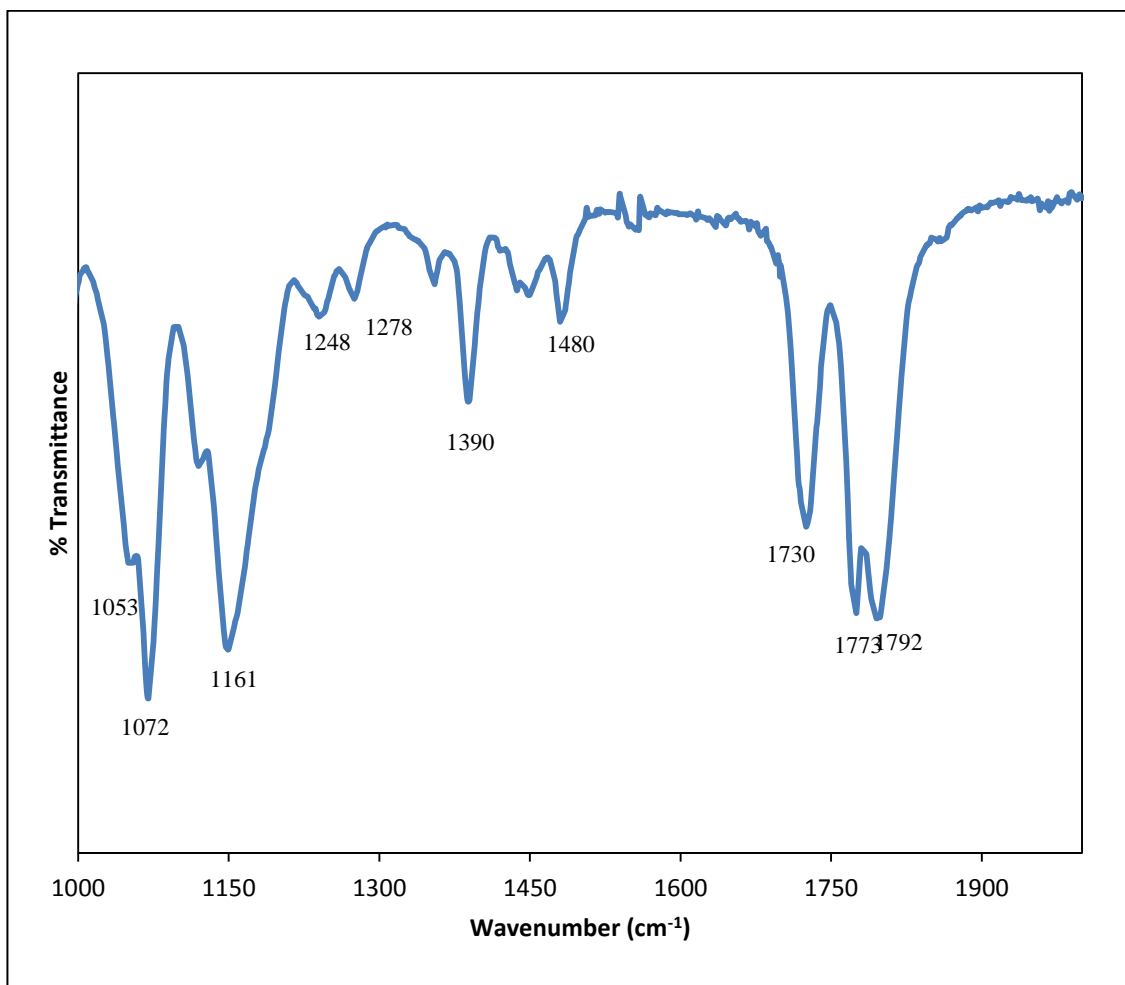


Figure 4.18: The FTIR spectrum of PMMA-EC-PC film in the range of 1000 cm^{-1} and 2000 cm^{-1} .

4.4.4 PMMA-EC-PC-Mg(CF₃SO₃)₂ system

Figure 4.19 shows the FTIR spectra of pure PMMA film, Mg(CF₃SO₃)₂ salt, PMMA-EC-PC film and GPE films containing 5 wt.% to 30 wt.% of Mg(CF₃SO₃)₂ salt in the wave number region of 650 cm⁻¹ – 2000 cm⁻¹. This is the region where the O-CH₃ stretching, O-CH₃ deformation and C=O stretching bands of PMMA, C=O stretching band of EC and PC are located. On addition of salt into the system, it can be observed that the peaks are shifted, intensity of the peaks is changed and the peaks became broader. This implies that the salt has interacts with the PMMA polymer and plasticizing solvent. This interaction will influence the local structure of the polymer backbone and certain modes of vibration will also be affected. Figure 4.20 depicts the FTIR spectra of pure PMMA film, Mg(CF₃SO₃)₂ salt, PMMA-EC-PC film and GPE films containing 5 wt.% to 30 wt.% of Mg(CF₃SO₃)₂ salt in the region between 650 cm⁻¹ and 850 cm⁻¹. The bands that peak at 716 cm⁻¹ and 774 cm⁻¹ in GPE film without salt is due to C=O bending of EC and ring deformation of PC, respectively. The intensity of this band is decreases and shifted towards higher wavenumbers as percentage of salt is increased. This indicates that the salt has interacts with the plasticizing solvent, EC and PC.

Figure 4.21 shows the FTIR spectra of of pure PMMA film, Mg(CF₃SO₃)₂ salt, PMMA-EC-PC film and GPE films containing 5 wt.% to 30 wt.% of Mg(CF₃SO₃)₂ salt in the region between 900 cm⁻¹ and 1600 cm⁻¹. Significant changes can be found in the band that peaks at 1030 cm⁻¹ which is assigned to $\nu_s(\text{SO}_3)$ of free triflate ions. It is to be noted that in the present work, the amount PMMA and plasticizing solvent (EC and PC) is fixed.

Therefore, as the salt concentrations increase (from 5 wt.% to 30 wt.%), the intensity of the peak is increasing as the amount of free triflate ions increased. Hence this will contribute to the higher conductivity in the GPE films. In Figure 4.21, the band at 1050 cm^{-1} and 1070 cm^{-1} are due to ring breathing and skeletal stretching of EC. It can be noticed that, there is no significant changes in the band at 1070 cm^{-1} when the salt is added. However, on addition of $\text{Mg}(\text{CF}_3\text{SO}_3)_2$ salt, a band at 1050 cm^{-1} decreases as the salt contents increase. This may be attributed to ring breathing of plasticizer, EC associated with the co-existence of ion $\nu_s(\text{SO}_3)$ modes of ion pairs of triflate anions (Jiří Vondrák et al., 2001).

Figure 4.22 presents the FTIR spectra of pure PMMA film, $\text{Mg}(\text{CF}_3\text{SO}_3)_2$ salt, PMMA-EC-PC film and GPE films containing 5 wt.% to 30 wt.% of $\text{Mg}(\text{CF}_3\text{SO}_3)_2$ salt in the wave number region of $1600\text{ cm}^{-1} - 2000\text{ cm}^{-1}$. It can be observed that the bands at 1725 cm^{-1} is correspond to C=O stretching of pure PMMA while the bands that peak at 1772 cm^{-1} and 1795 cm^{-1} are due to C=O stretching of EC and PC. It can also be observed that, on addition of the salt, the doublet bands of the plasticizing solvent (EC and PC) of GPE film without salt at 1772 cm^{-1} and 1795 cm^{-1} becomes slightly broader and decreases in intensity. These observations indicate that the magnesium ions (Mg^{2+}) have coordinated to lone pair electrons of oxygen atoms of C=O in PMMA, EC and PC.

Figure 4.23 shows the deconvolution part for all the GPE films in the range of 1000 cm^{-1} to 1100 cm^{-1} . Three decomposed bands that peak at approximately 1030 , 1050 and 1070 cm^{-1} have been observed from the Figure 4.23. A band that peaks at 1030 cm^{-1} is attributed to free ions while the bands that peak at 1050 and 1070 cm^{-1} are due to ion pairs and ion aggregates, respectively. At high concentration of $\text{Mg}(\text{CF}_3\text{SO}_3)_2$ salt, the viscosity of the GPE films increase thus the ions associated arise from various ions pairs and aggregates. The free ions curve exhibits a maxima and the ion aggregates curve exhibits a minimum at 20 wt.% salt concentration which is the highest conducting

GPE film. As salt concentration increases from 25 wt.% to 30 wt.%, the decrease in conductivity can be explained by the decrease in free ions and the increase in ion aggregates.

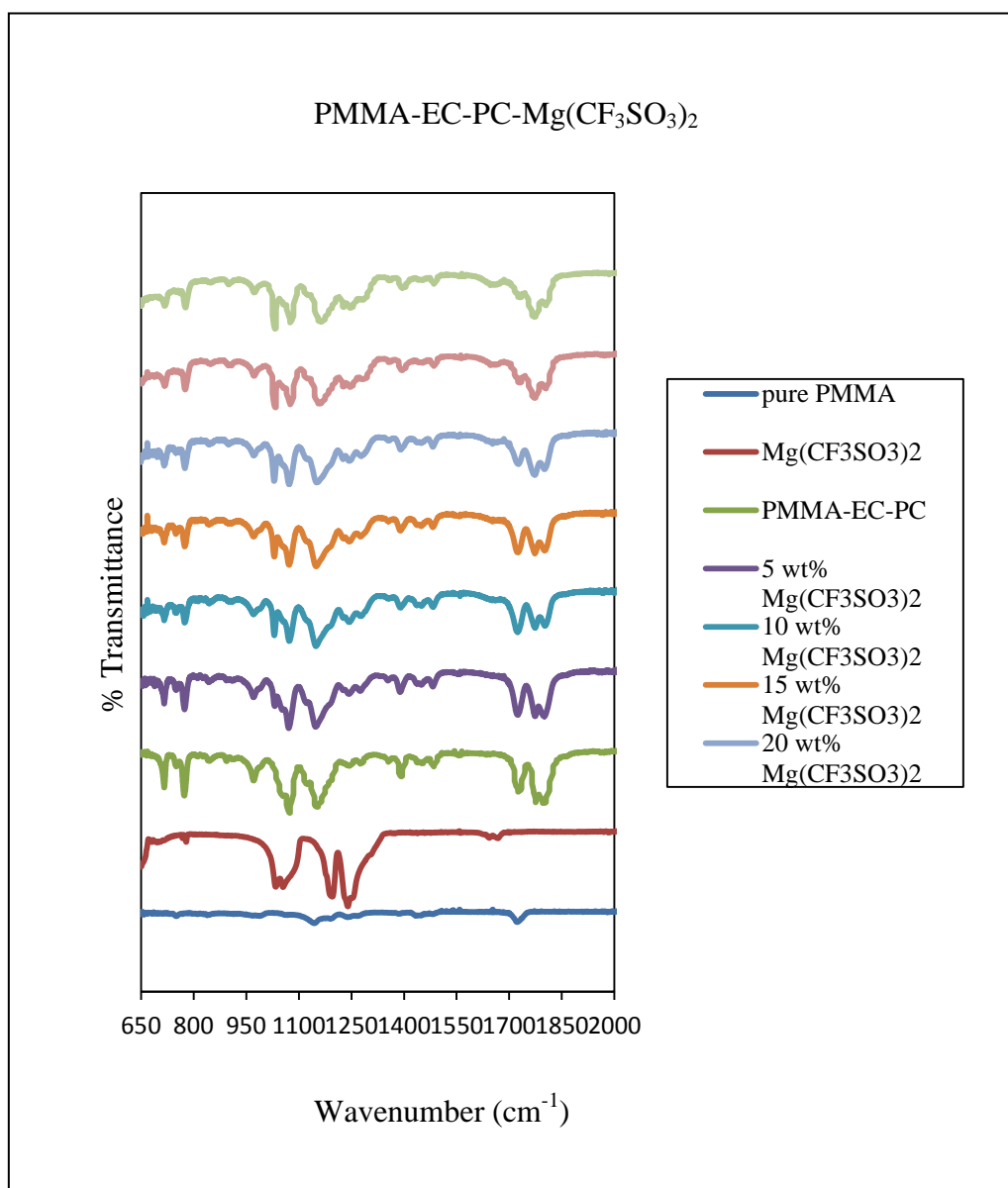


Figure 4.19: FTIR spectra of pure PMMA, pure Mg(CF₃SO₃)₂ and PMMA based GPE films with 5 wt% to 30 wt% of Mg(CF₃SO₃)₂

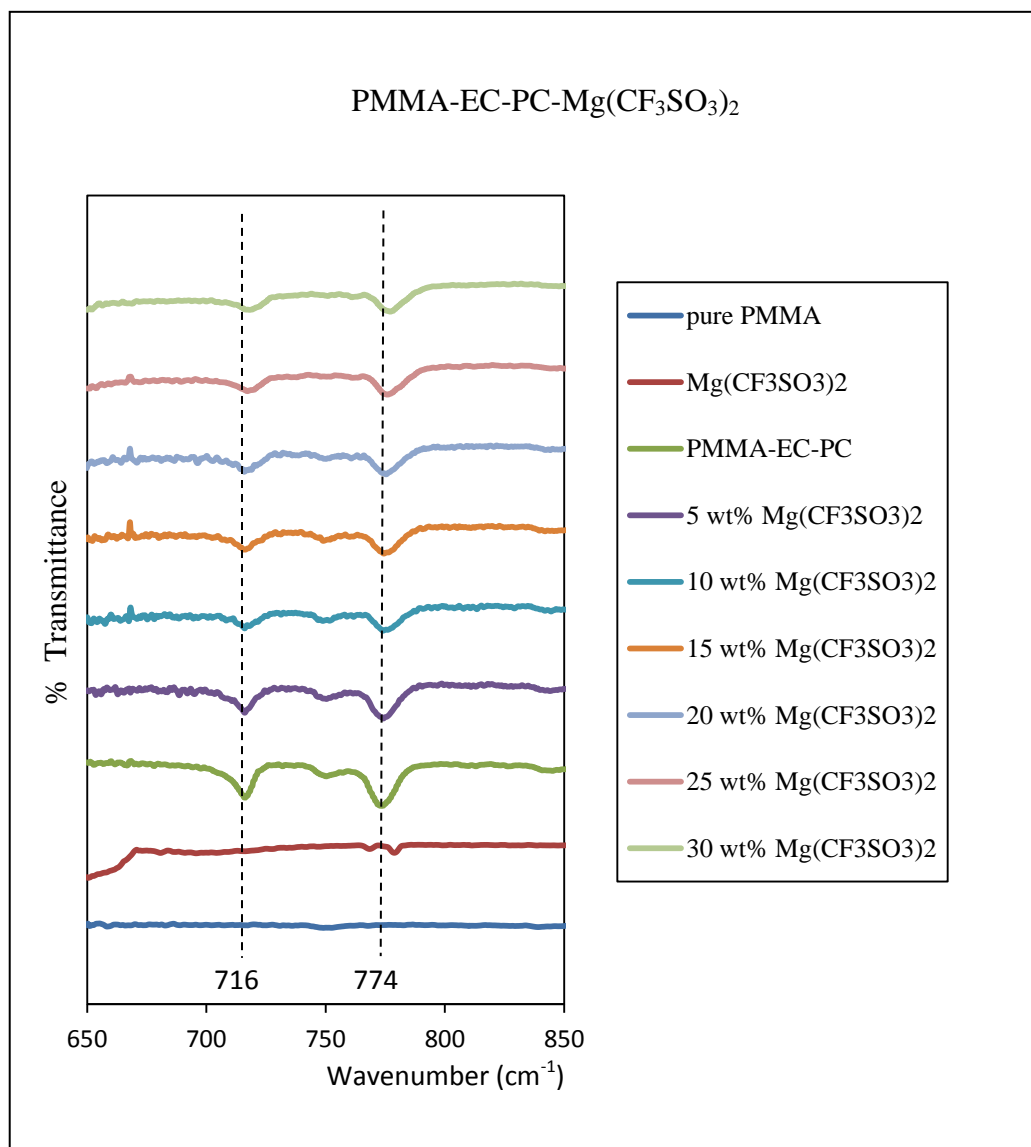


Figure 4.20: FTIR spectra of pure PMMA, pure Mg(CF₃SO₃)₂ and PMMA based GPE films with 5 wt% to 30 wt% of Mg(CF₃SO₃)₂

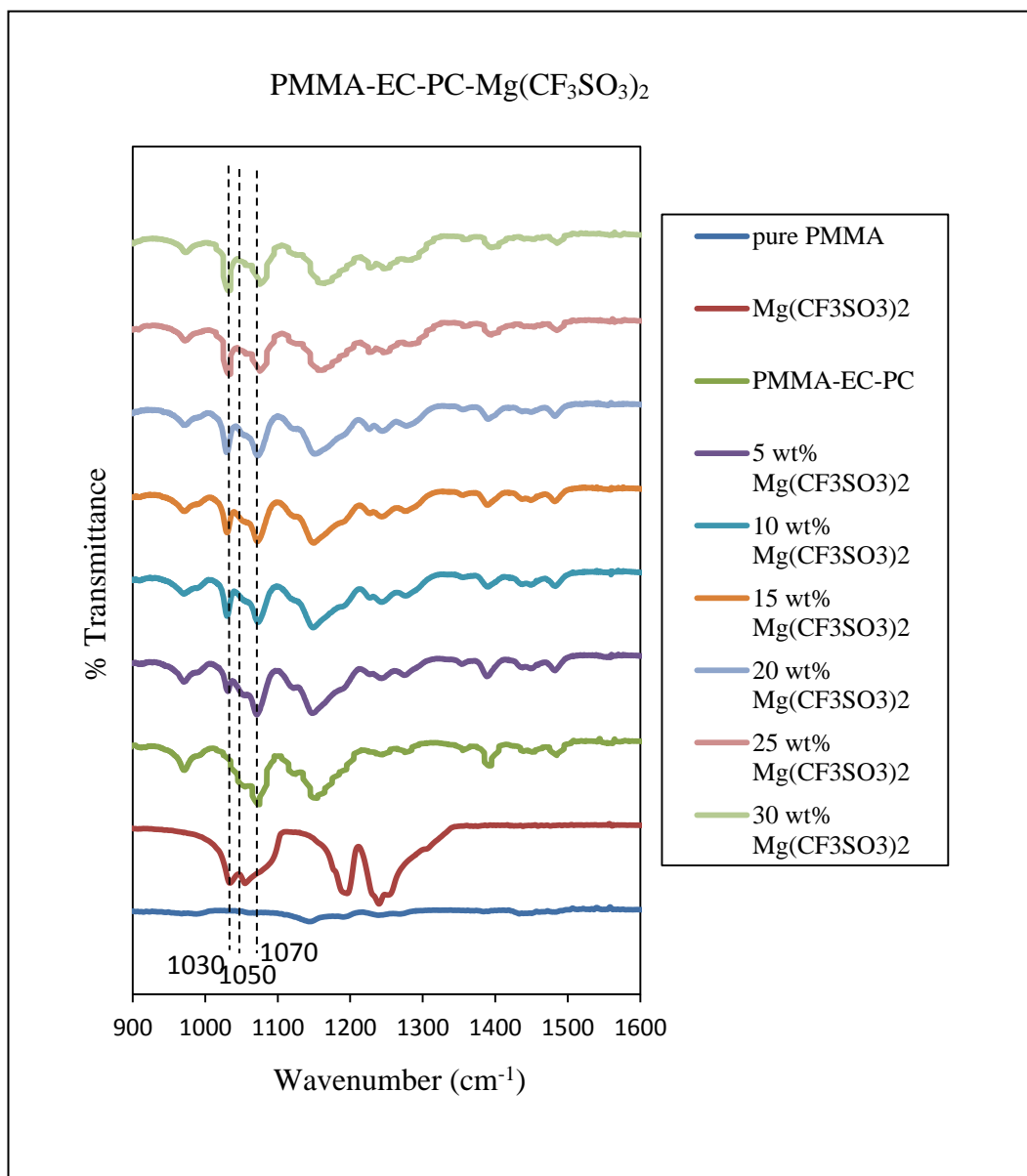


Figure 4.21: FTIR spectra of pure PMMA, pure Mg(CF₃SO₃)₂ and PMMA based GPE films with 5 wt% to 30 wt% of Mg(CF₃SO₃)₂

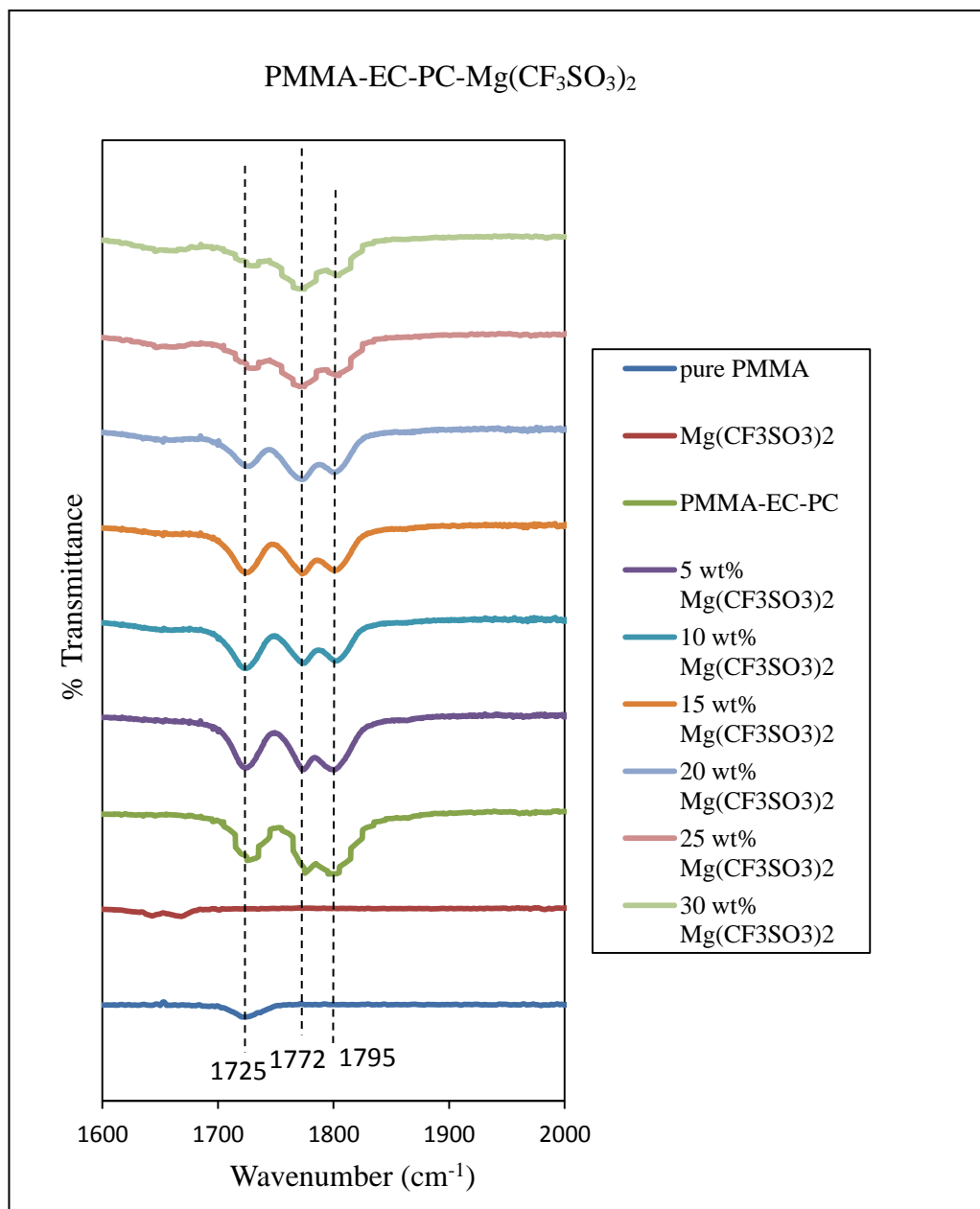


Figure 4.22: FTIR spectra of pure PMMA, pure Mg(CF₃SO₃)₂ and PMMA based GPE films with 5 wt% to 30 wt% of Mg(CF₃SO₃)₂

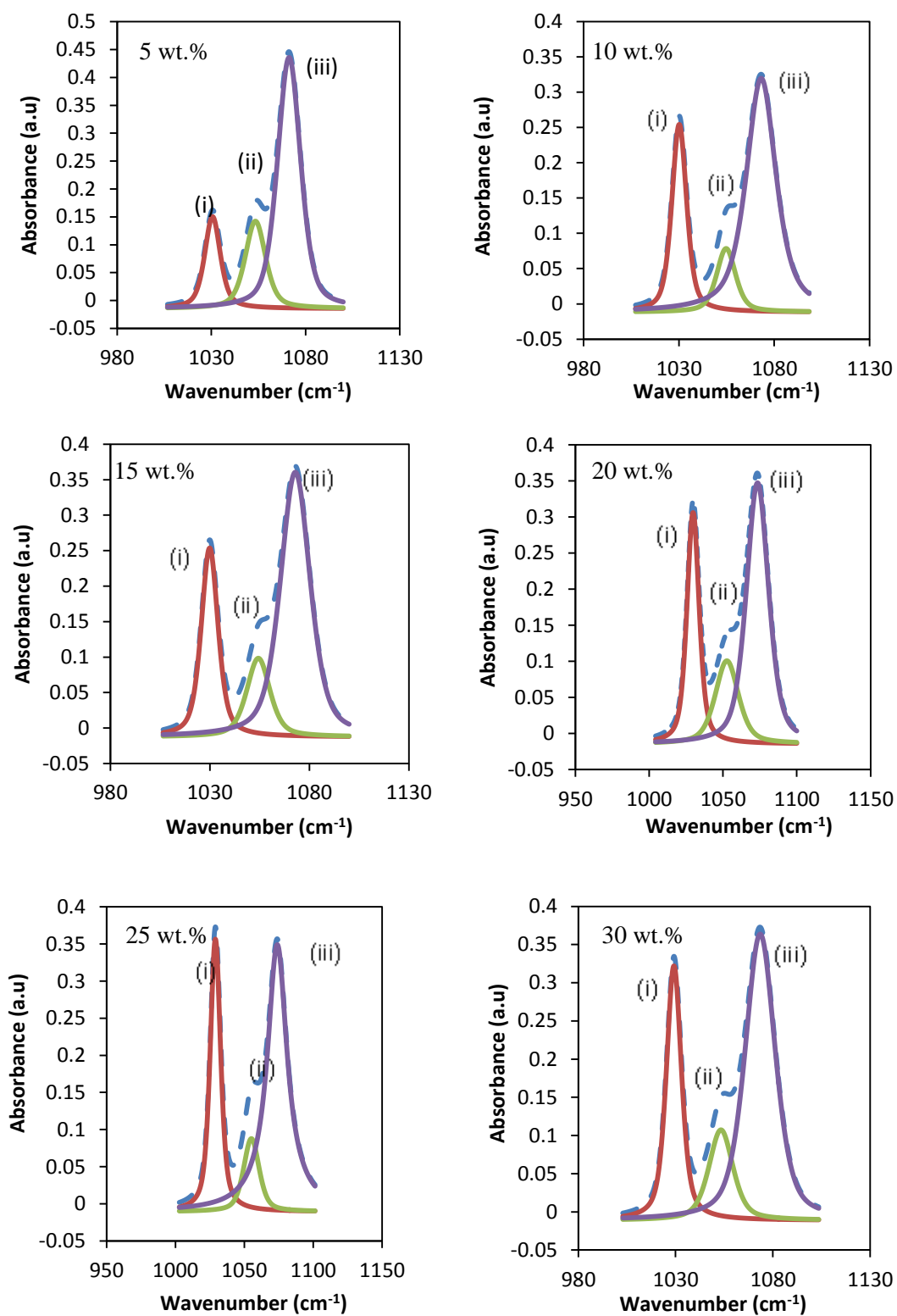


Figure 4.23: Deconvolution part for all the GPE films containing (i) free ions, (ii) ions pair and (iii) ions aggregates in the range of 1000 cm⁻¹ to 1100 cm⁻¹.

4.5 X-ray Diffraction (XRD) Analysis

X-ray Diffraction (XRD) measurements were performed on GPE films based on PMMA in order to examine the nature of crystallinity and the amorphousness of the films. The analysis was performed by using X'Pert PRO PANalytical diffractometer on the pure PMMA film, PMMA-EC-PC film, pure $\text{Mg}(\text{CF}_3\text{SO}_3)_2$ salt, and also for the GPE films containing 5 wt.%, 20 wt.% and 30 wt.% of $\text{Mg}(\text{CF}_3\text{SO}_3)_2$ salt.

4.5.1 Pure PMMA film

Figure 4.24 shows the x-ray diffractogram of pure PMMA film exhibits the typical characteristic of amorphous structure. No strong diffraction peaks is observed and this proved the amorphous nature of the polymer.

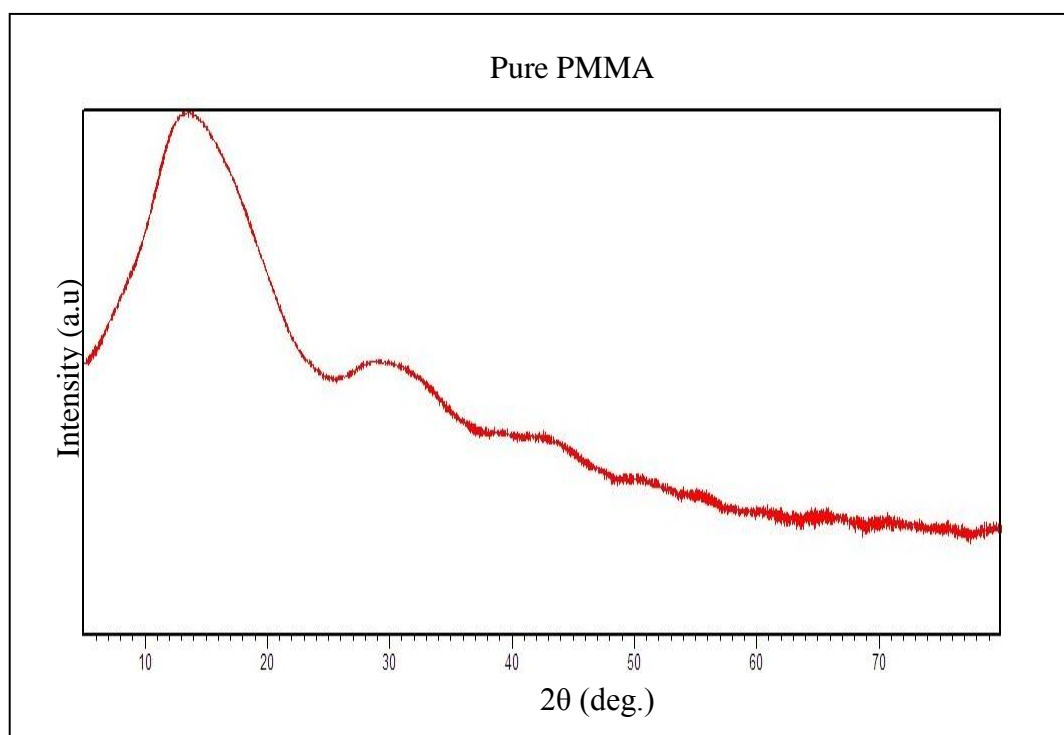


Figure 4.24: X-ray diffractogram of pure PMMA film

4.5.2 Pure EC

Figure 4.25 illustrates the x-ray diffractogram of pure EC film. In general, EC is crystalline in nature and shows its characteristic peaks at $2\theta = 17.4^\circ$, 20.1° , 25.5° , 46.1° and 50.2° .

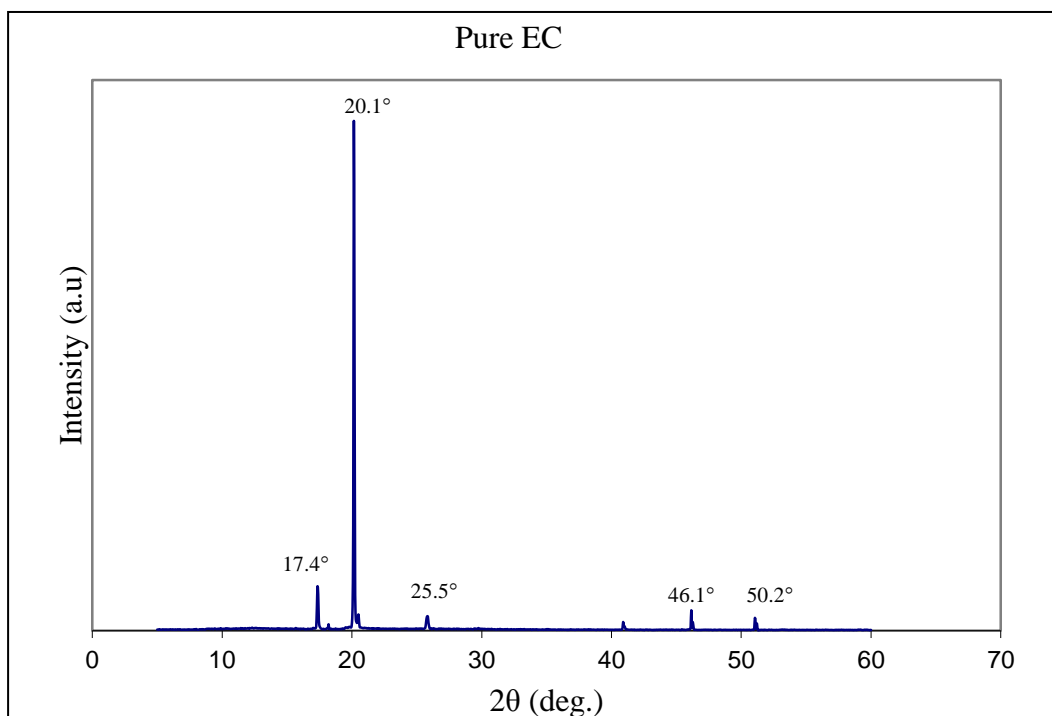


Figure 4.25: X-ray diffractogram of pure EC

4.5.3 PMMA-EC-PC film

The x-ray diffractogram of PMMA-EC-PC film is presented in Figure 4.26. It can be observed from Figure 4.27 that the predominant peak of pure PMMA film at $2\theta = 13.6^\circ$ has shifted to $2\theta = 18.9^\circ$ and the peak has broadened upon addition of plasticizing solvent, EC and PC. This indicates that the plasticizing solvent has interacted with PMMA and the amorphous region has been increased in this film.

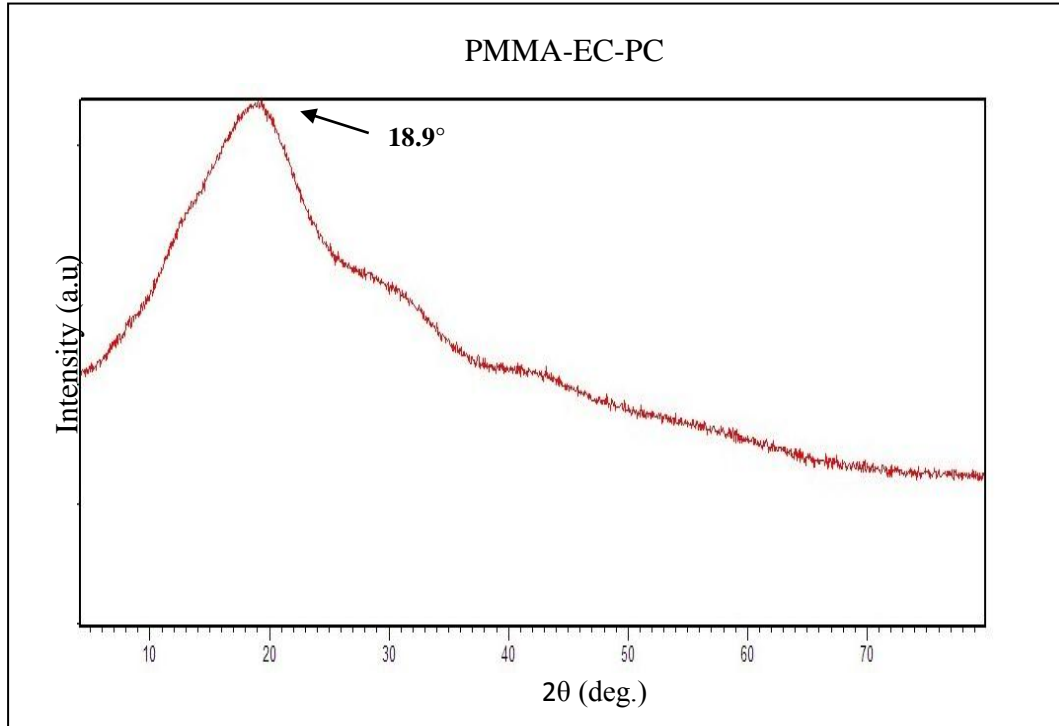


Figure 4.26: X-ray diffractogram of PMMA-EC-PC film

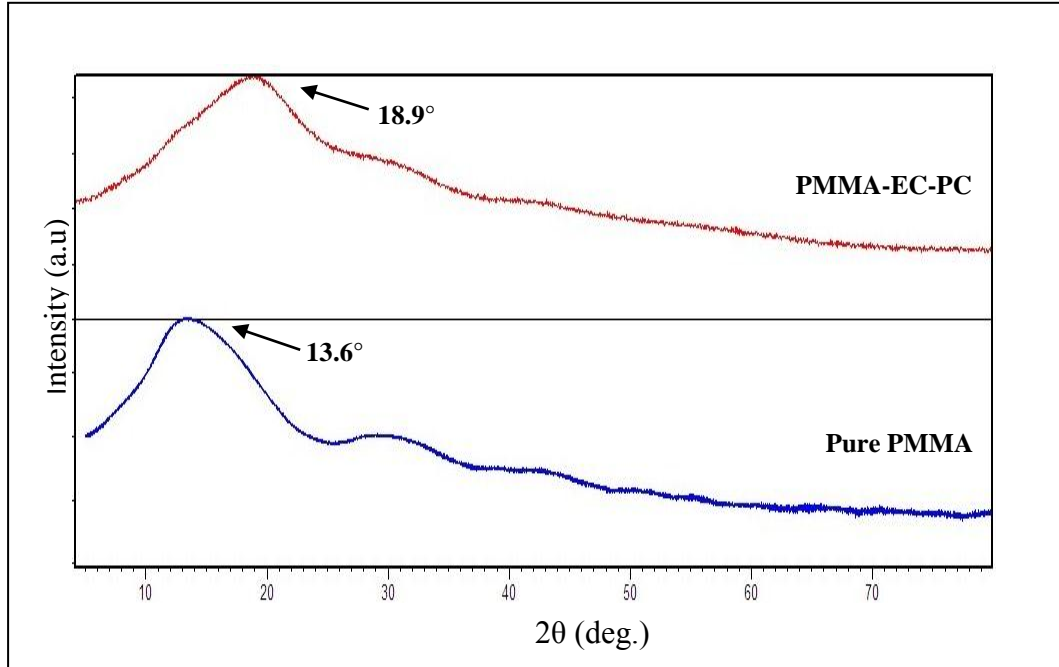


Figure 4.27: X-ray diffractogram of pure PMMA and PMMA-EC-PC films

4.5.4 Pure $\text{Mg}(\text{CF}_3\text{SO}_3)_2$ salt

Figure 4.28 exhibits the x-ray diffractogram of pure $\text{Mg}(\text{CF}_3\text{SO}_3)_2$ salt with several sharp peaks present signifying the crystalline state of the salt. This reveals that $\text{Mg}(\text{CF}_3\text{SO}_3)_2$ salt is crystalline in nature.

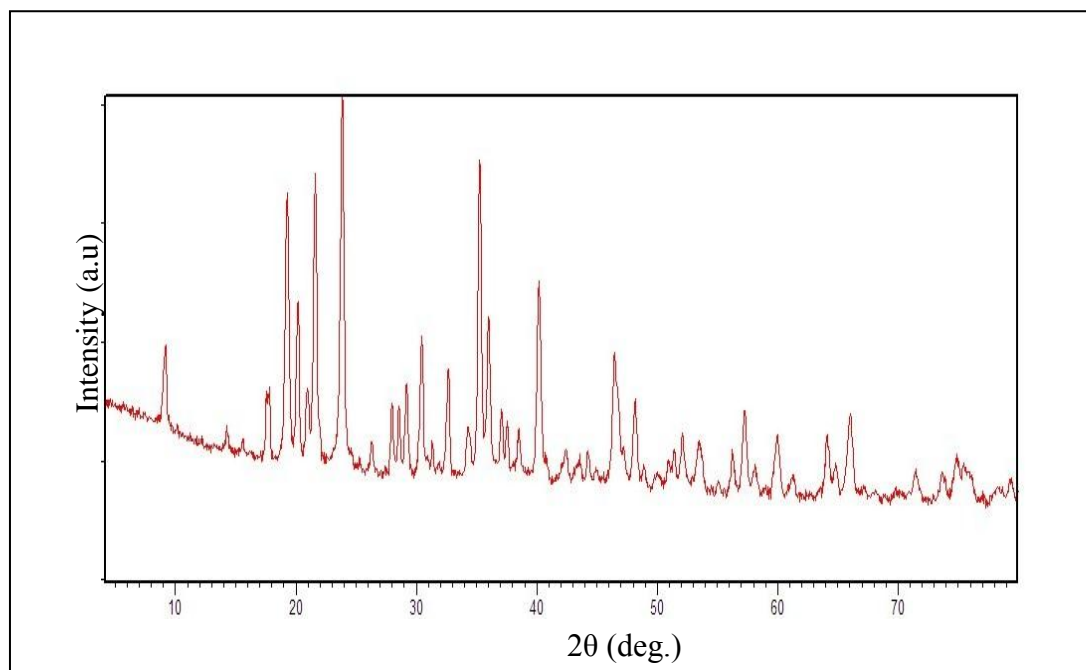


Figure 4.28: X-ray diffractogram of $\text{Mg}(\text{CF}_3\text{SO}_3)_2$ salt

4.5.5 PMMA-EC-PC-Mg(CF₃SO₃)₂ system

The XRD patterns of PMMA-EC-PC-Mg(CF₃SO₃)₂ system is shown in Figure 4.29. The disappearance of diffraction peaks of Mg(CF₃SO₃)₂ salt in this system can be attributed to the complete dissolution of the salt in plasticized polymer matrix. The intensity of the diffraction peak of PMMA-EC-PC film at $2\theta = 18.9^\circ$ is reduced and the peak also shifted to $2\theta = 19.1^\circ$, 19.4° and 19.8° in the 5 wt.%, 20 wt.% and 30 wt.% of Mg(CF₃SO₃)₂ salt, respectively. The highest conducting film containing 20 wt.% of Mg(CF₃SO₃)₂ salt shows the most amorphous region. Thus, it can be stated that higher conductivity results from the lower degree of crystallinity will assisted Mg²⁺ ions movement in the polymer network. From these observations, it is confirmed that the complexation has been occurred in the GPE films. Therefore, it can be inferred that the amorphous region in GPE films has increased significantly which leads to higher conductivity (Ganesan et al., 2008).

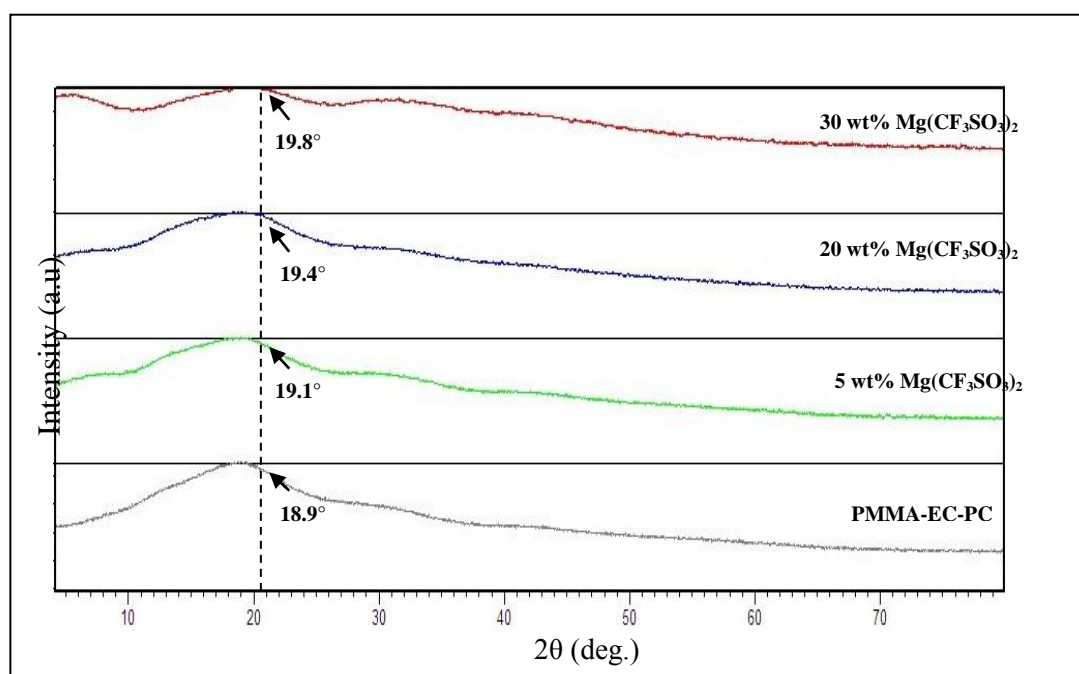


Figure 4.29: X-ray diffractogram of PMMA-EC-PC film and GPE film containing 5 wt%, 20 wt% and 30 wt% of Mg(CF₃SO₃)₂

Morphological Studies

4.6 Field Emission Scanning Electron Microscopy (FESEM) Analysis

The morphological properties of the gel polymer electrolyte films were observed using Field Emission Scanning Electron Microscopy (FESEM). The micrographs obtained from FESEM will provide important information on the surface structure and morphology features of the GPE films. In this work, FEI Quanta 200 system has been used to analyze surface morphology of the pure PMMA film, pure $\text{Mg}(\text{CF}_3\text{SO}_3)_2$ salt, PMMA-EC-PC film and GPE films from PMMA-EC-PC- $\text{Mg}(\text{CF}_3\text{SO}_3)_2$ system. FESEM micrographs of the films were obtained at a certain magnification to get better and clear images.

4.6.1 Pure PMMA film

Figure 4.30 shows the FESEM micrograph of pure PMMA film at magnification of 1000x. It can be observed that small craters with average pore size of 1 μm are formed and uniformly distributed at microscopic level. This image is similar to the surface of the pure PMMA film that reported in the literature (Deka & Kumar, 2010). A porous structure with small uniform pores is preferred for magnesium battery applications since these pores will act as a passage for Mg^{2+} ions during the charge-discharge cycle.

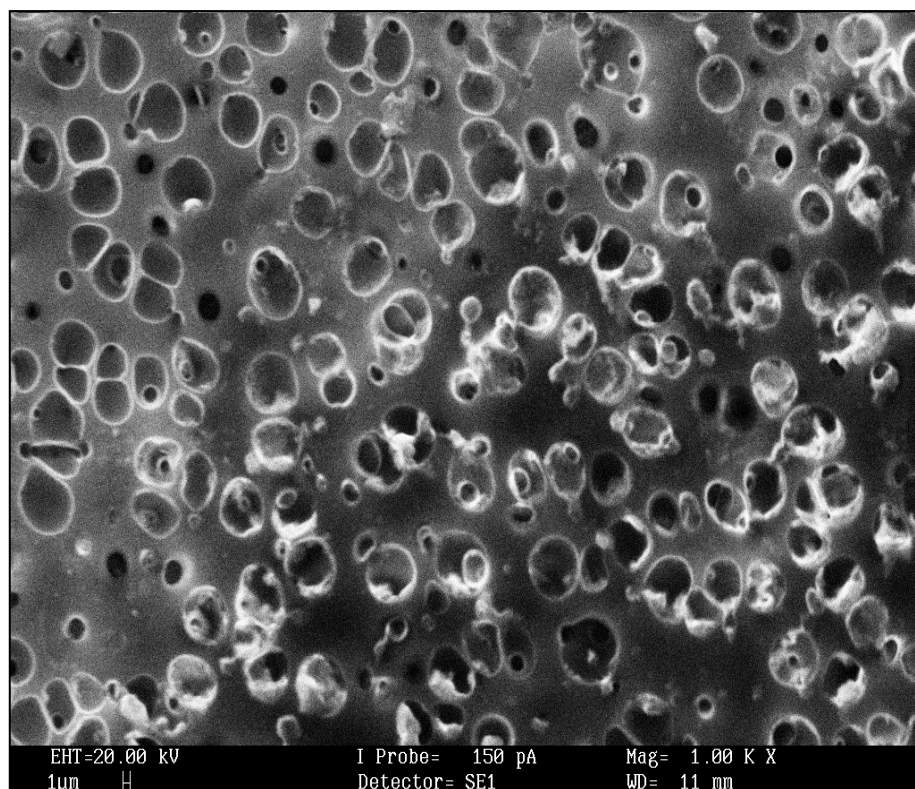


Figure 4.30: FESEM micrograph of pure PMMA film

4.6.2 Pure $\text{Mg}(\text{CF}_3\text{SO}_3)_2$ film

The FESEM micrograph for pure $\text{Mg}(\text{CF}_3\text{SO}_3)_2$ salt at magnification of 400x is presented in Figure 4.31. The crystalline structures with average size of 100 μm can be observed on the surface morphology of this film. Thus it proves that the crystalline phase is prominent in the pure $\text{Mg}(\text{CF}_3\text{SO}_3)_2$ salt.

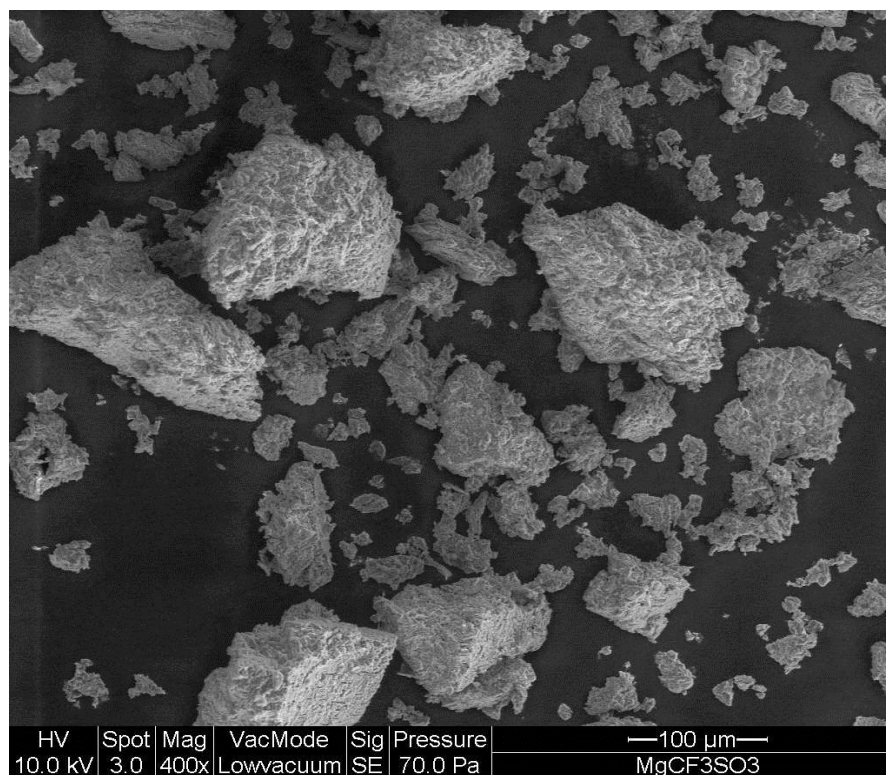


Figure 4.31: FESEM micrograph of pure $\text{Mg}(\text{CF}_3\text{SO}_3)_2$ salt

4.6.3 PMMA-EC-PC film

Figure 4.32 depicts the FESEM micrograph for the PMMA-EC-PC film at magnification of 3000x. The surface morphology of the film appears smooth and homogenous indicates that the amorphous phase has taken place on addition of plasticizers. It can therefore be inferred that the complexation between polymer, PMMA and the plasticizers, EC and PC has occurred. Due to this interaction, the crystalline phase in this film is reduced and more amorphous regions are formed. This result is consistent with the XRD result for PMMA-EC-PC film as discussed in Section 4.5.

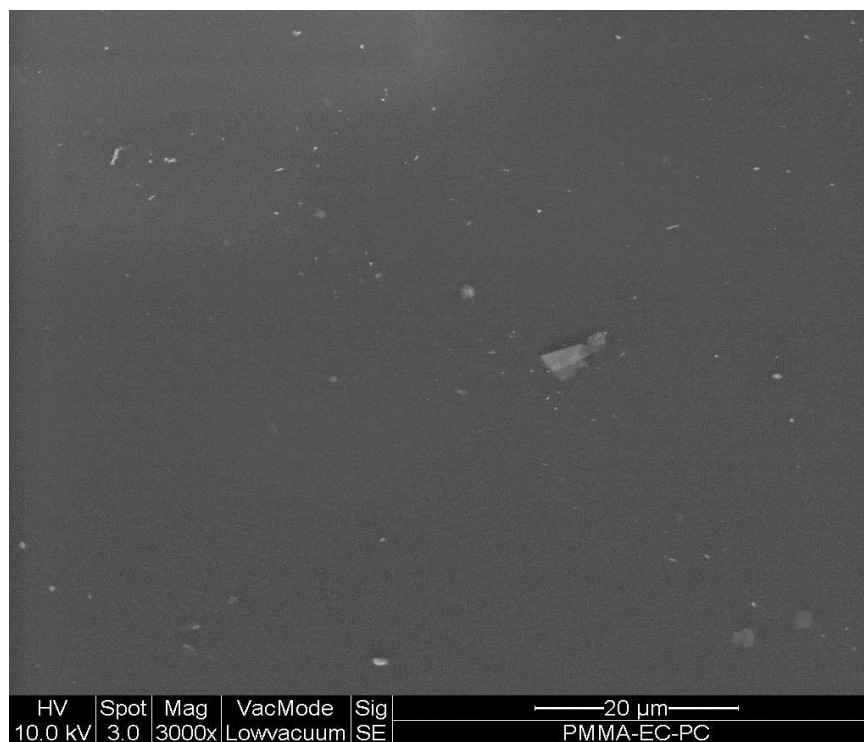


Figure 4.32: FESEM micrograph of PMMA-EC-PC film

4.6.4 PMMA-EC-PC-Mg(CF₃SO₃)₂ system

As 5 wt.% of Mg(CF₃SO₃)₂ salt is added, it can be seen that the pores in micro size of pure PMMA film are decreases and the surface of the film becomes smooth and homogenous as shown in Figure 4.33. The interconnected microspores in the GPE film helped in absorbing liquid electrolytes and hence the ionic conductivity of the GPE film is enhanced. The presence of pores in the microstructure is mainly due to the solvent removal and increased amorphous region and solvent retention ability in the electrolyte system (Ulaganathan, Nithya, & Rajendran, 2012). This confirmed that there is an interaction between the plasticized PMMA and Mg(CF₃SO₃)₂ salt. This result is in accordance with the XRD patterns as depicted in Figure 4.29.

On addition of 20wt.% of $\text{Mg}(\text{CF}_3\text{SO}_3)_2$ salt, the well distributed spherical and elongated grain structures in the film is observed as shown in Figure 4.34. Therefore, phase separation is absent in this GPE film. As a result, the charge carriers can be transported quickly and easily without the presence of blocking phase and hence the highest ionic conductivity is obtained in this film.

When more than 20 wt.% of salt is added, $\text{Mg}(\text{CF}_3\text{SO}_3)_2$ salt tends to aggregate as can be seen in Figure 4.35. The formation of globular agglomeration at higher salt content ultimately leads to the formation of phase separation thus hinders the migration of Mg^{2+} ions in the polymer matrix which in turn reduces the ionic conductivity and thus the crystalline region is increased. This result is supported by conductivity studies and XRD studies as discussed in Section 4.1 and 4.5, respectively.

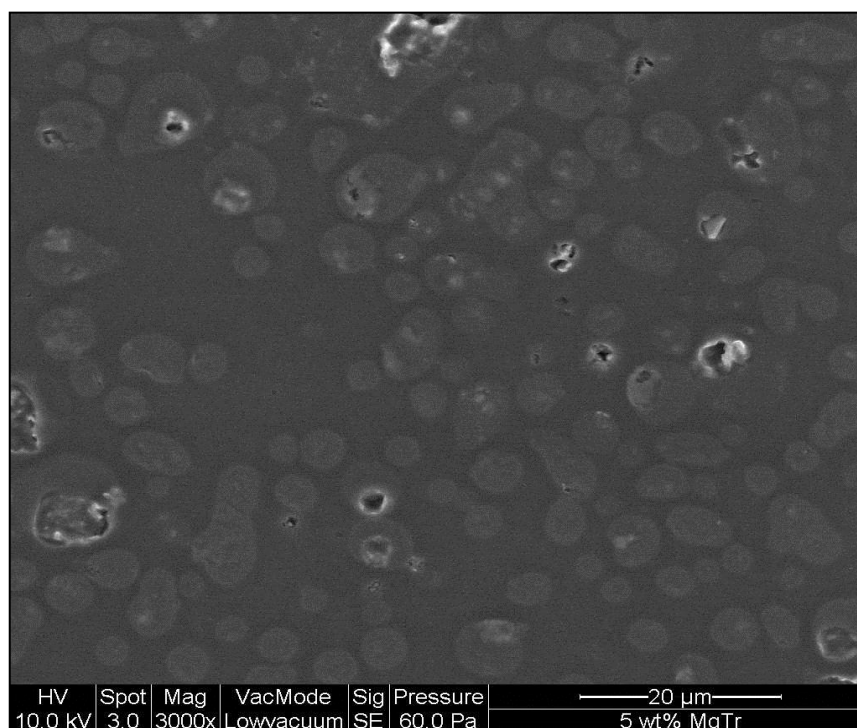


Figure 4.33: FESEM micrograph for GPE film containing 5 wt.% of $\text{Mg}(\text{CF}_3\text{SO}_3)_2$ salt

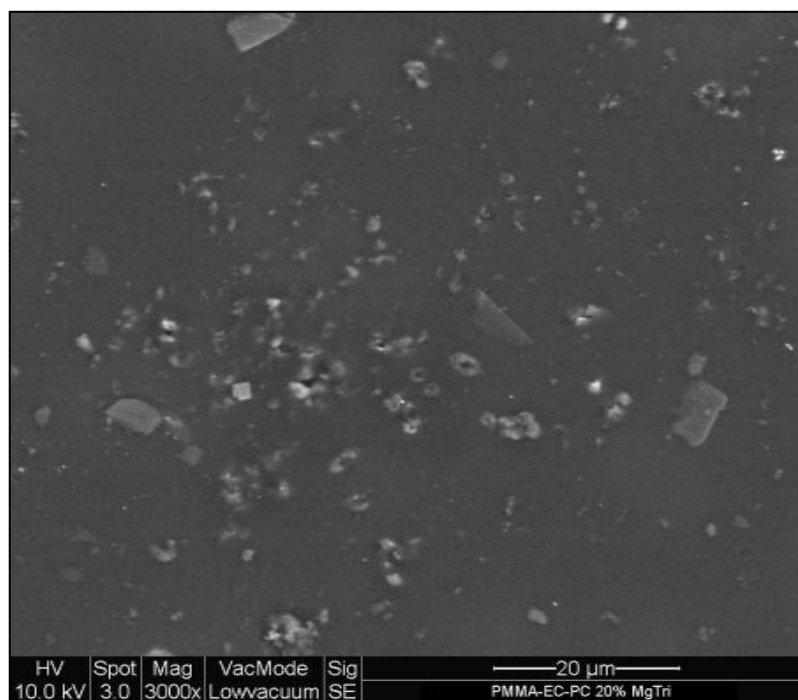


Figure 4.34: FESEM micrograph for GPE film containing 20 wt.% of $\text{Mg}(\text{CF}_3\text{SO}_3)_2$ salt

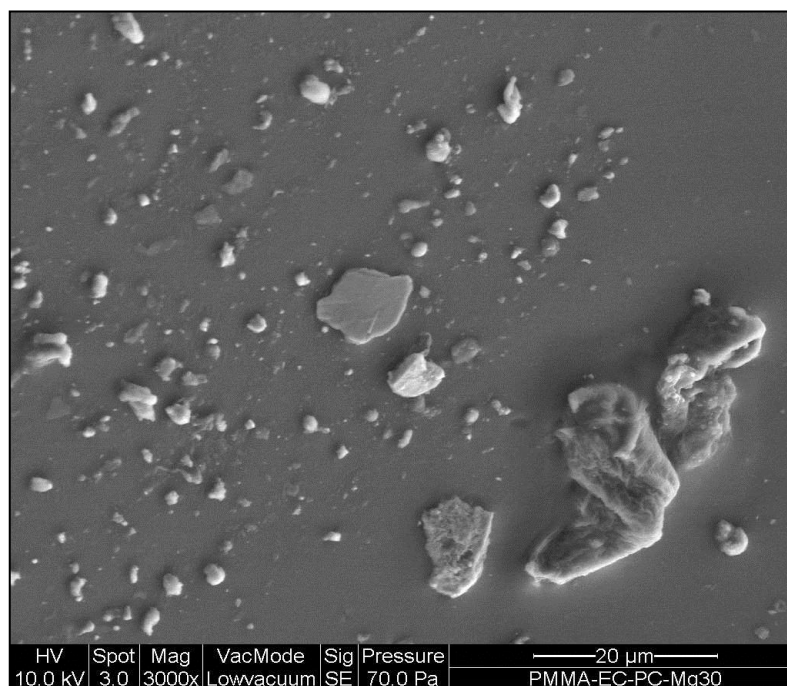


Figure 4.35: FESEM micrograph for GPE film containing 30 wt.% of $\text{Mg}(\text{CF}_3\text{SO}_3)_2$ salt

4.7 Thermal Properties Studies

Differential Scanning Calorimetry (DSC) Analysis

Thermal analyses were performed using DSC instrument with a Perkin Elmer DSC 8000 for all the GPE PMMA-EC-PC-Mg(CF₃SO₃)₂ films in the range of temperature between 30 °C to 180 °C. Films weighing 5.0 mg is hermetically sealed in aluminium pan. The GPE films were first heated to 180 °C at a heating rate of 10 °C/min to remove any trace amount of solvent and water. The GPE films were then cooled down to 30 °C and then reheated to 180 °C at the same heating rate of 10 °C/min. The glass transition temperature (T_g (midpoint), melting point (T_m) and decomposition temperature (T_d) of the films were determined from the TA Instrument software. T_g is a step transition from the glassy phase (brittle amorphous) into a more rubbery phase (solid) while T_m happens within the rubbery phase to liquid phase transition.

4.5.1 Pure PMMA film

It has been well established that crystalline and amorphous phase co-exist in most of the polymeric materials (Woo, Majid, & Arof, 2011). PMMA is a semi-crystalline polymer that exhibits both the glass transition (T_g) and melting transition (T_m). Figure 4.36 shows DSC thermogram of pure PMMA film and T_g obtained from this film is around 125 °C with T_m at 292 °C. The endothermic peak at 367 °C corresponds to the decomposition of PMMA while the enthalpy of melting and decomposition obtained for this film is 71.16 Jg⁻¹ and 319.8 Jg⁻¹, respectively. Generally, the T_g value is decreased with the increased of amorphous phase and GPE films that exhibits more amorphous phase structure is believed to allow the ionic conduction process more easily.

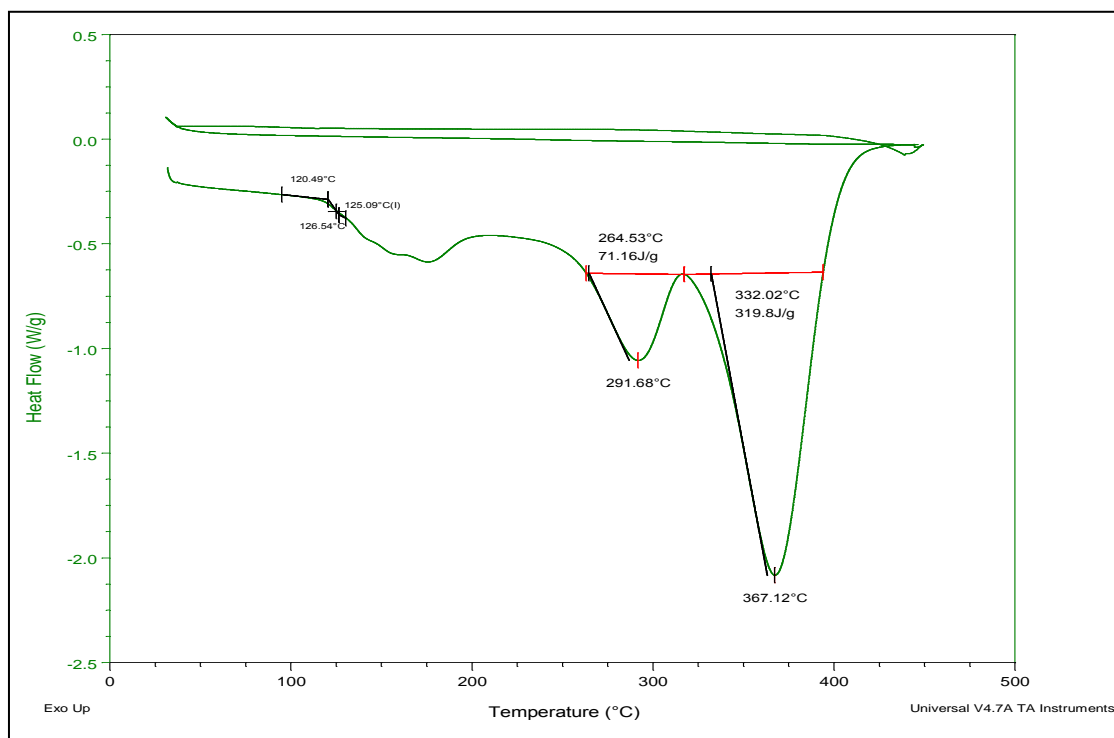


Figure 4.36: DSC thermogram of pure PMMA film

4.5.2 PMMA-EC-PC film

Figure 4.37 shows the DSC thermogram of the PMMA-EC-PC film. As can be observed from the figure, upon the addition of plasticizers, the value of T_g is decreased to 110 °C and melting temperature, T_m reduced to 189 °C. This shows the role of EC and PC, which possesses the properties of lower viscosity and act as a lubricant which softens the polymer backbone and decrease the crystallinity of PMMA. The T_g is associate with segmental flexibility of the host polymer, lower T_g value will enhance the segmental flexibility of polymeric chains thus increase in ionic conductivity.

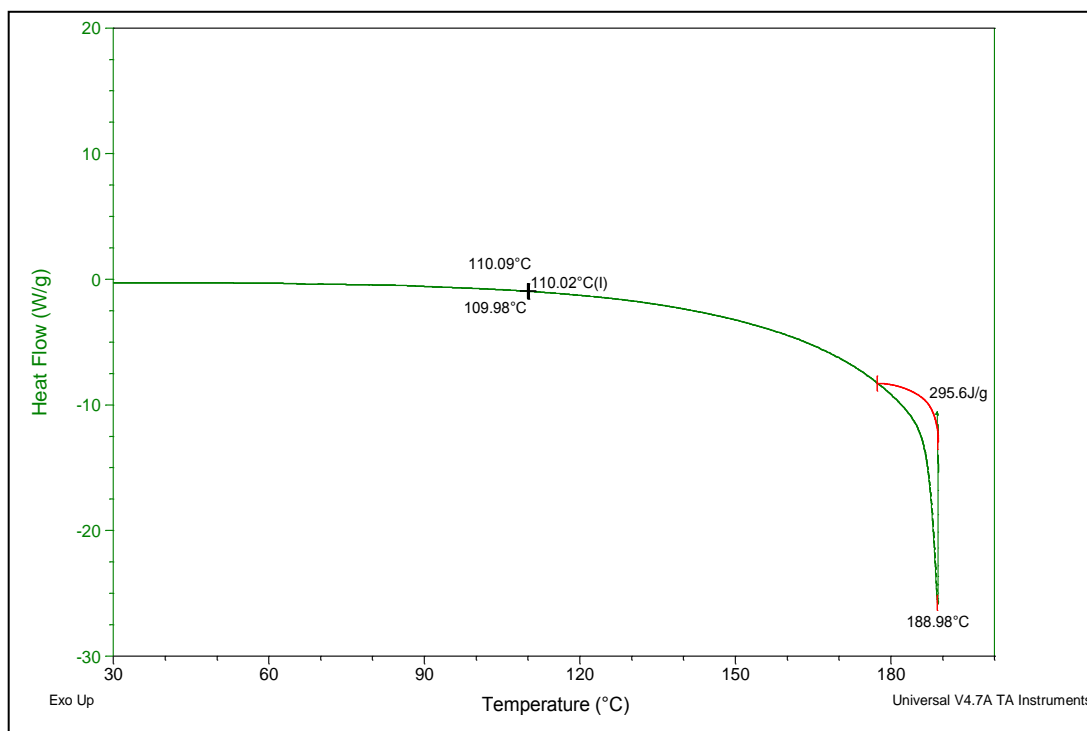


Figure 4.37: DSC thermogram of PMMA-EC-PC film

4.5.3 PMMA-EC-PC-Mg(CF₃SO₃)₂ films

The DSC thermograms for GPE films of PMMA-EC-PC-Mg(CF₃SO₃)₂ containing different weight percentages of Mg(CF₃SO₃)₂ salt ranging from 5 wt.% to 30 wt.% are shown in Figure 4.38 to Figure 4.43. The addition of salt to the polymer results in the formation of polymer-salt complexes and affect in the crystallization nature of the films. According to Figure 4.38 to Figure 4.43, T_g values are observed to decrease gradually with increasing of salt concentration. These results show that complexation has been occurred between the polymer host and the incorporating salt, Mg(CF₃SO₃)₂ salt (Idris, Glasse, Latham, Linford, & Schlindwein, 2001).

As higher salt contents were added into the films, the T_g values increased to 115 °C and 119 °C for GPE film containing 25 wt% and 30 wt% salt, respectively owing to the higher crystallinity in the films. This might be due to the cross-linked of polymer chains via ether oxygen and Mg^{2+} ions from the salt, which would lead to reduce the flexibility of PMMA backbones.

Figure 4.38 depicts the T_g value for GPE film containing 5 wt% of $Mg(CF_3SO_3)_2$ salt is 102 °C with T_m at 131 °C. As more salt is accommodated in the film, the salt acts as impurity and the melting peak is lowered (Cai, Hu, Egami, & Farrington, 1992). The melting point, T_m of the GPE films increase from 131 °C, 135 °C, 137 °C, then reduce to 124 °C for the highest conducting film, and increase again to 138 °C and 143 °C at higher salt concentrations i.e. 25 wt% and 30 wt% salt, respectively. This behavior might be due to strong interaction between the plasticizers polymer and the dissolved salt. Increasing the salt concentrations lead to high viscosity of the mixture in the film. This also indicates the possible formation of a separate crystalline phase due to the interaction of PMMA with Mg^{2+} cations thus increasing the melting point. Furthermore, no endothermic peak corresponding to decomposition is found in the plasticized PMMA- $Mg(CF_3SO_3)_2$ salt system suggesting that the present GPE films are stable over a wide temperature range from 30 °C - 130 °C. This indicates that the GPE films have potential applications in electrochemical devices. T_g and T_m values for all GPE films are tabulated in Table 4.5.

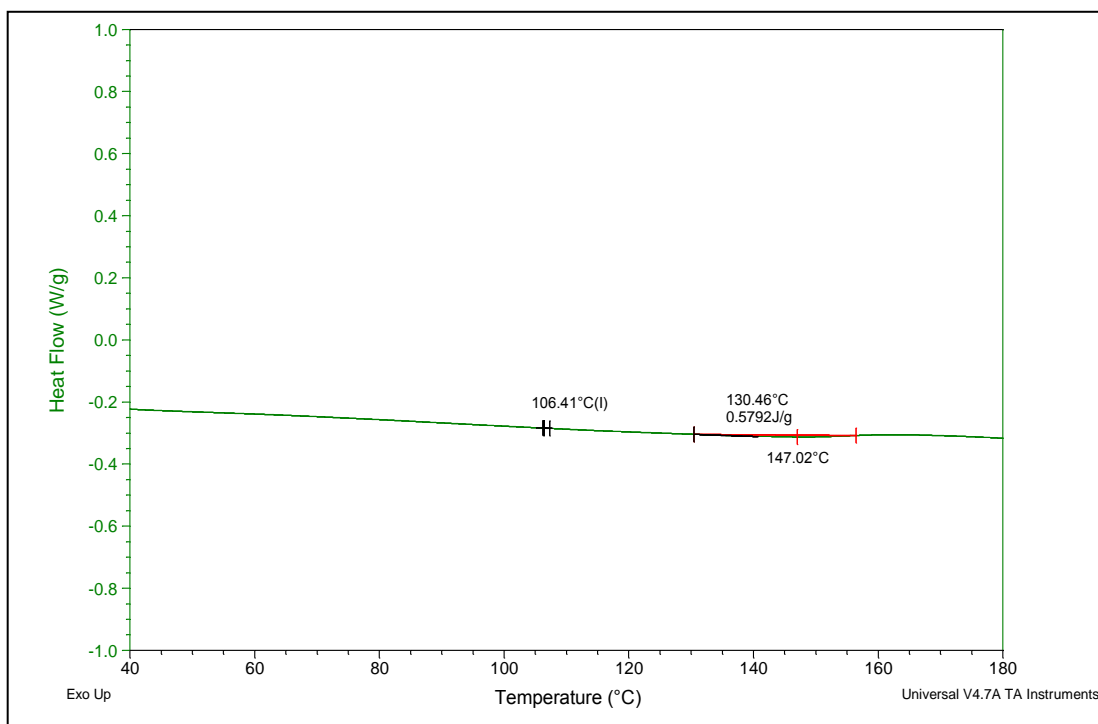


Figure 4.38: DSC thermogram of GPE film containing 5 wt% of $\text{Mg}(\text{CF}_3\text{SO}_3)_2$ salt

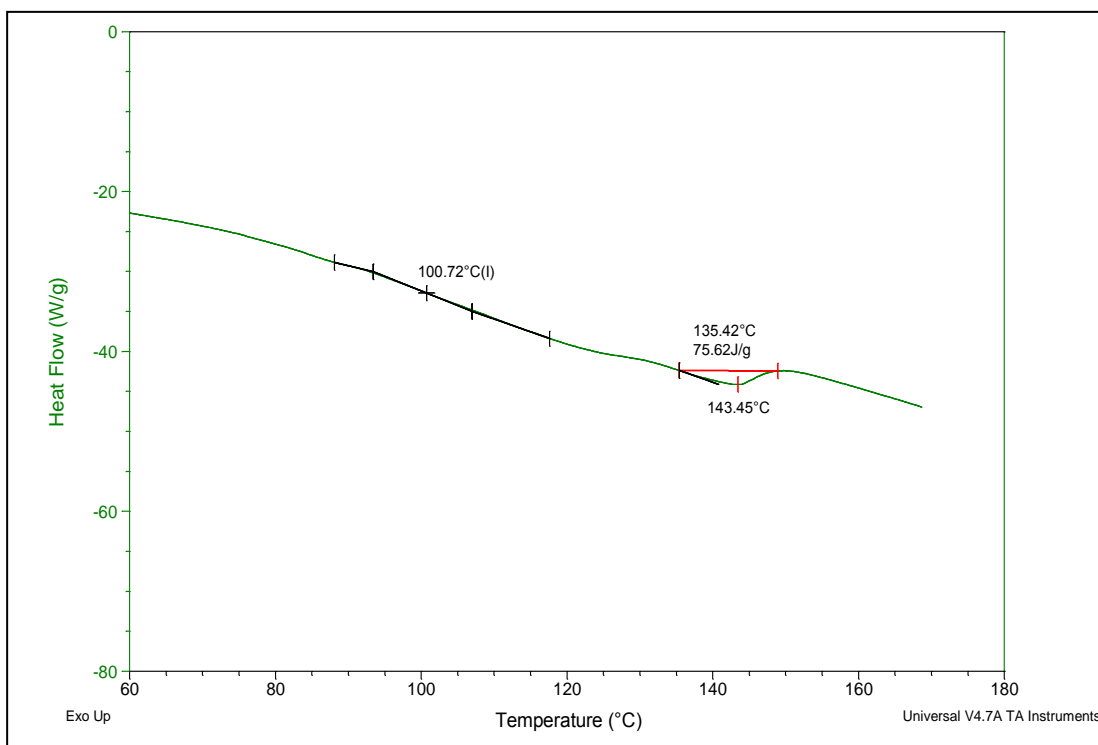


Figure 4.39: DSC thermogram of GPE film containing 10 wt% of $\text{Mg}(\text{CF}_3\text{SO}_3)_2$ salt

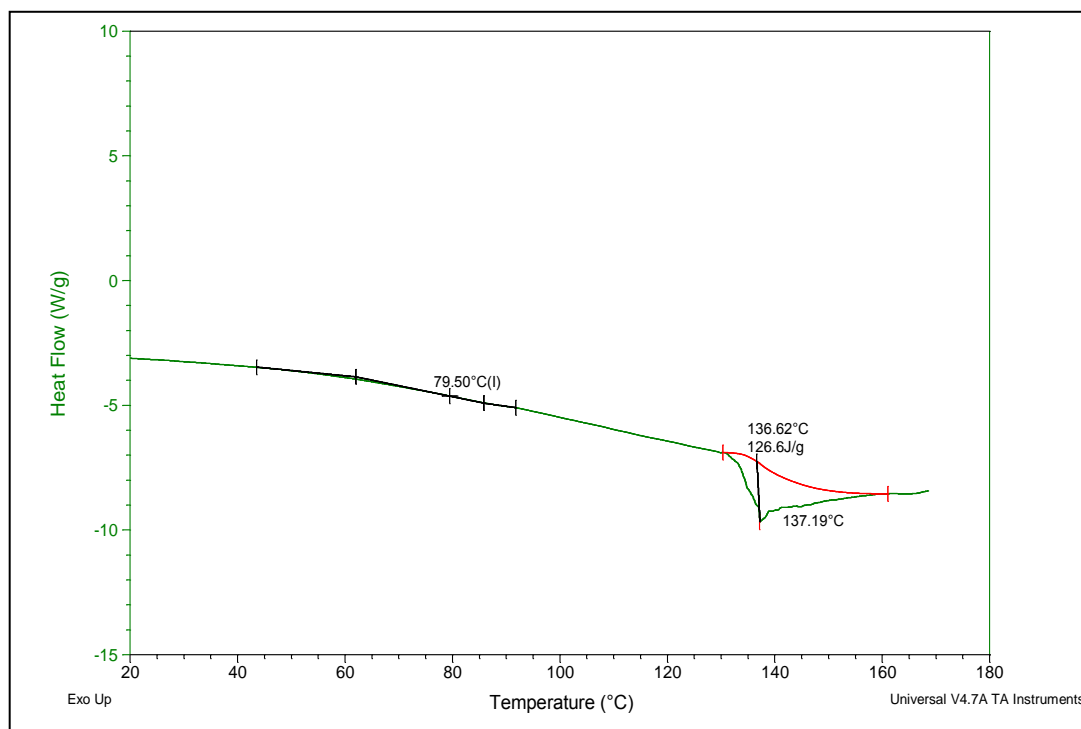


Figure 4.40: DSC thermogram of GPE film containing 15 wt% of $\text{Mg}(\text{CF}_3\text{SO}_3)_2$ salt

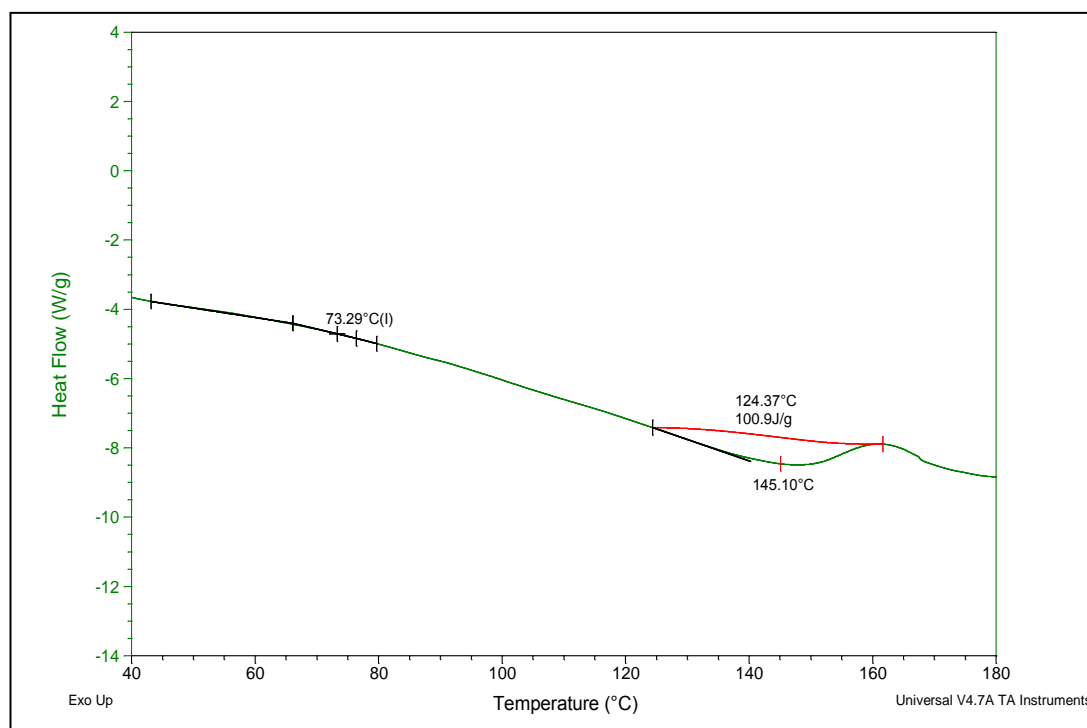


Figure 4.41: DSC thermogram of GPE film containing 20 wt% of $\text{Mg}(\text{CF}_3\text{SO}_3)_2$ salt

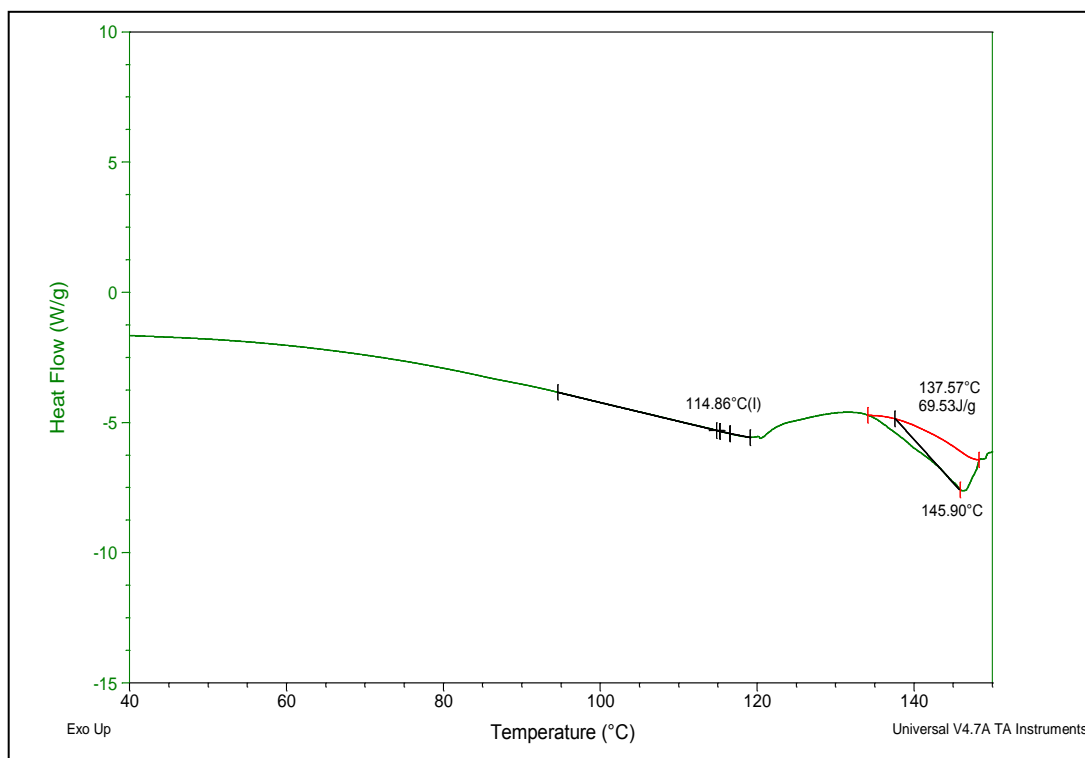


Figure 4.42: DSC thermogram of GPE film containing 25 wt% of $\text{Mg}(\text{CF}_3\text{SO}_3)_2$ salt

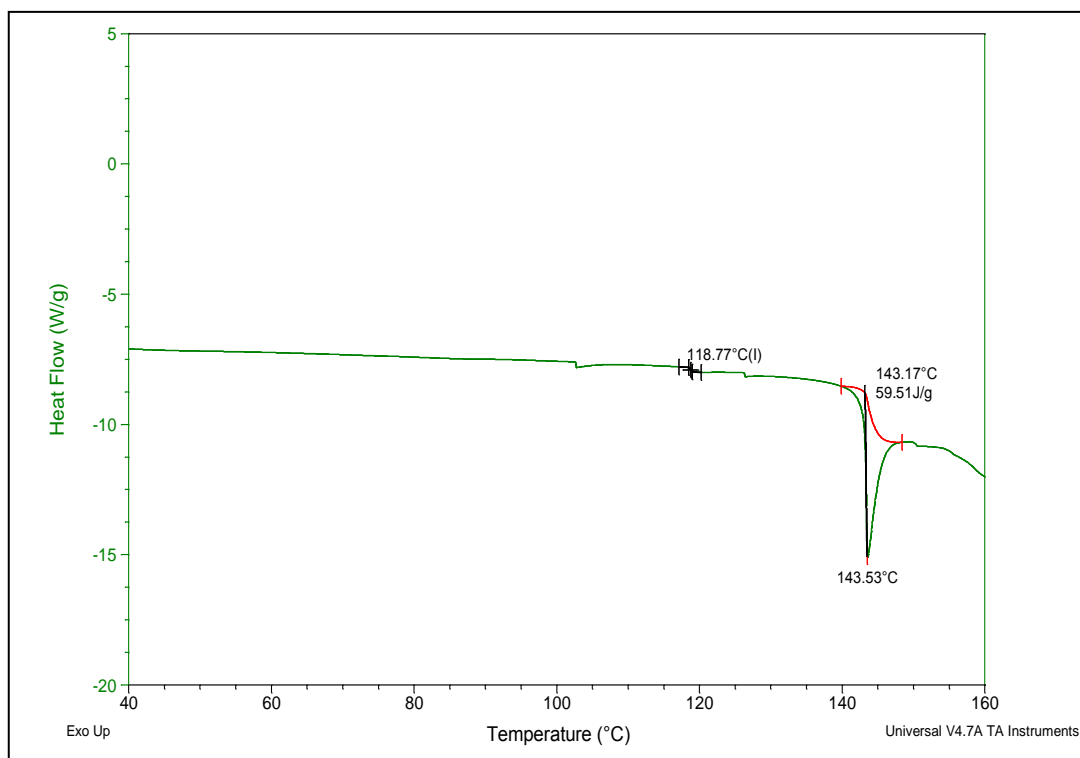


Figure 4.43: DSC thermogram of GPE film containing 30 wt% of $\text{Mg}(\text{CF}_3\text{SO}_3)_2$ salt

Table 4.5: T_g and T_m values for pure PMMA, PMMA-EC-PC and PMMA-EC-PC- $Mg(CF_3SO_3)_2$ GPE films.

System	Glass transition temperature, T_g (°C)	Melting temperature, T_m (°C)
PMMA	125	292
PMMA-EC-PC	110	189
PMMA-EC-PC-5 wt.% $Mg(CF_3SO_3)_2$	106	131
PMMA-EC-PC-10 wt.% $Mg(CF_3SO_3)_2$	101	135
PMMA-EC-PC-15 wt.% $Mg(CF_3SO_3)_2$	80	137
PMMA-EC-PC-20 wt.% $Mg(CF_3SO_3)_2$	73	124
PMMA-EC-PC-25 wt.% $Mg(CF_3SO_3)_2$	115	138
PMMA-EC-PC-30 wt.% $Mg(CF_3SO_3)_2$	119	143

4.8 Electrochemical Studies

The electrochemical studies were carried out by linear sweep voltammetry (LSV) and cyclic voltammetry (CV) using an electrochemical analyzer in order to estimate the electrochemical stability window (ESW) or working voltage limit of the gel polymer electrolytes. In this work, highest conducting film containing 20 wt.% of $\text{Mg}(\text{CF}_3\text{SO}_3)_2$ salt was characterized through LSV and CV techniques by using WPG100e potentiostat/galvanostat system and the results obtained will be analyzed.

To demonstrate the application of the GPE film as an electrolyte in rechargeable Mg-batteries, $\text{Mg}|\text{GPE}|\text{MnO}_2$ cell was assembled and its performance has been evaluated. The charge and discharge characteristics of the cell were briefly examined to figure out the applicability of the GPE film to rechargeable Mg-batteries. Several types of cathode materials that suitable for the rechargeable Mg-batteries have been reported (Y. Kumar, Hashmi, & Pandey, 2011) which are known for the insertion and de-insertion of the Mg^{2+} ions in themselves. Manganese oxide or MnO_2 was chosen as the positive electrode because it offers the advantages of relatively low cost, low toxicity and environmental safety as well as high theoretical capacitance (Girish Kumar & Munichandraiah, 2002). The capacitance of manganese oxide is attributed to the reversible redox transitions involving exchange of protons and/or cations with the electrolyte (Pandey, Agrawal, & Hashmi, 2011). Girish Kumar et al. (Girish Kumar & Munichandraiah, 2002) reported that the discharge capacity of about 90 mAh g^{-1} of MnO_2 is obtained during the discharge of $\text{Mg}|\text{GPE}|\text{MnO}_2$ cell.

4.8.1 Linear Sweep Voltammetry (LSV)

The electrochemical stability of the GPE film containing 20 wt.% of $\text{Mg}(\text{CF}_3\text{SO}_3)_2$ salt has been measured using linear sweep voltammetry (LSV) recorded on the SS|GPE|Mg cell. The stainless steel (SS) will act as a working electrode while Mg foil as the combined of counter and reference electrodes. Figure 4.44 displays the current-voltage response obtained by applying anodic voltage to the cell. The voltage is swept from 0 V towards anodic (positive) values with a scan rate of 5 mV s^{-1} until a large current is obtained. As the potential is swept, a sudden rise of current is observed at certain potential, which is due to the electrolyte decomposition at the inert electrode interface. It is found that the GPE film are stable up to $\sim 3.0 \text{ V}$ and this value of working voltage range appears to be high enough to use as an electrolyte in solid state Mg-batteries system.

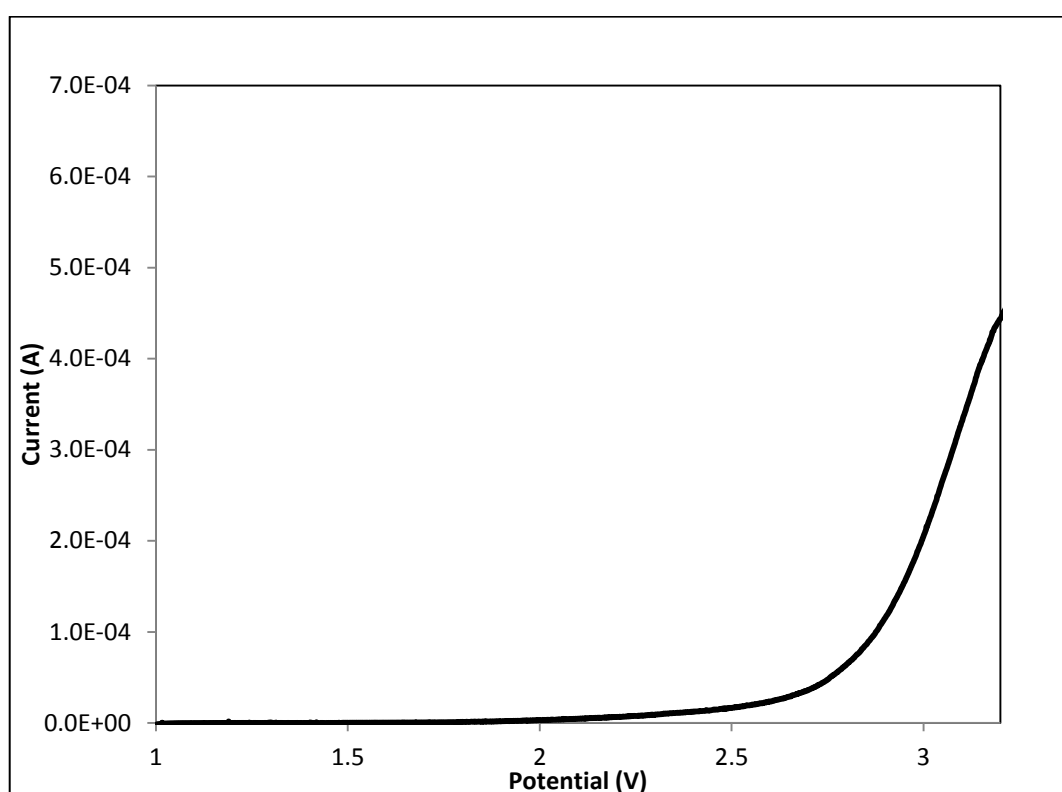


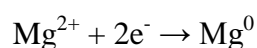
Figure 4.44: Linear sweep voltammogram of SS|GPE|Mg cell for GPE containing 20 wt.% of $\text{Mg}(\text{CF}_3\text{SO}_3)_2$ salt at scan rate of 5 mV s^{-1} .

4.8.2 Cyclic Voltammetry (CV)

Cyclic voltammetry and complex impedance studies have been carried out in order to confirm the Mg^{2+} ion conduction in the gel polymer electrolyte. It has been performed on symmetrical cells SS|GPE|SS (Cell-I) and Mg|GPE|Mg (Cell-II) for the GPE film containing 20 wt.% of $\text{Mg}(\text{CF}_3\text{SO}_3)_2$ salt at room temperature. Figure 4.45 shows the comparative impedance plots for the cells sandwiched between SS and Mg-electrodes, referred as Cell-I and Cell-II, respectively. The Cell-I offers a steep rising impedance pattern at lower frequency range, indicating the ion blocking nature of the SS electrodes. On the other hand, almost well-defined semicircular dispersion curve has been observed from the Cell-II, thus suggests the reversible nature of the Mg-electrodes (Y. Kumar et al., 2011). This behavior is similar to that reported by Pandey et al. (Pandey & Hashmi, 2009). These observations give the evidence of Mg^{2+} ion conduction in the gel polymer electrolyte.

Figure 4.46 shows the current response of the working electrode for Cell-I recorded at a scan rate of 5 mV s^{-1} . As can be observed, there is only a very small current through the working electrode until the applied voltage reached a potential of 2.5 V and the current related to GPE decomposition has increases on increase of the applied voltage above 2.5 V. However, the small hump around 2.4 V is ascribed to the oxidation of some trace species such as water and oxygen (Hu & Tsou, 2002) or from which hydroxyl functional groups could have attached to the electrode surface and changed the stainless steel electrode morphology. Thus, it can be inferred that the electrochemical stability window for the GPE film has been found in the range of -2.5 V to 2.5 V.

On the other hand, the cathodic and anodic current peaks are distinctly observed for the Cell-II (with Mg electrodes), whereas no such features are present for the Cell-I (with SS electrodes) in the same potential range. This suggests that the electrodeposition of Mg is very facile at the Mg electrodes and the gel polymer electrolyte interface due to the following reversible reaction:



The oxidation of Mg metal to Mg^{2+} ions takes place during discharge of the electrode and the reverse process, which is the electrodeposition of Mg occurs during charge. This is possible because the experiments were conducted with the symmetrical cell with a two-electrode geometry without using a reference electrode. Hence, this indicates the Mg^{2+} ion conduction in the gel polymer electrolyte film. This observation is similar to other systems are reported in the literatures (Novák, Imhof, & Haas, 1999). Figure 4.47 shows the cyclic voltammogram of cell-II, Mg|GPE|Mg with 20 wt.% of $\text{Mg}(\text{CF}_3\text{SO}_3)_2$ salt at scan rate of 5 mV s^{-1} .

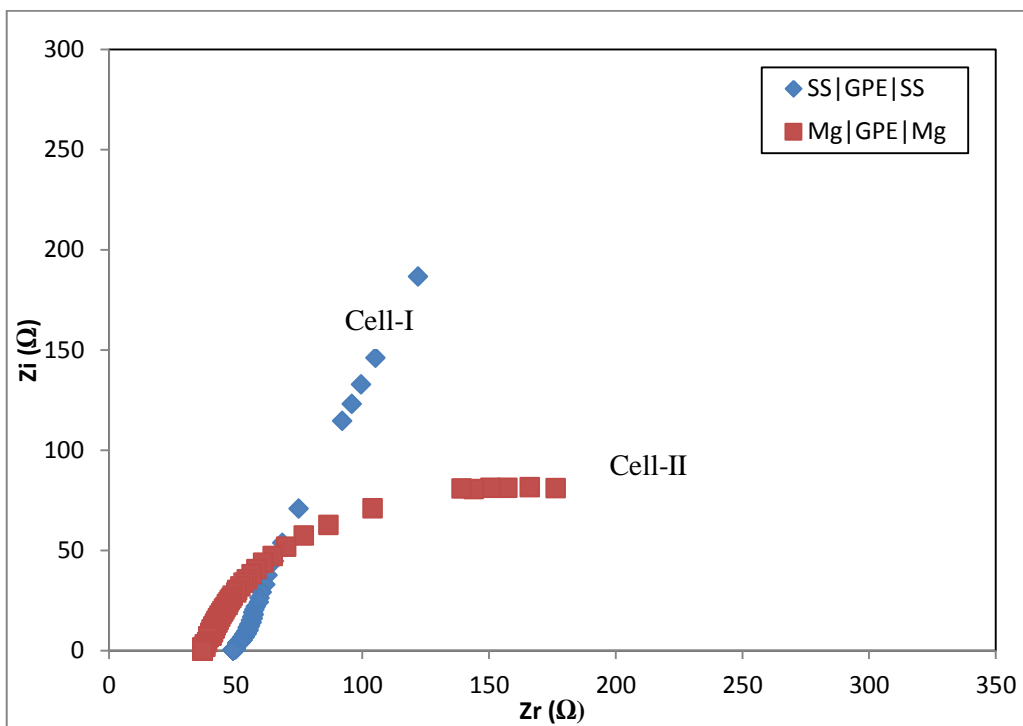


Figure 4.45: Complex impedance plots for Cell-I: SS|GPE|SS and Cell-II: Mg|GPE|Mg at room temperature.

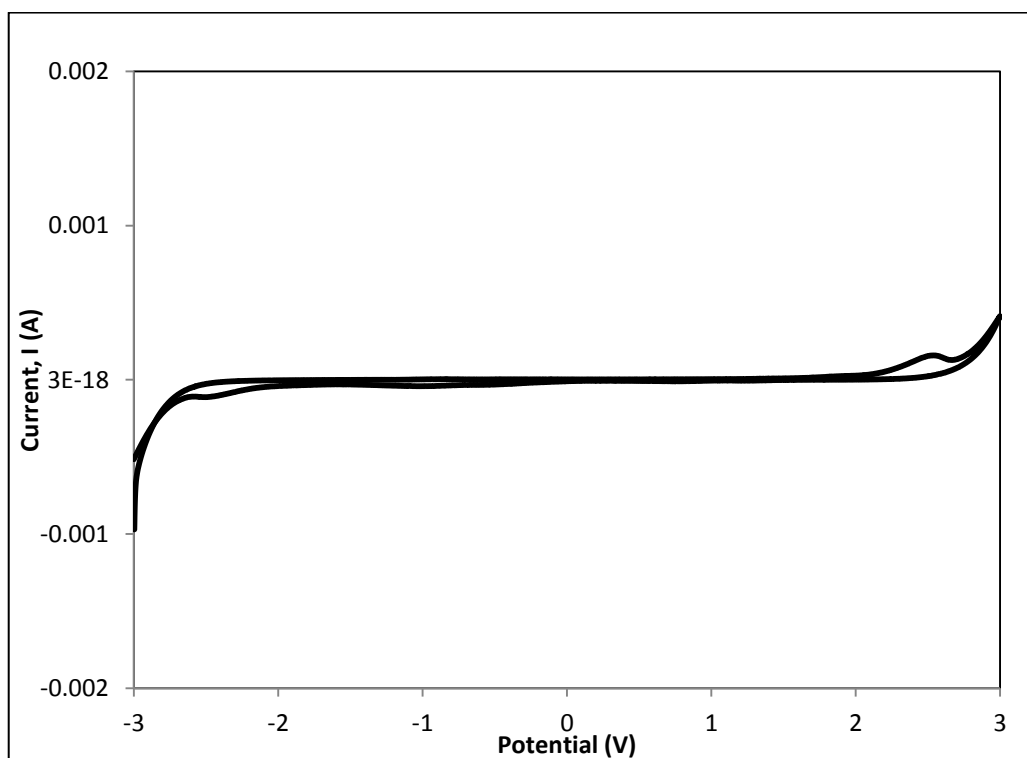


Figure 4.46: Cyclic voltammogram of cell-I: SS|GPE|SS with 20 wt.% of $\text{Mg}(\text{CF}_3\text{SO}_3)_2$ salt at scan rate of 5 mV s^{-1} .

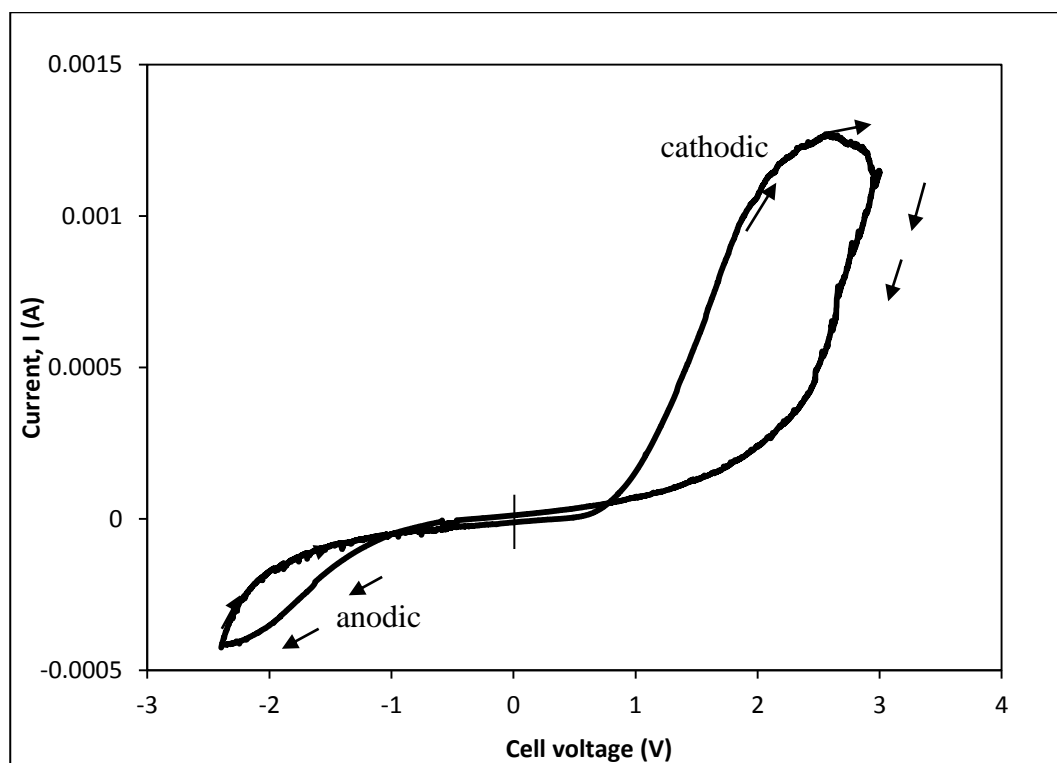
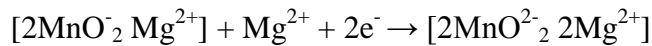
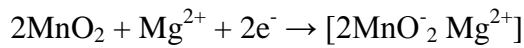


Figure 4.47: Cyclic voltammogram of cell-II: Mg|GPE|Mg with 20 wt.% of $\text{Mg}(\text{CF}_3\text{SO}_3)_2$ salt at scan rate of 5 mV s^{-1} .

4.9 Performances of Magnesium Cell

It is essential to construct a cell with the gel polymer as the electrolyte in order to examine its performances characteristics in the rechargeable magnesium batteries. The most extensively studied cathode material for magnesium batteries is MnO_2 which known to intercalate/deintercalate Mg^{2+} reversibly in the electrolyte. In this research work, the cell have been fabricated comprising a MnO_2 cathode, Mg-foil anode and optimized gel polymer electrolyte (GPE) film containing 20 wt.% of $\text{Mg}(\text{CF}_3\text{SO}_3)_2$ salt. As fabricated, the cell with GPE of optimum concentration shows an open circuit voltage (OCV) of 1.6 V and charged to 2.3 V with current of 0.2 mA. The cell was then discharge with the same current and the charge-discharge process was repeated up to 4 cycles.

These processes correspond to Mg^{2+} insertion into MnO_2 cathode from the gel polymer electrolyte, and desorbed from the MnO_2 cathode to the electrolyte during the charging process. The discharge curve is fairly flat and a potential plateau was observed over a long duration of charge. The discharge capacity obtained is about 32 mAh g^{-1} of MnO_2 and this value is quite low compared to the theoretical value. This might be due to accumulation of inert Mg^{2+} in the oxide phase that does not participate in the insertion/desorption reactions. The following reactions are considered to involve in the first Mg|GPE|MnO_2 cell discharge:



where the reduction of MnO_2 cathode occurs from Mn^{4+} to Mn^{3+} thus results in the formation of $[2\text{MnO}^-_2 \text{Mg}^{2+}]$. This product undergoes further reduction from Mn^{3+} to Mn^{2+} , which corresponds to the second voltage plateau (Girish Kumar & Munichandraiah, 2002). Figure 4.48 shows charge-discharge cycles as a function of time of Mg|GPE|MnO_2 cell.

Figure 4.48 shows the discharge curves against specific capacity of Mg|GPE|MnO_2 cell with constant current of 0.2 mA. As can be observed from the figure, it is found that the charging and discharging processes were gradually decreased with the repetition of the cycle between 2.3 and 0.8. The discharge capacity has been observed to be 32 mAh g^{-1} of MnO_2 . The cell has low capacity for recharging and cyclic performance is limited to 4 cycles. This is mainly due to the irreversibility of Mg metal and some degradation of the interface structure between the electrode and GPE film, where the surface film grows in thickness during repeated cycling.

The thick surface film in turn tends to passivate the Mg-electrode and this passivating layer will impede the reversibility process of Mg/Mg^{2+} electrochemical reaction in the $\text{Mg}|\text{GPE}|\text{MnO}_2$ cell. The similar pattern of charge-discharge curves has been reported by Pandey et al. (Pandey et al., 2011). In their work, they used V_2O_5 as a cathode material.

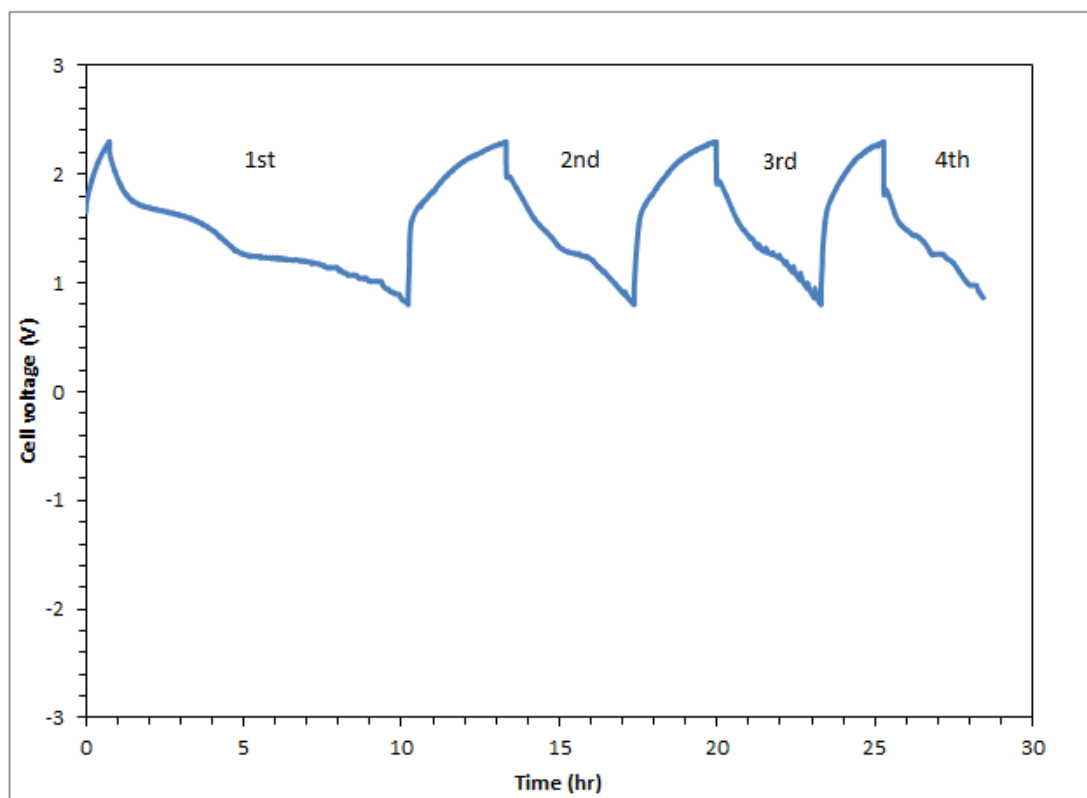


Figure 4.48: Charge-discharge cycles as a function of time of $\text{Mg}|\text{GPE}|\text{MnO}_2$ cell.

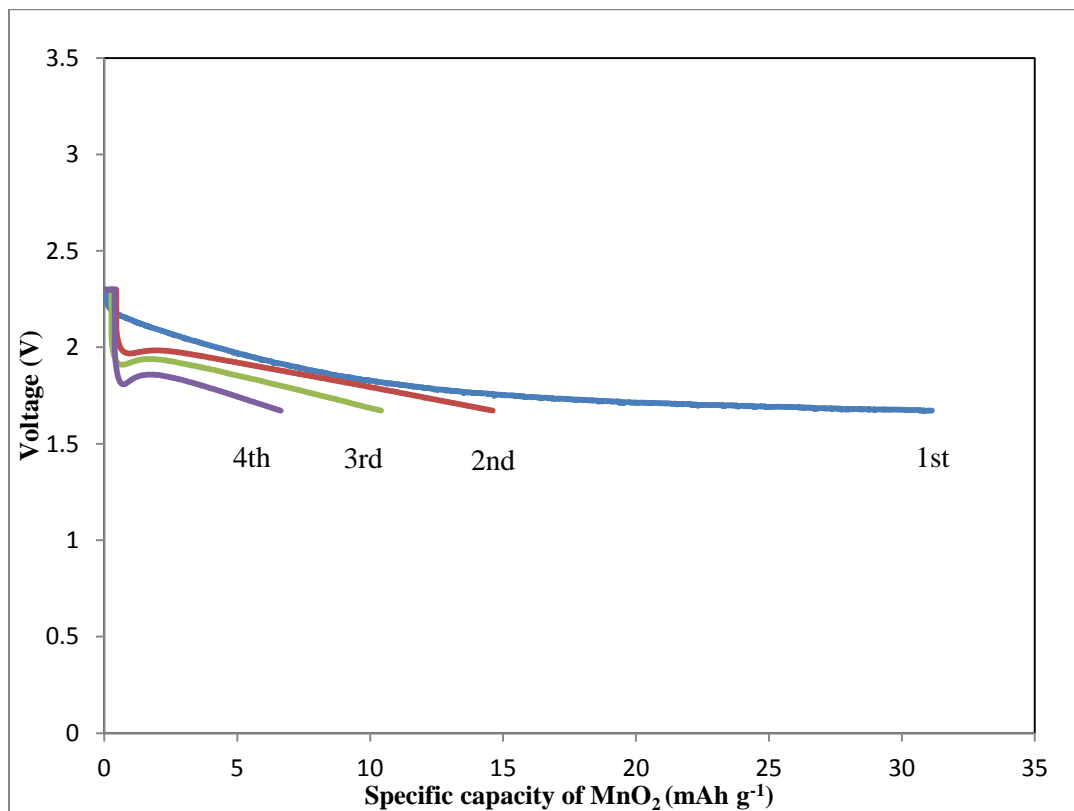


Figure 4.49: Discharge curves against specific capacity of Mg|GPE|MnO₂ cell with constant current of 0.2 mA.

CHAPTER 5

CONCLUSIONS AND SUGGESTIONS FOR FURTHER WORK

Gel polymer electrolyte is an attractive solid state material over conventional liquid electrolyte and solid polymer electrolyte because of its intrinsic properties i.e. improvement of safety performance by eliminating the leakage problem, better shape flexibility and significant enhancement of ionic conductivity with an addition of plasticizers (G. Pandey, Kumar, & Hashmi, 2010). Magnesium salt was chosen due to its green properties which are more environmental friendly and high safety with comparable high ionic conductivity as compared to lithium-based salts.

In the present work, the PMMA-based GPE films have been prepared via solution casting technique. Moreover, the effect of varying the concentrations of $\text{Mg}(\text{CF}_3\text{SO}_3)_2$ salt with addition of plasticizers in this system has also been investigated. The GPE films were then characterized using several experimental techniques in order to study the ionic conductivity, transport number, structural, morphological, thermal and electrochemical properties.

Generally, the conductivity of the GPE films was influenced by the ionic mobility of the charge carrier concentration and the degree of salt concentration. Higher dissociation of salt will result in higher number of mobile ions thus enhancing the ionic conductivity of the GPE films. By adding plasticizers with high dielectric constant into the system, it would help in ion dissociation of the salt by providing more charge carriers or free ions thus decrease the crystallinity of the polymer matrix. This effect softens the polymer backbone and enhances the flexibility of the polymer matrix, accelerating the polymer segmental motion and ionic transportation by providing more conducting pathways (S Ramesh, Liew, & Ramesh, 2011).

The highest room temperature conductivity was achieved at $1.27 \times 10^{-3} \text{ S cm}^{-1}$ for the GPE film containing 20 wt.% of $\text{Mg}(\text{CF}_3\text{SO}_3)_2$ salt. The ionic conductivity increases with increasing the salt concentrations and decreases as the salt concentrations are saturated. Table 5.1 summarizes the ionic conductivity obtained for the all GPE films.

Table 5.1: The ionic conductivity for the GPE films from PMMA-EC-PC- $\text{Mg}(\text{CF}_3\text{SO}_3)_2$ system.

Amount of $\text{Mg}(\text{CF}_3\text{SO}_3)_2$ (wt.%)	Ionic Conductivity (S cm^{-1})
5	4.65×10^{-5}
10	8.34×10^{-5}
15	5.58×10^{-4}
20	1.27×10^{-3}
25	1.49×10^{-4}
30	1.56×10^{-4}

From the dielectric properties study, the highest conducting film shows the highest value of dielectric constant, ϵ_r and dielectric loss, ϵ_i . As frequency decreases, the value of the dielectric constant, ϵ_r and dielectric loss, ϵ_i decreases. This inferred that the increase in ionic conductivity is due to an increasing of ions diffusion through their free volume. The conductivity-temperature studies proved that the GPE films follow the Arrhenius behavior with the regression value, R^2 almost close to unity. This study also indicates that the charge carriers were transport via ion hopping mechanism.

The values of activation energy, E_a obtained from this system are in the range of 0.18 - 0.26 eV. The low value of E_a suggests that ionic conduction is facile in GPE films due to the completely amorphous nature that facilitates the fast Mg^{2+} ion motion in the polymer network. The values of ionic conductivity, σ and activation energy, E_a obtained in this present work are within the range that reported by other researchers. The ionic transport number (t_{ion}) has been evaluated using the D.C. polarization method and the results confirmed that the total conductivity of the polymer electrolytes is predominantly due to ions. The Mg^{2+} ions transport number has been evaluated using a combination of A.C. impedance and D.C. polarization techniques and the value is found to be 0.38 for the highest conducting GPE film.

FTIR spectra studies have been carried out to study the structural properties of the GPE films and the results shown that the complexation of PMMA, EC, PC and $Mg(CF_3SO_3)_2$ salt has occurred. This can be observed by the appearance of new peaks, the absence of peaks along with the shift and the intensity of the existing peaks in FTIR spectra. Deconvolution has been done in the range of 1000 cm^{-1} to 1100 cm^{-1} to resolve the overlapping peaks which contain the free ions, ions pair and ions aggregates. These peaks are important to confirm the contribution of free ions which lead to high ionic conductivity while the decreasing of the ionic conductivity of the GPE film was due to the formation of ions pair and ions aggregates.

From XRD results, it reveals that the highest conducting GPE film exhibits most amorphous phase. The disappearance of diffraction peaks of $Mg(CF_3SO_3)_2$ salt can be attributed to complete dissolution of the salt in plasticized polymer matrix thus proved the complexation occurs between the salt, the plasticizing solvent and the polymer. Therefore,

it can be inferred from the XRD patterns that the amorphous region in GPE films has increased significantly which leads to higher conductivity.

The micrographs obtained from FESEM will provide important information on the surface structure and morphological properties of the GPE films. In this work, FESEM micrographs of the films were obtained for pure PMMA, PMMA-EC-PC and also the GPE films containing different weight percentages of $\text{Mg}(\text{CF}_3\text{SO}_3)_2$ salt. When salt is added, it can be observed that the size of pores is decreases and the surface of the film becomes smooth and homogenous. This confirmed that there is an interaction between the plasticized PMMA and the $\text{Mg}(\text{CF}_3\text{SO}_3)_2$ salt. When more salt is added, $\text{Mg}(\text{CF}_3\text{SO}_3)_2$ salt tends to aggregates. The formation of globular agglomeration at higher salt content ultimately leads to the formation of phase separation thus hinders the migration of Mg^{2+} ions in the polymer matrix which in turn reduces the ionic conductivity (S. Ramesh, Liew, Morris, & Durairaj, 2010).

DSC studies show that pure PMMA film has glass transition, T_g at 125 °C and upon the addition of plasticizers and salt, T_g values are decreases. The highest conducting film shows the lowest T_g value thus corresponds to the highest conductivity value obtained at room temperature. This is due to the increased in the segmental motion of the PMMA polymer backbone.

In this work, highest conducting film containing 20 wt.% of $\text{Mg}(\text{CF}_3\text{SO}_3)_2$ salt was characterized through LSV and CV techniques in order to estimate the electrochemical stability window (ESW) of the film and the results obtained have been analyzed. From the results, it is found that the GPE film are stable up to ~3.0 V and it can be inferred that the electrochemical stability window for the GPE film has been found in the range of -2.5 V to 2.5 V. This value of working voltage range appears to be high enough to be used as an electrolyte in solid state Mg-batteries system (G. P. Pandey, Agrawal, & Hashmi, 2009).

A cell of Mg|GPE|MnO₂ has been assembled and its performance has been characterized. The cell can be charged up to 2.3 V and the discharge curves gradually decrease to 0.8 V. The cyclic performance is limited to 4 cycles. This is mainly due to the electrochemical irreversibility of Mg metal and the growth of the layer at the interface between electrode and the GPE film.

As the suggestions for future work, the conductivity of the GPE films can be enhanced by blending the PMMA with other polymer such as PVdF and PEO. Blending polymer has been reported to be a useful method in order to develop new materials with improved mechanical stability. Another suggestion to improve the mechanical stability of the GPE films is by dispersing nano-sized ceramic fillers such as SiO₂ or TiO₂. Furthermore, we can also study the performance of the magnesium battery by using the different type of cathode materials such as V₂O₅ and MgNiO₂. Both of these materials are expected to give high discharge capacity with high stability of the battery.

REFERENCES

- Agnihotry, S. A., Pradeep, P., & Sekhon, S. S. (1999). PMMA based gel electrolyte for EC smart windows. *Electrochimica Acta*, 44(18), 3121-3126.
- Ahmad, S. (2009). Polymer electrolytes: characteristics and peculiarities. *Ionics*, 15(3), 309-321.
- Appetecchi, G. B., Croce, F., & Scrosati, B. (1995). Kinetics and stability of the lithium electrode in poly(methylmethacrylate)-based gel electrolytes. *Electrochimica Acta*, 40(8), 991-997.
- Armand, M. (1994). The history of polymer electrolytes. *Solid State Ionics*, 69(3-4), 309-319.
- Aurbach, D., Gofer, Y., Lu, Z., Schechter, A., Chusid, O., Gizbar, H., . . . Levi, E. (2001). A short review on the comparison between Li battery systems and rechargeable magnesium battery technology. *Journal of Power Sources*, 97-98(0), 28-32.
- basic_FTIR. (2012). Introduction to Fourier Transform Infrared Spectrometry
- battery_diagram.(2012). Retrieved from http://en.wikipedia.org/wiki/File:Diagram_of_a_battery_with_a_polymer_separator.jpg
- braggs_law.(2012). Retrieved from http://serc.carleton.edu/research_education/geochemsheets/BraggsLaw.html
- Bruce, P. G., Evans, J., & Vincent, C. A. (1988). Conductivity and transference number measurements on polymer electrolytes. *Solid State Ionics*, 28-30, Part 2(0), 918-922.
- C. Julien, G.-A. N. (1994). *Solid State Batteries: Materials Design and Optimization*. London: Kluwer Academic Publisher.
- Cai, H., Hu, R., Egami, T., & Farrington, G. C. (1992). The effect of salt concentration on the local atomic structure and conductivity of PEO-based NiBr₂ electrolytes. *Solid State Ionics*, 52(4), 333-338.
- cell, F. (2012). retrieved from <http://www.snupeel.com/xe/fuelcell>
- Chintapalli, S., & Frech, R. (1996). Effect of plasticizers on high molecular weight PEO-LiCF₃SO₃ complexes. *Solid State Ionics*, 86-88, Part 1(0), 341-346.
- Chusid, O., Gofer, Y., Gizbar, H., Vestfrid, Y., Levi, E., Aurbach, D., & Riech, I. (2003). Solid-State Rechargeable Magnesium Batteries. *Advanced Materials*, 15(7-8), 627-630.
- CV_voltammogram. (2012). Retrieved from <http://www.ceb.cam.ac.uk/pages/linear-sweep-and-cyclic-voltametry-the-principles.html>

- David Linden, T. R. (2001). *Handbook of Batteries* (pp. 1200).
- Deepa, M., Agnihotry, S. A., Gupta, D., & Chandra, R. (2004). Ion-pairing effects and ion-solvent-polymer interactions in LiN(CF₃SO₂)₂-PC-PMMA electrolytes: a FTIR study. *Electrochimica Acta*, 49(3), 373-383.
- Deka, M., & Kumar, A. (2010). Enhanced electrical and electrochemical properties of PMMA-clay nanocomposite gel polymer electrolytes. *Electrochimica Acta*, 55(5), 1836-1842.
- Device, E. (2012). Retrieved from <http://www.snupeel.com/xo/Electrochromic>
- DSC_thermogram. (2012). Retrieved from <http://www.flemingptc.co.uk/our-services/dsc-tga/>
- Dyre, J. C. (1991). Some remarks on ac conduction in disordered solids. *Journal of Non-Crystalline Solids*, 135(2-3), 219-226.
- Feuillade, G., & Perche, P. (1975). Ion-conductive macromolecular gels and membranes for solid lithium cells. *Journal of Applied Electrochemistry*, 5(1), 63-69.
- Ganesan, S., Muthuraaman, B., Mathew, V., Madhavan, J., Maruthamuthu, P., & Austin Suthanthiraraj, S. (2008). Performance of a new polymer electrolyte incorporated with diphenylamine in nanocrystalline dye-sensitized solar cell. *Solar Energy Materials and Solar Cells*, 92(12), 1718-1722.
- Girish Kumar, G., & Munichandraiah, N. (2000). Effect of plasticizers on magnesium-poly(ethyleneoxide) polymer electrolyte. *Journal of Electroanalytical Chemistry*, 495(1), 42-50.
- Girish Kumar, G., & Munichandraiah, N. (2002). Poly(methylmethacrylate)—magnesium triflate gel polymer electrolyte for solid state magnesium battery application. *Electrochimica Acta*, 47(7), 1013-1022.
- Girish Kumar, G., & Sampath, S. (2005). Electrochemical and spectroscopic investigations of a gel polymer electrolyte of poly(methylmethacrylate) and zinc triflate. *Solid State Ionics*, 176(7-8), 773-780.
- Granqvist, C. G. (1995). *Handbook of Inorganic Electrochromic Materials*
- Hu, C.-C., & Tsou, T.-W. (2002). Ideal capacitive behavior of hydrous manganese oxide prepared by anodic deposition. *Electrochemistry Communications*, 4(2), 105-109.
- Huang, B., Wang, Z., Li, G., Huang, H., Xue, R., Chen, L., & Wang, F. (1996). Lithium ion conduction in polymer electrolytes based on PAN. *Solid State Ionics*, 85(1-4), 79-84.
- Idris, R., Glasse, M. D., Latham, R. J., Linford, R. G., & Schlindwein, W. S. (2001). Polymer electrolytes based on modified natural rubber for use in rechargeable lithium batteries. *Journal of Power Sources*, 94(2), 206-211.
- Kumar, D., & Hashmi, S. A. (2010). Ionic liquid based sodium ion conducting gel polymer electrolytes. *Solid State Ionics*, 181(8-10), 416-423.

- Kumar, G. G., & Munichandraiah, N. (2000). Solid-state Mg/MnO₂ cell employing a gel polymer electrolyte of magnesium triflate. *Journal of Power Sources*, 91(2), 157-160.
- Kumar, Y., Hashmi, S. A., & Pandey, G. P. (2011). Ionic liquid mediated magnesium ion conduction in poly(ethylene oxide) based polymer electrolyte. *Electrochimica Acta*, 56(11), 3864-3873.
- LSV_voltammogram. (2012). from <http://www.ceb.cam.ac.uk/pages/linear-sweep-and-cyclic-voltametry-the-principles.html>
- MacCallum, J. R., Tomlin, A. S., & Vincent, C. A. (1986). An investigation of the conducting species in polymer electrolytes. *European Polymer Journal*, 22(10), 787-791.
- MacDonald, J. R. (1987). *Impedance Spectroscopy*. New York: Wiley.
- Novák, P., Imhof, R., & Haas, O. (1999). Magnesium insertion electrodes for rechargeable nonaqueous batteries — a competitive alternative to lithium? *Electrochimica Acta*, 45(1–2), 351-367.
- Oh, J.-S., Ko, J.-M., & Kim, D.-W. (2004). Preparation and characterization of gel polymer electrolytes for solid state magnesium batteries. *Electrochimica Acta*, 50(2–3), 903-906.
- Park, C. H., Kim, D. W., Prakash, J., & Sun, Y.-K. (2003). Electrochemical stability and conductivity enhancement of composite polymer electrolytes. *Solid State Ionics*, 159(1–2), 111-119.
- Pandey, G. P., & Hashmi, S. A. (2009). Experimental investigations of an ionic-liquid-based, magnesium ion conducting, polymer gel electrolyte. *Journal of Power Sources*, 187(2), 627-634.
- Pandey, G. P., Agrawal, R. C., & Hashmi, S. A. (2009). Magnesium ion-conducting gel polymer electrolytes dispersed with nanosized magnesium oxide. *Journal of Power Sources*, 190(2), 563-572.
- Pandey, G. P., Agrawal, R. C., & Hashmi, S. A. (2011). Performance studies on composite gel polymer electrolytes for rechargeable magnesium battery application. *Journal of Physics and Chemistry of Solids*, 72(12), 1408-1413.
- Pandey, G., Kumar, Y., & Hashmi, S. (2010). Ionic liquid incorporated polymer electrolytes for supercapacitor application. *Indian journal of chemistry. Section A, Inorganic, bio-inorganic, physical, theoretical & analytical chemistry*, 49(5), 743.
- Payne, D. R., & Wright, P. V. (1982). Morphology and ionic conductivity of some lithium ion complexes with poly(ethylene oxide). *Polymer*, 23(5), 690-693.
- Pitawala, H. M. J. C., Dissanayake, M. A. K. L., & Seneviratne, V. A. (2007). Combined effect of Al₂O₃ nano-fillers and EC plasticizer on ionic conductivity enhancement in the solid polymer electrolyte (PEO)₉LiTf. *Solid State Ionics*, 178(13–14), 885-888.
- Rajendran, S., & Uma, T. (2000). Characterization of plasticized PMMA-LiBF₄ based solid polymer electrolytes. *Bulletin of Materials Science*, 23(1), 27-29. doi: 10.1007/BF02708607

- Rajendran, S., Kannan, R., & Mahendran, O. (2001). Ionic conductivity studies in poly(methylmethacrylate)–polyethylene oxide hybrid polymer electrolytes with lithium salts. *Journal of Power Sources*, 96(2), 406-410.
- Rajendran, S., Mahendran, O., & Kannan, R. (2002). Lithium ion conduction in plasticized PMMA–PVdF polymer blend electrolytes. *Materials Chemistry and Physics*, 74(1), 52-57.
- Ramesh, S., Leen, K. H., Kumutha, K., & Arof, A. K. (2007). FTIR studies of PVC/PMMA blend based polymer electrolytes. *Spectrochimica Acta Part A: Molecular and Biomolecular Spectroscopy*, 66(4–5), 1237-1242.
- Ramesh, S., Liew, C.-W., & Ramesh, K. (2011). Evaluation and investigation on the effect of ionic liquid onto PMMA-PVC gel polymer blend electrolytes. *Journal of Non-Crystalline Solids*, 357, 2132-2138.
- Ramesh, S., Liew, C.-W., Morris, E., & Durairaj, R. (2010). Effect of PVC on ionic conductivity, crystallographic structural, morphological and thermal characterizations in PMMA–PVC blend-based polymer electrolytes. *Thermochimica Acta*, 511(1–2), 140-146.
- Ramesh, S., Yahaya, A. H., & Arof, A. K. (2002). Dielectric behaviour of PVC-based polymer electrolytes. *Solid State Ionics*, 152–153(0), 291-294.
- Ramya, C. S., Selvasekarapandian, S., Savitha, T., Hirankumar, G., & Angelo, P. C. (2007). Vibrational and impedance spectroscopic study on PVP–NH₄SCN based polymer electrolytes. *Physica B: Condensed Matter*, 393(1–2), 11-17.
- Saikia, D., & Kumar, A. (2005). Ionic transport in P(VDF-HFP)–PMMA–LiCF₃SO₃–(PC+DEC)–SiO₂ composite gel polymer electrolyte. *European Polymer Journal*, 41(3), 563-568.
- sample_analysis.(2012). Retrieved from http://chemwiki.ucdavis.edu/Physical_Chemistry/Spectroscopy/Fundamentals/The_Power_of_the_Fourier_Transform_for_Spectroscopists
- schematic_FTIR. (2012). Introduction to Fourier Transform Infrared Spectrometry
- schematic_SEM.(2012). Retrieved from <http://ncmn.unl.edu/cfem/microscopy/SEM.shtml>
- schematic_XRD.(2012). Retrieved from www.micro.magnet.fsu.edu/primer/java/interference/index.html
- Scrosati, B. (2000). Recent advances in lithium ion battery materials. *Electrochimica Acta*, 45(15–16), 2461-2466.
- Sekhon, S. S. (2003). Conductivity behaviour of polymer gel electrolytes: Role of polymer. *Bulletin of Materials Science*, 26(3), 321-328.
- SEM_principal.(2012). Retrieved from <http://www.nslc.wustl.edu/courses/Bio2960/labs/04Organelle/microscopy.html>
- Song, J. Y., Wang, Y. Y., & Wan, C. C. (1999). Review of gel-type polymer electrolytes for lithium-ion batteries. *Journal of Power Sources*, 77(2), 183-197.

- Tripathi, S. K., Jain, A., Gupta, A., & Mishra, M. (2012). Electrical and electrochemical studies on magnesium ion-based polymer gel electrolytes. *Journal of Solid State Electrochemistry*, 16(5), 1799-1806.
- Ulaganathan, M., Nithya, R., & Rajendran, S. (2012). Surface Analysis Studies on Polymer Electrolyte Membranes Using Scanning Electron Microscope and Atomic Force Microscope.
- Uma, T., Mahalingam, T., & Stimming, U. (2003). Mixed phase solid polymer electrolytes based on poly(methylmethacrylate) systems. *Materials Chemistry and Physics*, 82(2), 478-483.
- Uma, T., Mahalingam, T., & Stimming, U. (2005). Conductivity studies on poly(methyl methacrylate)-Li₂SO₄ polymer electrolyte systems. *Materials Chemistry and Physics*, 90(2-3), 245-249.
- vibrational_modes.(2012). Retrieved from http://chemwiki.ucdavis.edu/Organic_Chemistry/Organic_Chemistry_With_a_Biological_Emphasis/Chapter_4%3A_Structure_Determination_I/Section_4.2%3A__Infrared_spectroscopy
- Vondrák, J., Sedlaříkova, M., Velická, J., Klapšte, B., Novak, V., & Reiter, J. (2001). Gel polymer electrolytes based on PMMA. *Electrochimica Acta*, 46(13-14), 2047-2048.
- Vondrák, J., Sedlaříkova, M., Velická, J., Klapšte, B., Novak, V., & Reiter, J. (2003). Gel polymer electrolytes based on PMMA: III. PMMA gels containing cadmium. *Electrochimica Acta*, 48(8), 1001-1004.
- Vondrák, J., Reiter, J., Velická, J., & Sedlaříková, M. (2004). PMMA-based aprotic gel electrolytes. *Solid State Ionics*, 170(1-2), 79-82.
- Woo, H. J., Majid, S. R., & Arof, A. K. (2011). Conduction and thermal properties of a proton conducting polymer electrolyte based on poly (ϵ -caprolactone). *Solid State Ionics*, 199-200(0), 14-20.
- Yoshimoto, N., Yakushiji, S., Ishikawa, M., & Morita, M. (2003). Rechargeable magnesium batteries with polymeric gel electrolytes containing magnesium salts. *Electrochimica Acta*, 48(14-16), 2317-2322.

Magnesium Ion-Based Gel Polymer Electrolytes: Ionic Conduction and Infrared Spectroscopy Studies

*N. H. Zainol, S.M. Samin, L. Othman, K.B. Md Isa, W.G. Chong and Z. Osman**

Department of Physics, University of Malaya, 50603, Kuala Lumpur, Malaysia

*E-mail: zurinaosman@um.edu.my

Received: 12 January 2013 / Accepted: 6 February 2013 / Published: 1 March 2013

The gel polymer electrolyte (GPE) films based on polymethylmethacrylate (PMMA) containing the mixture of ethylene carbonate (EC) and propylene carbonate (PC) as a plasticizing solvent and various concentrations of magnesium triflate or $Mg(CF_3SO_3)_2$ salt have been prepared using the solution casting technique. The maximum room temperature ionic conductivity of $1.27 \times 10^{-3} S cm^{-1}$ was obtained from the GPE film containing 20 wt.% of $Mg(CF_3SO_3)_2$ salt. The conductivity-temperature studies of the GPE films follow the Arrhenius behavior with activation energy for ionic conduction are determined to be 0.18 - 0.26 eV. The transport number of magnesium ions in the GPEs was evaluated using the combination of a.c. impedance spectroscopy and d.c. polarization techniques. Fourier Transform Infrared Spectroscopy (FTIR) studies confirmed the increased in conductivity is due to increase of free ions and decrease in ion aggregates.

Keywords: Gel polymer electrolytes; magnesium ion; ionic conductivity; transport number; FTIR spectroscopy

1. INTRODUCTION

Electrochemical energy storage systems have a tremendous role in technical applications such as supercapacitors, electrochemical devices, sensors, fuel cells, etc. [1-2]. In the midst of technologies emerging today, an even higher demand for rechargeable batteries with high specific energy, high power which provides good metal surface stability and high electrochemical stability are expected [2-4]. Although lithium batteries are widely been used in high power application due to its highest electrode potential with an average voltage of 3.8 V, the lithium itself has brought out serious environmental issues due to its reactive nature and safety concern to the device and even the users [5-6]. At the same time, the accessibility of the raw material for the conventional battery is a great challenge that is likely to impact its sustainability in the future. Therefore, an alternative energy

Transport and Morphological Properties of Gel Polymer Electrolytes containing $Mg(CF_3SO_3)_2$

N.H.Zainol^a, Z.Osman^b, L.Othman^c and K.B. Md. Isa^d

Physics Department, Faculty of Science, University of Malaya, 50603, Kuala Lumpur, Malaysia

^ahusna.zai87@gmail.com, ^bzurinaosman@um.edu.my, ^camoda78@yahoo.com,

^dwlppyne@yahoo.com

Keywords: Gel polymer electrolyte; $Mg(CF_3SO_3)_2$; ionic conductivity; transport number; morphological properties

Abstract: Magnesium-ion conducting gel polymer electrolytes (GPEs) based on PMMA with ethylene carbonate (EC) and propylene carbonate (PC) as a plasticizing solvent were prepared via the solution casting technique. $Mg(CF_3SO_3)_2$ salt was used as source of magnesium ions, Mg^{2+} . The variation of conductivity with salt concentrations, from 5 wt.% to 30 wt.% was studied. The gel polymer electrolyte with composition 20 wt.% of $Mg(CF_3SO_3)_2$ exhibited the highest conductivity of $1.27 \times 10^{-3} S cm^{-1}$ at room temperature. The conductivity-temperature dependence of gel polymer electrolyte films obeys Arrhenius behaviour with activation energy in the range of 0.18 eV to 0.26 eV. Ionic transport number was evaluated using DC polarization technique and it reveals the conducting species are predominantly ions. It is found that the ionic conductivity and transport properties of the prepared GPEs are consistent with the X-Ray Diffraction (XRD) and Field Emission Scanning Electron Microscopy (FESEM) studies.

Introduction

Many research works on polymer electrolytes have been directed towards advanced batteries technology based on lithium since the rechargeable lithium-ion battery has been one of the best choices in view of its specific capacity and cycle stability. However, lithium-ion batteries are relatively expensive and suffered from safety problem as it requires a high purity argon or helium atmosphere to be handled [1]. Therefore, magnesium-based batteries have attracted researchers in materials science and electrochemical fields owing to their electrochemical properties that closed to lithium-based system [2]. Magnesium is a promising candidate due to its high electrochemical equivalence ($2.2 Ah g^{-1}$), relatively low equivalent weight (12g per Faraday), high melting point (649°C), low cost, high safety, ease of handling, and low toxicity which allows for urban waste disposal [3-6].

At present, various gel-type polymer electrolytes that are made by immobilizing magnesium salt and plasticizing organic solvents are proposed in the literature for possible application as electrolytes in electrochemical devices [7-9]. The addition of an extra amount of polymeric component may prove to provide mechanical stability by increasing the viscosity of electrolyte. In addition, the plasticizing effect would facilitate the ionic transportation within the polymer matrix by forming highly flexible polymer backbone [10]. Compared with other types of polymer electrolytes, gel polymer electrolytes possess higher room temperature ionic conductivity of about $10^{-3} S cm^{-1}$ and the development of solid-state Mg^{2+} conducting electrolytes has become one of the main issues to realize rechargeable solid-state magnesium batteries.

In this work, conductivity, ionic transport, structural and morphological studies have been carried out on poly (methylmethacrylate) (PMMA) based gel polymer electrolytes. Magnesium triflate ($MgCF_3SO_3$) has been used as source of magnesium ions while the mixture of ethylene carbonate (EC) and propylene carbonate (PC) will act as a plasticizing solvent. This system has been prepared by using solution casting technique. Ionic conductivity and transport number of the GPE samples have been measured by using impedance spectroscopy technique and DC polarization method, respectively. XRD and FESEM studies have been conducted in order to investigate the structural and morphological features of the GPE films.